PERSISTENT REMODELING AND NEURODEGENERATION IN LATE-STAGE RETINAL DEGENERATION

by

Rebecca Lynne Pfeiffer

A dissertation submitted to the faculty of
The University of Utah
in partial fulfillment of the requirements for the degree of

Doctor of Philosophy

in

Neuroscience

Interdepartmental Program in Neuroscience

The University of Utah

December 2017

The University of Utah Graduate School

STATEMENT OF DISSERTATION APPROVAL

The dissertation of **Rebecca Lynne Pfeiffer**

has been approved by the following supervisory committee members:

Robert E. Marc	, Chair	**April 13th, 2017** Date Approved
Alessandra Angelucci	, Member	**April 13th, 2017** Date Approved
David Krizaj	, Member	**April 13th, 2017** Date Approved
Karen S. Wilcox	, Member	**April 13th, 2017** Date Approved
Megan E. Williams	, Member	**April 13th, 2017** Date Approved

and by **Richard Dorsky** , Chair/Dean of

the Department/College/School of **Interdepartmental Program in Neuroscience**

and by David B. Kieda, Dean of The Graduate School.

ABSTRACT

Human retinitis pigmentosa (RP) typically involves decades of progressive vision loss before some patients become blind, and prospective therapies target patients who have been blind for substantial time, even decades. Evaluations of molecular and cellular therapies have primarily employed short-lived mouse models lacking the scope of remodeling common in human RP. The *Rho* Tg P347L transgenic rabbit offers a unique opportunity to evaluate the primary degeneration event and subsequent progressive remodeling that ensues over a timespan that recapitulates the human disease phenotype. Retinas from a TgP347L rabbit model of human dominant RP and wild-type litter mates were harvested over an 8-year span and processed for transmission electron microscope connectomics, immunocytochemistry for a range of macromolecules, and computational molecular phenotyping for small molecules, including transport tracing with D-Asp. Early time points in the TgP347L rabbit recapitulate the established sequence of photoreceptor loss, retinal remodeling, and reprogramming, and also reveal progressive disruptions in Müller cell metabolism, where rather than observing a homogeneous glial population, chaotic metabolic signatures emerge. By 4 years, virtually all remnants of photoreceptors are gone and the neural retina manifests severe cell loss and near complete loss of glutamine synthetase, though glial glutamate transport persists. By 6 years, there is a global >90% neuronal loss. In some regions the retina is devoid of identifiable cells and replaced by unknown debris-like assemblies. Though the 6-year retina does have locations with

recognizable neurons, all cell types are drastically reduced in number and some have altered metabolic phenotypes. These results are never seen in wt littermates, including rabbits which are 8 years old. Electron microscopic analysis using wide-field connectomics imaging of the 6-year TgP347L sample demonstrates some structurally normal synapses, indicating that survivor neurons in these regions are not quiescent despite the lack of sensory input for a substantial period of time. These results indicate that, although photoreceptor degeneration is the trigger, retinal remodeling ultimately gives way to neurodegeneration, which is a separate unrelenting disease process independent of the initial insult, closely resembling slow progressive CNS neurodegenerations. Indeed, both metabolic disruption and debris-related degeneration predicts the existence of a persistent neuropathy, and increases in α-synuclein levels support a proteinopathy component. Remodeling and neurodegeneration progress until the retina is devoid of recognizable cells. There is no stable state into which the retina settles and no cell type is spared. This has profound implications for current therapeutics. There will likely be critical windows for implementation but, ultimately, suspension of neurodegenerative remodeling will be required for long-term success.

TABLE OF CONTENTS

ABSTRACT iii

LIST OF FIGURES viii

Chapters

1. INTRODUCTION 1

1.1 Architecture of the Retina 2
1.1.1 Photoreceptors 3
1.1.2 Horizontal Cells 4
1.1.3 Bipolar Cells 5
1.1.4 Amacrine Cells 6
1.1.5 Ganglion Cells 7
1.1.6 Glia 8
1.2 Retinal Degenerative Diseases 9
1.2.1 Retinitis Pigmentosa 9
1.2.2 Age-Related Macular Degeneration 10
1.3 Phases of Retinal Remodeling 11
1.3.1 Phase 0: The Healthy Retina 12
1.3.2 Phase 1: Rod Degeneration 13
1.3.3 Phase 2: Cone Degeneration 14
1.3.4 Early Phase 3: Neurite Remodeling 14
1.3.5 Mid Phase 3: Global Remodeling 15
1.3.6 Late Phase 3: Plateau Remodeling 16
1.4 Therapeutic Approaches to Vision Restoration 16
1.4.1 Optogenetics 17
1.4.2 Chemical Photoswitches 18
1.4.3 Cellular Replacement Strategies 19
1.4.4 Bionic Implants 20
1.4.5 Genetic Approaches 21
1.4.6 Requirements for Therapeutic Interventions to Be Effective 22
1.5 References 27

2. MATERIALS AND METHODS 35

2.1 Computational Molecular Phenotyping (CMP) 35
2.1.1 Molecular Trapping and IgG Labeling 36

2.1.2 CMP Analysis: Pattern Recognition 40
2.2 P347L Transgenic Rabbit Model of Retinitis Pigmentosa 43
2.3 References 48

3. MÜLLER CELL METABOLIC CHAOS DURING RETINAL DEGENERATION 52

3.1 Introduction 53
3.1.1 Retinal Degeneration and Remodeling 53
3.1.2 Müller Glia in Degenerating Retina 54
3.1.3 Müller Glia Functions and Homogeneity 54
3.1.4 Transgenic P347L Rabbit Model of Autosomal-Dominant Retinitis Pigmentosa (adRP) 54
3.1.5 Computational Molecular Phenotyping 54
3.2 Methods 54
3.2.1 Model Systems 54
3.2.2 Tissue Processing 55
3.2.3 CMP and Nomenclature 55
3.2.4 Analysis 55
3.3 Results 55
3.3.1 CMP Signatures 56
3.3.2 Clustering, Histograms, and Analysis 56
3.4 Discussion 58
3.5 Acknowledgements 60
3.6 References 60

4. EVALUATION OF EXCITOTOXICITY AS A MECHANISM OF RETINAL DEGENERATION 62

4.1 Introduction 62
4.1.1 Excitotoxicity Hypothesis 63
4.1.2 Evidence Disputing Excitotoxicity 65
4.2 Materials and Methods 67
4.2.1 Model Systems 67
4.2.2 Tissue Processing 68
4.2.3 CMP Analysis 68
4.3 Results 69
4.4 Conclusions and Discussion 72
4.5 References 79

5. LONG-TERM RETINAL DEGENERATION LEADS TO EXTENSIVE NEURODEGENERATION AND ALPHA SYNUCLEIN AGGREGATION 82

5.1 Effects of Long-term Remodeling on Therapeutic Interventions 82
5.2 Animal Models of Retinal Remodeling and Possible Caveats 83
5.3 Materials and Methods 84
5.3.1 Model Systems 84

5.3.2 Tissue Processing 84
5.3.3 Computational Molecular Phenotyping (CMP) 85
5.3.4 Protein Variation Quantification 86
5.4 Characterization of Aged P347L Rabbit 87
5.5 Ubiquitin Expression in Retinal Degeneration 88
5.6 Alpha Synuclein Aggregation in Older Transgenic Retina 89
5.7 Discussion 91
5.8 References 104

6. DISCUSSION AND FUTURE DIRECTIONS 107

6.1 Müller Cell Metabolic Chaos 107
6.2 Excitotoxicity in the Retina 110
6.3 Retinal Neurodegeneration 112
6.4 Implications for Therapeutic Interventions 113
6.5 Future Directions 114
6.6 References 121

LIST OF FIGURES

Figures

1.1 Schematic of the major histological and cellular classifications of the retina 25

1.2 Remodeling of the mammalian retina in retinal degenerations 26

2.1 K-means generation of theme maps 46

3.1 Comparison of WT amino acid levels to that of Tg P347L 56

3.2 Representative τQE and theme maps of WT retina vs degenerate retina 57

3.3 Univariate amino acid probability density distributions (histograms) for each of the amino acids displayed in Fig 3.2 58

3.4 τQE → rgb mappings of registered amino acid signals in serial 100 nm sections 59

3.5 Cumulative distribution frequencies (CDFs) of the entire Müller cell cohorts in the regions displayed in 3.4C-F (red Normal Distribution (ND) line) in addition to 10 4x4 µm regions from WT and degenerate retina (MC1-10 CDFs) as gray lines. 60

4.1 Müller cell metabolic variation across retinal regions and species 75

4.2 Müller cell metabolic variation within Müller cells 76

4.3 GS/Q/E variability in WT compared to degenerate retina 77

4.4 D-Aspartate loading in retinal chips 78

5.1 Representative registered images of amino acid immunoreactivity in 100nm sections of WT, Phase 2, and Phase 3 remodeling in rabbit retina 94

5.2 Representative images from WT rabbit (A-C), 2yr (d-F), 4yr (G-I), 5(yr (J-L), and 6yr (M-O) Tg P347L rabbit retina 95

5.3 Theme map overlay of TEM image of retina 98

5.4 Grayscale ubiquitin labeling in rabbit retinas 99

5.5 Endogenous signaling of phosphorylated α-synuclein (α-syn), and GFAP 100

5.6 Western Blot: Beta actin demonstrated some increase in Tg retinas when compared to WT. 102

5.7 Antibody inhibition experiment 103

6.1 Retinal degeneration, a combination of remodeling and neurodegenerative processes 117

6.2 Workflow for generation of pathoconnectome 119

6.3 Preliminary RPC1 data 120

CHAPTER 1

INTRODUCTION

Diseases such as diabetic retinopathy, age-related macular degeneration, glaucoma, and retinitis pigmentosa, cause irreversible vision loss affecting millions of people worldwide.[1] Of these diseases, degenerations that onset with the loss of photoreceptors (age-related macular degeneration and retinitis pigmentosa) have received special attention with the goal of restoring vision through therapeutic interventions, primarily after photoreceptors have degenerated.[2-13] Ultimately this dissertation aims to describe the long term effects of retinal degeneration, factors contributing to degeneration following the loss of photoreceptors, identify potential complications in implementing therapeutics long-term, and propose windows of degeneration in which therapeutic interventions have the greatest likelihood of success.

This chapter aims to introduce the reader to the structure of the healthy retina and its general roles in vision. In addition, this chapter will give a broad overview of retinal degenerative diseases, phases of degeneration, therapeutic interventions currently in development, and describe probable requirements for long-term vision restoration, which will be recurrent themes throughout this dissertation.

1.1 Architecture of the Retina

The retina is a thin multilaminar strip of nervous tissue along the posterior surface of the eye, which developmentally originates from the frontal cortex, making it part of the central nervous system. The retina is subdivided into six major histological layers: the photoreceptor layer (which may be further subdivided into the outersegment, innersegment, and outer nuclear layer), the outer plexiform layer (OPL), the inner nuclear layer (INL), the inner plexiform layer (IPL), the ganglion cell layer (GCL), and the optic fiber layer (OFL) (Figure 1.1). It is composed of five major neuronal cell types: photoreceptors, horizontal cells, bipolar cells, amacrine cells, and ganglion cells.[14] These cells working together play important roles in processing color, motion, intensity, and directionality from visual stimulus.[15] In addition to neurons, the retina also has numerous glial cells: Müller cells, astrocytes, and microglia of immune system origin, providing critical functions in the retina. The retinal circuitry is primarily divided into two major pathways: vertical and horizontal. The vertical pathway is the path from the photoreceptors, bipolar cells, and ganglion cells, which ultimately project axons into the brain. It is primarily thought of as an amplification pathway, though the presence of ON and OFF cells permits the first level of light-detection processing, and ON-OFF motifs are preserved from bipolar cells through processing in the brain. The horizontal pathway tunes signals from the vertical pathway from being extremely broad regions of light detection to more defined regions of higher light intensity with less light intense regions surrounding. The higher intensity regions of focus are termed *centers* while the surrounding regions are aptly named the *surround*. Together, the vertical and horizontal pathways provide initial processing of visual information, prior to action potentials relaying signals to the brain

1.1.1 Photoreceptors

In most species, photoreceptors are the neurons of the retina found closest to the back of the eye. They are the first cells to receive visual stimulus via light, and consist of two major types: cones and rods. Rods and cones are responsible for translating light information (photons) into neurochemical signals, which is how most information is passed throughout the nervous system. In photoreceptors, the neurotransmitter released is glutamate. Mammals tend to have two to three types of cones and a single type of rod. The opsins (light-sensitive proteins) for both classes of photoreceptors are contained in the outersegment portion of the photoreceptor. Outer segments are composed of bilipid membrane stacked disks, which are continuously shed distally, and replaced proximal to the cell body. Rod outer segments are stacked in thin rod shaped columns, while cone outer segments are conical. Cones provide responses to bright light and have different opsins (light-sensing molecules) tuned to different wavelengths. The mixing of information from cones containing different opsins is the mechanism by which we see color. In contrast to cones, there is only one type of rod in mammals. Rods contain the opsin rhodopsin, and the rod transduction pathway makes it extremely sensitive to light, facilitating vision at low levels of light (e.g., starlight). A fundamental principle associated with all neurons is that when they are depolarized, the rate of synaptic vesicle fusion leading to neurotransmitter release is increased. When neurons are hyperpolarized the opposite is true. In response to light, photoreceptors hyperpolarize, meaning the amount of glutamate released decreases as the intensity of light increases. In darkness, photoreceptors are depolarized and constitutively release glutamate, leading to a large concentration of glutamate in the synaptic cleft. Though this may seem counterintuitive, the balance of glutamate being

released versus being removed from the synapse via transporters creates a concentration gradient making the system very sensitive to even small variations in light. The hyperpolarization and depolarization responses to photon capture are not an all-or-none response (e.g., an action potential), but rather a graded potential, allowing small and large changes in available photons to be rapidly relayed to neurons of the inner retina. The postsynaptic partners of photoreceptors (horizontal cells and bipolar cells) have evolved mechanisms to detect and respond to slight changes in glutamate release by photoreceptors.

1.1.2 Horizontal Cells

Horizontal cells are found immediately below the outer plexiform layer and, as the name would suggest, are oriented horizontal to the vertical pathway of the retina. The primary function of horizontal cells in most mammals is feedback onto cone photoreceptors helping to generate center-surround response curves and assist in tuning luminosity, though in nonmammalian vertebrates, they also help to tune chromatic information. Horizontal cells are extensively coupled to one another via large gap junctions, facilitating wide spreading of depolarization and hyperpolarization events throughout the retina. A common theme in neuroscience is sign-conserving versus sign-inverting synapses. Sign-conserving synapses are cases where the postsynaptic neuron has the same polarity response as the presynaptic neuron, though not necessarily the same kinetics. An example of this is the synapse between cones and horizontal cells. Horizontal cells are predominately activated via ionotropic glutamate receptors, which depolarize in response to glutamate released by cones and hyperpolarize when glutamate release is decreased, thereby matching the polarization state of the cones that directly drive them. In contrast, the “synapses” back

onto cones from horizontal cells are sign-inverting: as horizontal cells hyperpolarize, they trigger depolarization of the photoreceptor, albeit using nonconventional signaling pathways though to involve ephaptic mechanisms or alkalization of the perisynaptic space. These sign-inverting and sign-conserving feedback loops are a common motif that, combined with graded potentials, are fundamental to initial visual processing performed by the retina. The number and types of horizontal cells is variable between animals, but in mammals it is generally accepted that there are two types: type A (axon-less) and type B (axon-bearing). Despite the two morphological types, horizontal cells are often referred to as having three functional types; this is because the rod-associated axon terminals and cone-associated somas of type B cells function independently of one another. It is now thought that horizontal cell axon terminals may provide some feedback function for rods as well. The three functional types of horizontal cell's feedback with photoreceptors create the first level of center-surround tuning.

1.1.3 Bipolar Cells

Bipolar cells are specialized interneurons, which pass signals from photoreceptors onto the rest of the retina. In mammals bipolar cells are subdivided into three major classes: ON-cone, OFF-cone, and rod. As described above, photoreceptors are persistently depolarized in darkness, and hyperpolarize in response to light. Bipolar cells respond to increases or decreases in light by either sign-conserving or sign-inverting responses via ionotropic glutamate receptors (iGluRs) or group III metabotropic glutamate receptors (mGluRs), respectively, on dendrites that synapse with photoreceptors within the OPL. Metabotropic glutamate receptors transduce sign-inverting signaling, which close cation

permeable channels in the plasma membrane in response to glutamate, decreasing inward currents and causing hyperpolarization. Alternatively, ionotropic glutamate receptors gate opening of cation channels in response to glutamate, increasing inward currants and initiate depolarization. Thus iGluRs mimick the response of the photoreceptors, leading to sign-conserving signaling. ON-cone and rod bipolar cells express mGluR6 metabotropic glutamate receptors, causing them to depolarize in the presence of light. OFF-cone bipolar cells have ionotropic glutamate receptors, causing them to be depolarized in the absence of light. Bipolar cells, like photoreceptors, are glutamatergic in their neurotransmission to synaptic partners, with glutamate packaged into synaptic vesicles and associated with ribbon synapses in bipolar cell axons. Synaptic ribbons perform important tasks in amplifying signals from photoreceptors and pass the information to amacrine and ganglion cells either via AMPA receptors or a mixture of AMPA and NMDA receptors. Cone bipolar cells synapse directly onto ganglion cell dendrites, while rod bipolar cell axons do not.[16] Rod signals reach ganglion cells indirectly via the AII amacrine cell network. The layers of the retina where bipolar cells make their synaptic connections is mostly segregated: ON-bipolar cells synapse in the proximal IPL (closer to the GCL), and OFF-bipolar cells synapse in the distal IPL (closer to the INL)[17]; although this is a generalization and some synaptic crossover does occur.[18]

1.1.4 Amacrine Cells

Amacrine cells play multiple roles in visual processing in the retina. They are the most diverse cell type in the retina, with the mammalian retina possessing at least 30 classes of amacrine cells. The main neurotransmitters associated with amacrine cells are GABA

and glycine.[19-21] These neurotransmitters are inhibitory and they act on synapses in a sign-inverting manner. In addition to chemical synapses, amacrine cells also couple with one another via a large network of gap junctions, permitting the transfer of graded potentials electrically. GABAergic amacrine cells are predominantly thought of as gain modulators of the retina helping to organize vision beyond ON versus OFF with a complex network of feedback synapses onto bipolar cells and feed forward synapses with ganglion cells. Beyond the synaptic contacts amacrine cells make onto bipolar and ganglion cells, one type of amacrine cell, the AII amacrine cell, plays a unique role in the vertical pathway as a sign-conserving interneuron. The AII amacrine cell receives sign-conserving synaptic input from the rod-bipolar cell axons causing it to depolarize. This depolarization then spreads to nearby ON-bipolar cells via gap junctions, leading to the depolarization and release of glutamate by these cells onto ganglion cells. Simultaneously, the depolarization of AII amacrine cells causes the release of the neurotransmitter glycine onto OFF-bipolar cells, thereby inhibiting them.[16, 22] These two paths inject rod-ON and rod-OFF signals into ON and OFF ganglion cells, respectively.

1.1.5 Ganglion Cells

Ganglion cells are the only neuron of the retina to directly synapse within the brain. In mammals, ganglion cells project to the lateral geniculate nucleus, superior colliculus, suprachiasmatic nucleus, and accessory optic nuclei in the midbrain.[23] The dendrites of ganglion cells arborize in the IPL and are postsynaptic to both bipolar cells and amacrine cells. Depending on the combination of bipolar and amacrine cell synapses onto ganglion cells and the spatial properties of the amacrine cells, different features of the visual world

are encoded into a sequence of action potentials to discreet nuclei in the brain. In addition to ganglion cells firing depending on whether they receive ON or OFF input, thereby preserving the initial encoding by bipolar cells, some ganglions cells are specially tuned to respond only to signals moving in certain directions, or are temporally responsive, giving transient or sustained responses to the same visual stimulus. Other ganglion cells are also intrinsically photosensitive due to their expression of melanopsin; these ganglion cells play important roles in the regulation of pupil size and maintenance of circadian rhythm.

1.1.6 Glia

Glia are traditionally referred to as the support cells of the nervous system. In the retina, the predominant glial cell type is the Müller cell. Müller glia have been shown to play important structural roles within the neural retina[24] including sealing the retina off from the vitreous and separating the ONL from the INL. They play a key role in retinal homeostasis through removal of neural waste products such as CO_2 and NH_3, redistribution of K+, and are important in the glutamate-glutamine cycle by metabolizing glutamate to glutamine via the enzyme glutamine synthetase.[25-27] The other macroglia found in the retina is astrocytes; they are predominantly restricted to the OFL, though they make some vascular contacts in the GCL, contributing to the blood-retinal-barrier (BRB). One distinction between brain astrocytes and retinal astrocytes is the absence of glutamine synthetase in astrocytes of the retina. In addition to macroglia, microglia may be found distributed throughout the retina, though they are typically found in the ONL, OPL, IPL, and GCL in healthy retina. In conditions of stress microglia may be found in different activation states throughout the retina.

In summary, the retina is a complex neural system, consisting of over 70 neural types (in mammals), which form chemical and electrical connections responsible for initial visual processing. The precise patterning of these connections, in addition to the metabolic system requirements to allow for constant signaling, work together to provide the brain with the information it needs to interpret the visual world.

1.2 Retinal Degenerative Diseases

Retinal degenerative diseases including retinitis pigmentosa (RP) and age-related macular degeneration (AMD) cause irreversible vision impairment, by directly or indirectly leading to photoreceptor loss. Though the initial progression rate of photoreceptor loss may vary between diseases, the ultimate outcome is the same: global loss of photoreceptors across the retina, leaving a deafferented neural retina.

1.2.1 Retinitis Pigmentosa

Retinitis pigmentosa (RP) refers to a range of hereditary disorders, which onset with degeneration of the photoreceptors. The name retinitis pigmentosa originates from the ophthalmoscopic observation of exposed pigmentation in the neural retina, arising from migration of pigmented RPE cells into the neural retina.[28] The prevalence of RP is approximately 1 in 4000, with varying modes of inheritance: 50-60% of cases are inherited autosomal-recessive, 30-40% autosomal-dominant, and 5-15% X-linked. In fact, RP is known to arise from almost 300 gene defects,[*] which are subclassified by their genetic

[*] https://sph.uth.edu/Retnet/ (Accessed March 5th,2017)

component, mode of inheritance, and whether the defect is constrained to the eye or also affects nonocular tissues. Examples of associated nonocular diseases are Bardet-Biedl syndrome and Usher syndrome, which are both autosomal-recessive. Bardet-Biedl syndrome, in addition to photoreceptor loss, is associated with polydactyly, truncal obesity, hypogonadism, renal dysfunction, and learning difficulties.[29] Usher syndrome is associated with hearing-loss in addition to RP.[30] Despite the many modes of inheritance and genes involved with RP, outer segments of rod degenerate in a patchy fashion across the retina, followed by cones, and gradually lead to loss of vision in patients.

The speed of vision loss and the mechanism causing the photoreceptor degeneration varies widely across RP diseases, along with the prevalence of that specific genetic defect. Some patients will present with vision loss early in life, while others will remain asymptomatic until mid-adulthood. In most cases, RP patients are legally blind by their mid-forties, and photoreceptor degeneration continues until the retina is completely devoid of photoreceptors, leaving patients completely unable to perceive light for years to decades of life.[31]

1.2.2 Age-Related Macular Degeneration

As the name would imply, *Age-Related Macular Degeneration* (AMD) predominately affects older people, and is the leading cause of vision loss in individuals over the age of 50.[†] Unlike RP, AMD is only partially associated with genetic inheritance. Rather, AMD is also associated with environmental factors such as smoking, which can

[†] https://nei.nih.gov/health/maculardegen/armd_facts

greatly increase an individual's risk.[32] Clinically, patients often complain about blurriness in their central vision, which progresses to a loss of central vision which then advances outward towards the periphery.[33] Histologically, dry AMD presents with drusen (lipid deposits under the retina) separating the RPE from the choroid, metabolic alterations of RPE cells,[34] and subsequent stress and loss of photoreceptors. Wet AMD arises from new blood vessel formation (neovascularization) in the retina and subsequent leakage of blood and serum into the neural retina.

1.3 Phases of Retinal Remodeling

Early studies evaluating the progression of advanced RP in humans noted clear gliosis, cellular disorganization, and displaced RPE cells scattered around the neural retina.[16] Other early ophthalmologists have also noted RP associated atrophy in humans, with an emphasis on an apparent loss of ganglion cells.[35-36] These early observations however have not been recapitulated in animal models, and therefore have largely not been factored into strategies for therapeutic interventions.[37] This was in part due to limitations of conventional histology and the result of short-lived experimental animal models. Recent post mortem studies of humans and the further extensive characterization of animal models[38] have shown that neurons and glia of the retina undergo metabolic and morphologic remodeling as a key component of retinal degeneration, antecedent and subsequent to photoreceptor loss in both humans and animal models of RP.[33, 37-40] Remodeling includes neuronal rewiring, neurite growth, and reprogramming of neurons' characteristic gene expression. Some remodeling begins as soon as photoreceptor stress is initiated, while other remodeling processes emerge following the complete regional loss of

photoreceptors. The phases of remodeling follow the loss of photoreceptors, so different regions of the retina are often in different phases of remodeling because photoreceptor loss appears in a patchy fashion in most instances. The description presented below assumes a rod-initiated RP-like process, but the long term progression, particularly in phase 3 (described below), is similar in all forms.[28] Ultimately, remodeling leads to large-scale corruption of neural networks in the retina, both through neural rewiring and cell death, making it unclear whether a retina which has undergone these alterations is capable of supporting therapeutic interventions to vision loss.[41] In the interest of clarity, our lab has classified the extent of remodeling into 3 distinct phases (Figure 1.2).[28, 40]

1.3.1 Phase 0: The Healthy Retina

The healthy retina is described more completely in section 1.1 of this chapter. In brief, the retina is composed of two major components that will be referenced throughout this section: the sensory retina and the neural retina. The sensory retina is composed of the photoreceptors (both their outer segments and nuclei), which are responsible for the primary detection of light. The neural retina then performs extensive processing of the light information before transmitting the information to the brain via ganglion cell action potential. The neural retina is composed of five main cell types: horizontal cells (HCs), bipolar cells (BCs), amacrine cells (ACs), ganglion cells (GCs), and glia (predominantly Müller cells (Müller cells), but also including microglia and astrocytes).

1.3.2 Phase 1: Rod Degeneration

Rod degenerations are triggered through a number of gene defects including those listed in section 1.2 of this chapter, or through some sort of trauma (retinal detachment or light-induced retinal degeneration). Regardless of the initiating insult, rod outer segments become shortened, followed by rod stress, deconstruction, and ultimately cell death. Prior to this, some rods will extend their axons and terminate in the GCL, rather than the conventional termination in the OPL.[42] During the initial stress of the outer segments, rod bipolar cells begin to retract their dendrites from their previously associated rod terminal (spherule).[43] Some of these rod bipolar cells will initiate rewiring and extend their dendrites toward cone terminals (pedicles).[44] In addition, most or all rod bipolar cells change their expressed receptors from metabotropic to ionotropic, causing them to functionally change from being ON-type cells to OFF-type. Beyond the neural responses seen from the rod bipolar cells, glia also respond to the rod degeneration. Microglia begin to invade the subretinal space, presumably to aid in the removal of debris of rod degeneration. In the neural retina, Müller cells also respond to the stress signals by beginning to become hypertrophic and increasing expression of glial fibrillary acidic protein (GFAP), which is typically maintained at very low to undetectable levels in Müller cells of the healthy retina. In addition to GFAP increase, Müller cells also show a variable increase in glutathione levels, which is thought to be an indicator of oxidative stress.[45] During the later period of rod degeneration, cones also begin to truncate their outer segments, even if the precipitating event was rod-specific. The mechanisms leading to the cone degeneration are currently unclear, though several models of bystander killing have been proposed.[28, 33, 37-38, 46]

1.3.3 Phase 2: Cone Degeneration

As phase 1 remodeling transitions into phase 2, rods are continually degenerating, leading to a collapse of the outer nuclear layer and concurrently cone stress and degeneration. The main feature distinguishing phase 2 remodeling is the widespread death of photoreceptors.[28] This process is likely the result of a number of factors, including microglial invasion of the subretinal space. RPE dysfunction caused by the rapid disassembly of rods, leading to debris accumulation in the subretinal space, is another theory for why cones die. The end result is the same; cones will degenerate and die, even in cases where the precipitating gene mutation is rod specific. This process may be fast or slow; there are forms of RP in which rod death causes cone outer segment loss, but the cone nuclei remain for extended periods of time, these are termed cone-sparing RP,[47] and delay most late-stage remodeling as long as cones are present. When cones deconstruct, BCs retract their dendrites.[43] HCs become hypertrophic and some extend multiple axon-like processes into the neural retina, in some cases, reaching the GCL.[48] Simultaneously, Müller cells elaborate a seal of their distal microvilli across the neural retina, gluing it together with intermediate junctions and fully separating the remnant cones from the RPE.[37-38] Though there is some cell death in the neural retina during this period, it is a small and not seen in regular histological analysis.

1.3.4 Early Phase 3: Neurite Remodeling

The primary feature signaling the initiation of phase 3 remodeling is the loss of all photoreceptors. The preservation of even a small portion of cone cell bodies in a region of retina is sufficient to prevent much of the gross remodeling in that local region.[38] As the

last of the cone cell bodies disappear, the glial seal separating the neural retina from the RPE completes, causing a total separation of the neural retina from the RPE and choroidal vasculature. In addition to the seal, Müller cells also hypertrophy along their trunks leading to the formation of large columns that fractionate the IPL,[49] though the impacts of these elaborated columns on IPL connectivity is unknown, they appear to be conduits for neuronal migration.[38] Cell death begins to become detectable within the neural retina by analysis of cell loss in phase 3, although the rate is so low that it cannot be tracked by techniques such as TUNEL labeling. At this point, anomalous neurites are produced by all classes of the remaining neurons.

1.3.5 Mid Phase 3: Global Remodeling

Following the extension of neurites by amacrine, bipolar, and ganglion cells into new neurite fascicles, many new neuron processes form *de* novo clusters of neurites that form new synapses between one another.[38] These collections of synapses between ectopic neurites are termed *microneuromas* and contain pre- and postsynaptic structures from all cell types, though whether they maintain the selectivity seen in healthy retina is unknown. Some neurons translocate their cell bodies to ectopic locations throughout the retina (e.g., ganglion cells migrate to the distal retina and bipolar and amacrine cells migrate into the ganglion cell layer), though most of these translocations occur along the elaborated Müller columns that appear earlier in remodeling.[38] Not all neurons survive this global remodeling, and there is a noticeable cell loss throughout the retina, with no apparent preference among any neural type. Throughout all of these changes, surviving neurons appear to maintain their core molecular signatures, regardless of positional location within the retina.[38]

1.3.6 Late Phase 3: Plateau Remodeling

As phase 3 continues, cell death leads to a depleted neural retina, with all layers being reduced in cell number. Microneuromas persist, though they may decrease in volume due to loss of neurons.[40] Müller cells break through the inner limiting membrane and form an epi-retinal membrane between the vitreous and the neural retina. The RPE begins to break apart and RPE cells can be found dispersed throughout the neural retina.[38]

In summary, regardless of the primary insult, the neural retina undergoes a series of increasingly deleterious changes in response to loss of photoreceptors. These processes will likely have an impact on any therapeutic scheme introduced to restore/preserve vision once remodeling is initiated. Further understanding of these components will be essential to recommending the best potential therapeutic for different stages of remodeling.[41]

1.4 Therapeutic Approaches to Vision Restoration

A primary interest for current vision research is the advancement of new therapies for the treatment of photoreceptor-associated vision loss. Therapies including small electrode array implants to stimulate remaining neurons,[2-4, 50] optogenetic approaches involving the transfection of specialized opsins into remnant neurons,[6-7] and a number of genetic and cellular based approaches are currently being investigated.[13, 51] Although these therapies may hold promise for future treatment of retinal degenerative diseases, it is difficult to fully assess their probability of success or improve upon the initial concept without better understanding the remodeling associated with retinal degenerative diseases.

1.4.1 Optogenetics

The fundamental concept behind optogenetics as a treatment for retinal degenerative disorders is that during and following the loss of outer segments of photoreceptors, if another cell type could be genetically encoded to detect light, vision could be rescued. Early studies demonstrated that when the algal channelrhodopsin-2 (ChR2) is inserted into the membrane of mammalian cells, a depolarization event can be initiated via light[52] and Archean halorhodopsin (NpHR) can induce hyperpolarization.[53-55] From this, the hypothesis was proposed that by genetically inserting these apoproteins into neurons, any neuron could be made light sensitive.[56] Ultimately, the idea that neurons of the retina could be given new light detecting capabilities following the loss of photoreceptors[57] was born. From here the discussion quickly turned to determining which cell type of the retina is optimal for targeting to induce, or restore, light-sensitivity. One early avenue was to restore light-sensitivity to cone somas, following the loss of outer segments with the goal of preserving native processing in the retina.[5, 7] Though this has the caveat that in many forms of retinal degeneration, cone cell death occurs relatively early in the progression of the disease in humans, this may yet be a potential treatment in cases of cone-sparing RP. Subsequently, the neurons of the inner retina were targeted to compensate for the loss of photoreceptors, either through a broadly delivered intravitreal injection approach, which predominantly targets ganglion cells[58-61] or through targeted delivery to specific cells of the inner retina.[8, 12] The discussion is still ongoing which cell is the best for inducing light sensitivity, in what combination, and which are the best promoters for cell-specific targeting. A major problem with all the algal and protozoan opsins is their very low photosensitivity, requiring extremely bright light displays to generate responses.[41]

Some groups have demonstrated that native opsins, such as rhodopsin, transduced into mouse bipolar cells offer improved performance.[62] Others have successfully transduced melanopsin into retinals, but the time course of melanopsin signaling is, so far, much too slow to provide functional vision.[63] And of course virtually all of these studies are performed in retinas of mice in the very early stages of retinal degeneration, usually mid-phase 2.

1.4.2 Chemical Photoswitches

A method for temporarily inducing photosensitivity in neurons involves the application of chemical photoswitches. These photosensitive small molecules regulate neuronal electrical activity by transiently blocking ion channels. An early study used the photochemical AAQ (acrylamide-azobenzene-quaternary ammonium), which in its *trans* form blocks K^+ channels, thereby increasing excitability, and in its *cis* form unblocks K^+ channels. AAQ photoisomerizes from its *trans* to *cis* conformation in the presence of short wavelength (~380nm) light, which unblocks K^+ channels and decreases excitability. Relaxation from *cis* to *trans* occurs slowly in darkness, or reisomerization can be rapidly induced using long wavelength (~540nm) light,[64] allowing bi-directional optical control. Polosukhina et al. unexpectedly found that 380nm light elicited action potentials, though K^+ channels become unblocked at that wavelength. This turned out to be the result of AAQ primarily effecting amacrine cells, causing ganglion cells to fire due to disinhibition. A distinct problem with AAQ is the necessity of high intensity UV light for isomerization. Another chemical photoswitch that has been investigated is DENAQ (diethylamino-azobenzene-quaternary ammonium).[65] DENAQ is also a K^+ channel photoswitch that

blocks K^+ channels in its *trans* confirmation and unblocks in *cis*. A main difference is that DENAQ is red-shifted and photoisomerizes *trans* to *cis* within the visible spectrum (450-550nm) then rapidly relaxes back to the *trans* conformation in the dark (within ~600msec). Also, DENAQ has been shown to be responsive to lower intensity light than either AAQ or many optogenetic strategies. Recently investigators have begun exploring new photoswitches capable of acting in AMPA receptors, via the photoswitchable excitatory amino acid (ATA).[66] ATA is active in the dark, and photoisomerizes from *trans* to *cis* in blue light (480nm). The distribution of AMPA receptors causes a group of RGCs to respond to blue light, while another group fires in response to darkness.[67] A combination of specific photoswitches may facilitate restoring ON-OFF responses, though remodeling leading to altered glutamate receptor expression levels will likely be of concern.[68] Photoswitches also demonstrate a shorter lifespan than optogenetics, which may make them a potential diagnostic tool.[41]

1.4.3 Cellular Replacement Strategies

In the majority of the central nervous system of mammals, once a neuron dies it is not replaced, which is the case in the mammalian retina. The advent of stem cell techniques brought with it the capabilities of differentiating new cells *in vitro*, with the hope of replacement of cells or entire organs grown specifically for an individual. Since the death of photoreceptors is the precipitating feature of all retinal degenerative diseases, photoreceptor replacement strategies are being investigated as a potential treatment. Photoreceptor transplants have had early success with surviving, for at least a few weeks, and have been found to generate synapses in the neural retina.[69-70] It has been shown that

following introduction of embryonic stem cell derived photoreceptors, pupillary responses are increased in visually deficient mice,[71] though it is unclear whether that is a response of photoreceptors or a change in the response of intrinsically-photosensitive retinal ganglion cells (ipRGCs). Further research is still ongoing to determine the long-term viability of transplanted cells and their functionality in the context of the total retina. In addition, our group has found that following the transplantation of fetal retina there is subsequent remodeling that occurs as fast as, or potentially faster than, that seen in degenerate retina without intervention.[72]

1.4.4 Bionic Implants

Beyond the biologic interventions currently being proposed, another methodology aims to intervene using principles similar to the widely successful cochlear implant; in this case, the retinal implant. Certain retinal implants, such as the Argus II epiretinal implant that is placed next to the ganglion cell layer in the vitreous, stimulate nearby neurons to fire action potentials in a pattern controlled by a video camera headset. This approach has the potential to provide for coarse vision, allowing increased independence and mobility among individuals affected by retinal degenerations.[50, 73-74] There are two types of retinal implants: subretinal and epiretinal.[3] A subretinal implant is surgically implanted under the retina between the photoreceptor layer (or former photoreceptor layer in the case of retinal degenerations) and the RPE, and uses thousands of microdiodes to generate light responses to be processed through the neural retina. An epiretinal implant is surgically placed along the ganglion cell layer of the retina, which does not require detachment of the retina from the RPE and generates action potentials in the associated ganglion cells based on images

from an external camera, bypassing neural retina processing. Both of these techniques have certain advantages. The subretinal implant has the capacity to utilize any circuitry remaining in the neural retina; however, as discussed in the remodeling section, it is likely that the circuitry of late retinal degenerations is corrupted. The epiretinal implant is currently in clinical trials (Argus II), which are showing distinct promise,[73-75] although it is unable to mimic the wide variation in signals normally encoded by ganglions cells[41] (direction selectivity, ON versus OFF versus ON-OFF signals, and only minimal center-surround responses).

1.4.5 Genetic Approaches

Among the therapeutic interventions for vision loss, genetic approaches are especially favored in cases where a specific gene defect is known to be the direct cause of vision loss. One such disorder is Leber's Congenital Amaurosis (LCA), in which one form is specifically caused by a loss of function mutation in the RPE specific gene *RPE-65*. LCA is an early onset retinal degeneration, where affected individuals typically experience severe vision loss in the first few years of life. Gene-replacement therapy delivered via adeno-associated viruses (AAVs) has been used to introduce functional *RPE-65*, and has shown promise in restoring proper RPE function in animal models, especially the Briard dog[76], and patients.[77-81] Other gene therapies for replacing defective genes have been tested with x-linked mutations leading to RP with successful prevention of much of the early photoreceptor loss.[82] A primary difficulty for the exclusive use of gene therapy to prevent or slow vision loss is the wide array of genetic defects that can lead to inherited retinal degenerations and the multiple environmental factors that contribute to the generation of

AMD.[32] More importantly, intercession in most cases of recessive disease must occur perinatally, posing severe challenges for the medical ethics of early genetic manipulation. Also, many diseases are autosomal dominant in which a single defective gene can override the function of a normal gene and lead to photoreceptor death. Approaches to these disorders require suppression of the defective gene with methods such as shRNA targeting or new CRISPR/Cas9 gene editing methods. Even with these tools, there is currently no therapeutic path for human autosomal disease. While autosomal diseases tend to progress more slowly, extending into adulthood (via unknown mechanisms), it is not clear that the critical defect leading to widespread degeneration is operation of the defective gene per se or accumulation of toxic protein, in which case late intervention will be of little use. It is also important to note that despite the success of *RPE65* gene therapy, the treated individuals still experience progressive cell death and slow rod kinetics[83] which will require further research before the gene therapy can be deemed a full rescue.

1.4.6 Requirements for Therapeutic Interventions to Be Effective

The generation of therapeutic interventions and treatment for photoreceptor-initiated vision loss is a lofty goal with a number of avenues of exploration. All therapeutic interventions require a functional neural retina.

Therapies that hope to utilize the neural processing afforded by the inner retina have a number of difficult problems to overcome. Cell-replacement therapies are unlikely to result in long-term vision restoration or preservation unless the initial insult leading to photoreceptor degeneration is also directly treated. It also has not been shown that the synapses made by newly introduced photoreceptors produce the same visual acuity as

native photoreceptors (not even within an order of magnitude), nor have they been shown to persist. For most therapeutics targeted at stimulation of bipolar cells to be effective, regardless of whether via optogenetics, photoswitches, or subretinal implant, the primary circuitry of the retina must remain intact in addition to the metabolic support of surrounding glia. The basic idea that an epiretinal implant only stimulates ganglion cells, or that ganglion cells transduced by optogenetics or photoswitches could function independently is complicated by extensive coupling between ganglion cells and amacrine cells, as well as penetration of currents deep into retinal tissue. Previous data indicate that alterations in circuitry are present early in remodeling and it is unclear to what extent this affects the signals that are communicated to ganglion cells. We certainly know that retinal ganglion cells begin to display massive uncorrelated spiking in late phase 2.[84-87] In addition, the early subtle variation of Müller cell metabolic phenotypes leads to questions regarding how widely Müller cells will vary with respect to one another, and how it will affect the metabolic support provided by Müller cells, particularly in the case of glutamate because excitotoxicity has been proposed as a potential contributing factor to retinal degeneration.[25, 88-89] Clarifying these mechanisms is a goal of this dissertation.

Retinal degenerative diseases have predominately been evaluated in rodent models, which have short life-spans, or shortly after the total loss of photo-receptors in large-eye model organisms. In contrast, humans live for decades with these disorders and are often functionally blind for years to decades of life. Many proposed interventions must target late-stage patients that are unable to perceive light, and some target ganglion cells with the assumption they will be the last remaining targets of intervention. We do not know the complete order or extent to which the neural retina deteriorates years after most

photoreceptors have died. Again, this dissertation will clarify much of that uncertainty.

In summary, this dissertation aims to characterize the structural, biochemical, and metabolic changes in late-stage retinal remodeling years after all photoreceptors have degenerated, and evaluate their implications for therapeutic interventions.

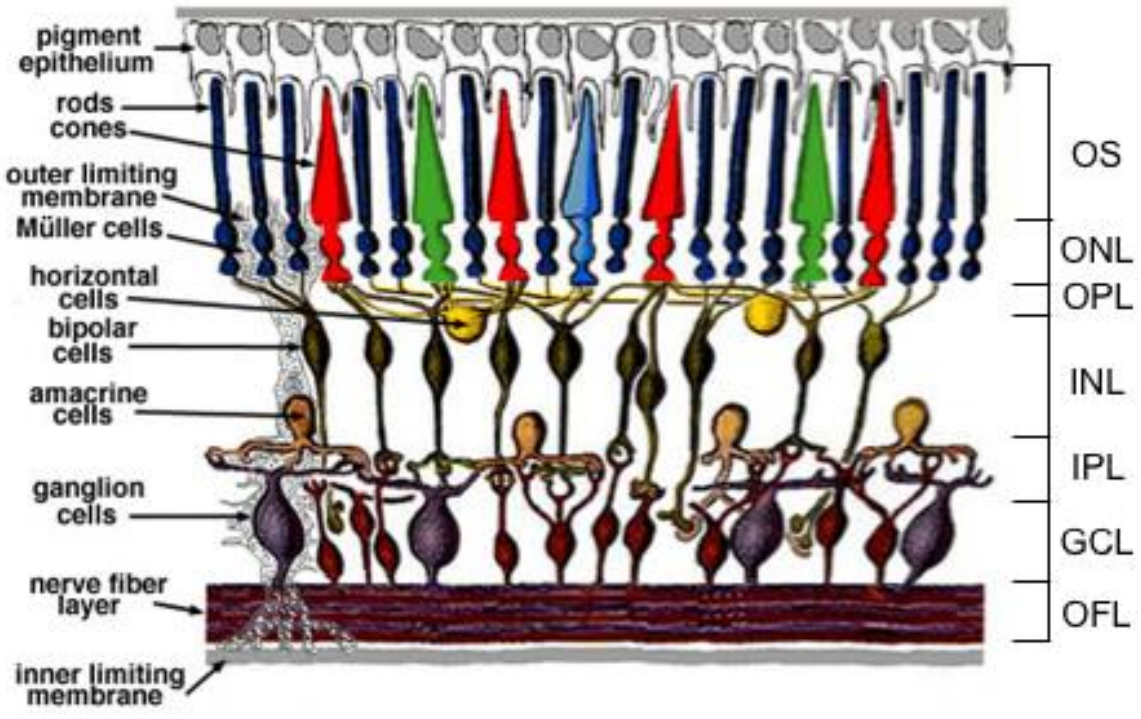

Figure 1.1 Schematic of the major histological and cellular classifications of the retina. Adapted from (http://webvision.med.utah.edu/book/part-i-foundations/simple-anatomy-of-the-retina/)

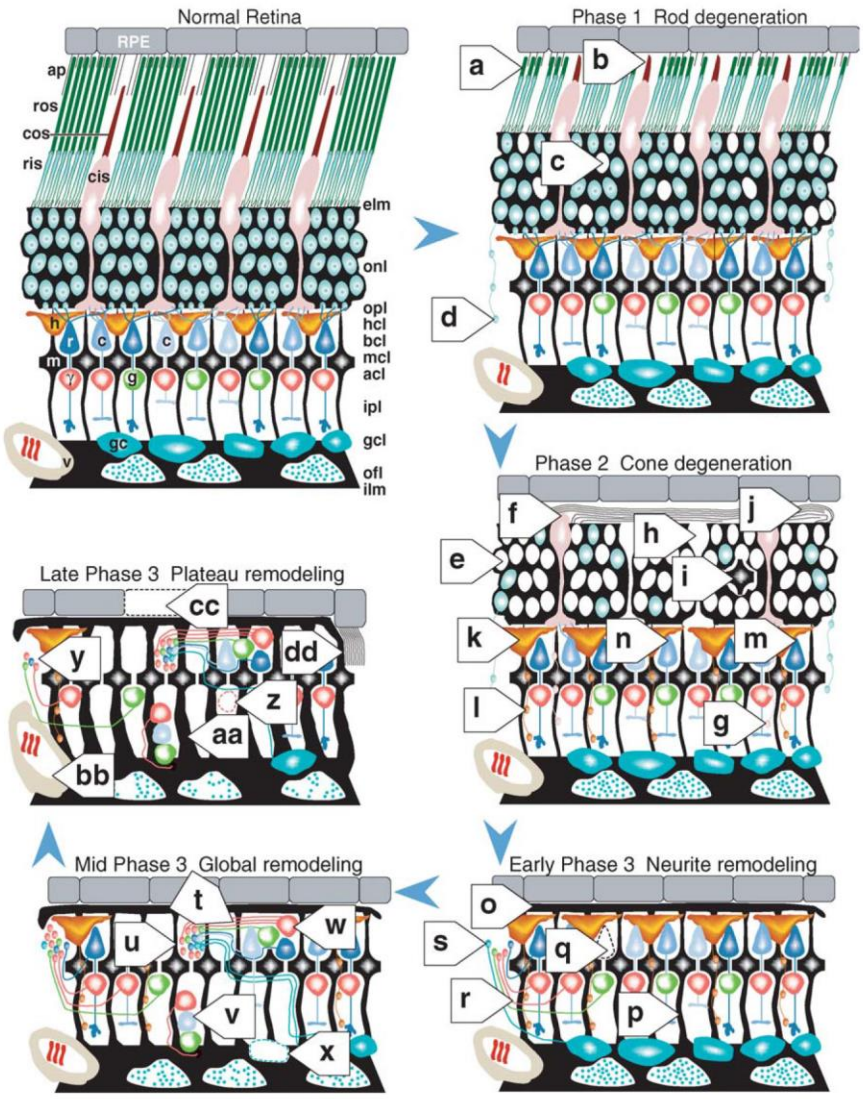

Figure 1.2 Remodeling of the mammalian retina in retinal degenerations. (From Marc et al. 2003[37]) *Normal retina* demonstrating proper lamination and organization of the mammalian retina. Some slight variations, such as vasculature, may vary with species. *Phase 1* (a) shortening of rod outer segments. (b) Shortening of cone outer segments. (c) Initial death of rod soma. (d) Ectopic rod axons descending beyond opl. *Phase 2* (e) Widespread rod death. (f) Loss of cone outer segments. (g) Ectopic neurite sprouting by amacrine cells. (h) Cone cell death. (i)Müller cell soma translocation. (j)Early stage of the glial seal. (k) Horizontal cell hypertrophy. (l) Horizontal cell neurite sprouting. (m+n) Bipolar cell dendritic retraction. *Early Phase 3* (o) Fully formed glial seal. (p) Increased Müller cell hypertrophy. (q) Initial neural retina neuronal loss. (r) Neurite fascicle formation. (s) Early microneuroma formation. *Mid Phase 3* (t) Increased multicellular fascicle formation. (u) Microneuroma growth. (v+w) Neuronal translocation. (x) Progressive cell death. *Late Phase 3* (y) Regression of microneuromas due to cell death. (z) Progressive cell death. (aa) Continued Müller cell hypertrophy. (bb) Hypertrophy and vessel invasion. (cc) RPE cell death. (dd) Invasion of the RPE into the neural retina.

1.5 References

1. Foster, A.; Resnikoff, S., The Impact of Vision 2020 on Global Blindness. *Eye (Lond)* **2005,** *19* (10), 1133-1135.

2. Stingl, K.; Bartz-Schmidt, K. U.; Besch, D.; Braun, A.; Bruckmann, A.; Gekeler, F.; Greppmaier, U.; Hipp, S.; Hortdorfer, G.; Kernstock, C.; Koitschev, A.; Kusnyerik, A.; Sachs, H.; Schatz, A.; Stingl, K. T.; Peters, T.; Wilhelm, B.; Zrenner, E., Artificial Vision with Wirelessly Powered Subretinal Electronic Implant Alpha-IMS. *Proc Biol Sci* **2013,** *280* (1757), 20130077.

3. Zrenner, E., The Subretinal Implant: Can Microphotodiode Arrays Replace Degenerated Retinal Photoreceptors to Restore Vision? *Ophthalmologica* **2002,** *216* 8-20; discussion 52-23.

4. Zrenner, E., Fighting Blindness with Microelectronics. *Sci Transl Med* **2013,** *5* (210), 210.

5. Busskamp, V.; Duebel, J.; Balya, D.; Fradot, M.; Viney, T. J.; Siegert, S.; Groner, A. C.; Cabuy, E.; Forster, V.; Seeliger, M.; Biel, M.; Humphries, P.; Paques, M.; Mohand-Said, S.; Trono, D.; Deisseroth, K.; Sahel, J. A.; Picaud, S.; Roska, B., Genetic Reactivation of Cone Photoreceptors Restores Visual Responses in Retinitis Pigmentosa. *Science* **2010,** *329* (5990), 413-417.

6. Busskamp, V.; Picaud, S.; Sahel, J. A.; Roska, B., Optogenetic Therapy for Retinitis Pigmentosa. *Gene Ther* **2012,** *19* (2), 169-175.

7. Busskamp, V.; Roska, B., Optogenetic Approaches to Restoring Visual Function in Retinitis Pigmentosa. *Curr Opin Neurobiol* **2011,** *21* (6), 942-946.

8. Lagali, P. S.; Balya, D.; Awatramani, G. B.; Munch, T. A.; Kim, D. S.; Busskamp, V.; Cepko, C. L.; Roska, B., Light-Activated Channels Targeted to ON Bipolar Cells Restore Visual Function in Retinal Degeneration. *Nat Neurosci* **2008,** *11* (6), 667-675.

9. Nirenberg, S.; Pandarinath, C., Retinal Prosthetic Strategy with the Capacity to Restore Normal Vision. *Proc Natl Acad Sci U S A* **2012,** *109* (37), 15012-15017.

10. Margalit, E.; Maia, M.; Weiland, J. D.; Greenberg, R. J.; Fujii, G. Y.; Torres, G.; Piyathaisere, D. V.; O'Hearn, T. M.; Liu, W.; Lazzi, G.; Dagnelie, G.; Scribner, D. A.; de Juan, E., Jr.; Humayun, M. S., Retinal Prosthesis for the Blind. *Surv Ophthalmol* **2002,** *47* (4), 335-356.

11. Jiang, L.; Zhang, H.; Dizhoor, A. M.; Boye, S. E.; Hauswirth, W. W.; Frederick, J. M.; Baehr, W., Long-Term RNA Interference Gene Therapy in a Dominant Retinitis Pigmentosa Mouse Model. *Proc Natl Acad Sci U S A* **2011,** *108* (45), 18476-18481.

12. Doroudchi, M. M.; Greenberg, K. P.; Liu, J.; Silka, K. A.; Boyden, E. S.; Lockridge, J. A.; Arman, A. C.; Janani, R.; Boye, S. E.; Boye, S. L.; Gordon, G. M.; Matteo, B. C.; Sampath, A. P.; Hauswirth, W. W.; Horsager, A., Virally Delivered Channelrhodopsin-2 Safely and Effectively Restores Visual Function in Multiple Mouse Models of Blindness. *Mol Ther* **2011,** *19* (7), 1220-1229.

13. Petrs-Silva, H.; Linden, R., Advances in Gene Therapy Technologies to Treat Retinitis Pigmentosa. *Clin Ophthalmol* **2014,** *8*, 127-136.

14. Marc, R. E., The Structure of Vertebrate Retinas. In *The Retinal Basis of Vision*, Toyoda, J.-I.; Murakami, M.; Kaneko, A.; Saito, T., Eds. Elsevier: Amsterdam, 1999; pp 3-19.

15. Masland, R. H., The Neuronal Organization of the Retina. *Neuron* **2012,** *76* (2), 266-280.

16. Kolb, H.; Gouras, P., Electron Microscopic Observations of Human Retinitis Pigmentosa, Dominantly Inherited. *Invest Ophthalmol* **1974,** *13* (7), 487-498.

17. Famiglietti, E. V., Jr.; Kaneko, A.; Tachibana, M., Neuronal Architecture of On and Off Pathways to Ganglion Cells in Carp Retina. *Science* **1977,** *198* (4323), 1267-1269.

18. Lauritzen, J. S.; Anderson, J. R.; Jones, B. W.; Watt, C. B.; Mohammed, S.; Hoang, J. V.; Marc, R. E., ON Cone Bipolar Cell Axonal Synapses in the OFF Inner Plexiform Layer of the Rabbit Retina. *J Comp Neurol* **2013,** *521* (5), 977-1000.

19. Marc, R. E., Retinal Neurotransmitters. In *The Visual Neurosciences*, Chalupa, L. M.; Werner, J., Eds. MIT Press: Cambridge MA, 2004; pp 315-330.

20. Marc, R. E., Information Processing: Amacrine Cells. In *Encyclopedia of the Eye*, Dartt, D., Ed. Elsevier: 2010; Vol. 2, pp 330-337.

21. Marc, R. E., Functional Neuroanatomy of the Retina. In *Duane's Ophthalmology*, Tasman, W.; Jaeger, E. A., Eds. Lippincott Williams & Wilkins: Philadelphia, 2009.

22. Dowling, J. E.; Werblin, F. S., Organization of Retina of the Mudpuppy, Necturus Maculosus. I. Synaptic Structure. *J Neurophysiol* **1969,** *32* (3), 315-338.

23. Rodieck, R. W., Visual Pathways. *Annu Rev Neurosci* **1979,** *2*, 193-225.

24. Byrne, L. C.; Khalid, F.; Lee, T.; Zin, E. A.; Greenberg, K. P.; Visel, M.; Schaffer, D. V.; Flannery, J. G., AAV-Mediated, Optogenetic Ablation of Muller Glia Leads to Structural and Functional Changes in the Mouse Retina. *PLoS One* **2013,** *8* (9), e76075.

25. Reichenbach, A.; Bringmann, A., New Functions of Muller Cells. *Glia* **2013,** *61* (5), 651-678.

26. Riepe, R. E.; Norenburg, M. D., Muller Cell Localisation of Glutamine Synthetase in Rat Retina. *Nature* **1977,** *268* (5621), 654-655.

27. Pow, D. V.; Robinson, S. R., Glutamate in Some Retinal Neurons is Derived Solely from Glia. *Neuroscience* **1994,** *60* (2), 355-366.

28. Jones, B. W.; Marc, R. E., Retinal Remodeling During Retinal Degeneration. *Exp Eye Res* **2005,** *81* (2), 123-137.

29. Medicine, U. S. N. L. o. Bardet-Biedl Syndrome. https://ghr.nlm.nih.gov/condition/bardet-biedl-syndrome (accessed March, 22).

30. Koenig, R., Bardet-Biedl Syndrome and Usher Syndrome. *Dev Ophthalmol* **2003,** *37*, 126-140.

31. Hartong, D. T.; Berson, E. L.; Dryja, T. P., Retinitis Pigmentosa. *Lancet* **2006,** *368* (9549), 1795-1809.

32. Armstrong, R. A.; Mousavi, M., Overview of Risk Factors for Age-Related Macular Degeneration (AMD). *J Stem Cells* **2015,** *10* (3), 171-191.

33. Jones, B. W.; Marc, R. E.; Pfeiffer, R. L. Retinal Remodeling and Plasticity. http://webvision.med.utah.edu/.

34. Jones, B. W.; Pfeiffer, R. L.; Ferrell, W. D.; Watt, C. B.; Tucker, J. F.; Marc, R. E., Retinal Remodeling And Metabolic Alterations in Human AMD. *Front Cell Neurosci* **2016,** *10*, 103.

35. Wolff, E., *A Pathology of the Eye*. 1st edition ed.; Blakiston: Philadelphia, 1935.

36. Humayun, M. S.; Prince, M.; de Juan, E., Jr.; Barron, Y.; Moskowitz, M.; Klock, I. B.; Milam, A. H., Morphometric Analysis of the Extramacular Retina from Postmortem Eyes with Retinitis Pigmentosa. *Invest Ophthalmol Vis Sci* **1999,** *40* (1), 143-148.

37. Marc, R. E.; Jones, B. W.; Watt, C. B.; Strettoi, E., Neural Remodeling in Retinal Degeneration. *Prog Retin Eye Res* **2003,** *22* (5), 607-655.

38. Marc, R. E.; Jones, B. W.; Watt, C. B.; Strettoi, E., Neural remodeling in retinal degeneration. *Prog Retin Eye Res* **2003,** *22* (5), 607-655.

39. Jones, B. W.; Pfeiffer, R. L.; Ferrell, W. D.; Watt, C. B.; Marmor, M.; Marc, R. E., Retinal Remodeling in Human Retinitis Pigmentosa. *Exp Eye Res* **2016,** *150*, 149-165.

40. Marc, R. E., Injury and Repair: Retinal Remodeling. In *Encyclopedia of the Eye*, Dartt, D., Ed. Elsevier: 2010; Vol. 2, pp 414-420.

41. Marc, R.; Pfeiffer, R.; Jones, B., Retinal Prosthetics, Optogenetics, and Chemical Photoswitches. *ACS Chem Neurosci* **2014,** *5* (10), 895-901.

42. Strettoi, E.; Porciatti, V.; Falsini, B.; Pignatelli, V.; Rossi, C., Morphological and Functional Abnormalities in the Inner Retina of the rd/rd Mouse. *J Neurosci* **2002,** *22* (13), 5492-5504.

43. Strettoi, E.; Pignatelli, V.; Rossi, C.; Porciatti, V.; Falsini, B., Remodeling of Second-Order Neurons in the Retina of rd/rd Mutant Mice. *Vision Res* **2003,** *43* (8), 867-877.

44. Lewis, G. P.; Linberg, K. A.; Fisher, S. K., Neurite Outgrowth from Bipolar and Horizontal Cells After Experimental Retinal Detachment. *Invest Ophthalmol Vis Sci* **1998,** *39* (2), 424-434.

45. Jones, B. W.; Kondo, M.; Terasaki, H.; Watt, C. B.; Rapp, K.; Anderson, J.; Lin, Y.; Shaw, M. V.; Yang, J. H.; Marc, R. E., Retinal Remodeling in the Tg P347L Rabbit, a Large-Eye Model of Retinal Degeneration. *J Comp Neurol* **2011,** *519* (14), 2713-27133.

46. Jones, B. W.; Kondo, M.; Terasaki, H.; Lin, Y.; McCall, M.; Marc, R. E., Retinal remodeling. *Jpn J Ophthalmol* **2012,** *56* (4), 289-306.

47. Marc, R. E.; Jones, B. W.; Anderson, J. R.; Kinard, K.; Marshak, D. W.; Wilson, J. H.; Wensel, T.; Lucas, R. J., Neural Reprogramming in Retinal Degeneration. *Invest Ophthalmol Vis Sci* **2007,** *48* (7), 3364-3371.

48. Fariss, R. N.; Li, Z. Y.; Milam, A. H., Abnormalities in Rod Photoreceptors, Amacrine Cells, and Horizontal Cells in Human Retinas with Retinitis Pigmentosa. *Am J Ophthalmol* **2000,** *129* (2), 215-223.

49. Marc, R. E.; Jones, B. W., Retinal Remodeling in Inherited Photoreceptor Degenerations. *Mol Neurobiol* **2003,** *28* (2), 139-147.

50. Ahuja, A. K.; Dorn, J. D.; Caspi, A.; McMahon, M. J.; Dagnelie, G.; Dacruz, L.; Stanga, P.; Humayun, M. S.; Greenberg, R. J.; Argus, I. I. S. G., Blind Subjects Implanted with the Argus II Retinal Prosthesis are able to Improve Performance in a Spatial-Motor Task. *Br J Ophthalmol* **2011,** *95* (4), 539-543.

51. Lamba, D. A.; Karl, M. O.; Reh, T. A., Strategies for Retinal Repair: Cell Replacement and Regeneration. *Prog Brain Res* **2009,** *175*, 23-31.

52. Nagel, G.; Szellas, T.; Huhn, W.; Kateriya, S.; Adeishvili, N.; Berthold, P.; Ollig, D.; Hegemann, P.; Bamberg, E., Channelrhodopsin-2, a Directly Light-Gated Cation-Selective Membrane Channel. *Proc Natl Acad Sci U S A* **2003,** *100* (24), 13940-13945.

53. Schobert, B.; Lanyi, J. K., Halorhodopsin is a Light-Driven Chloride Pump. *J Biol Chem* **1982,** *257* (17), 10306-10313.

54. Han, X.; Boyden, E. S., Multiple-Color Optical Activation, Silencing, and Desynchronization of Neural Activity, with Single-Spike Temporal Resolution. *PLoS One* **2007,** *2* (3), e299.

55. Zhang, F.; Wang, L. P.; Brauner, M.; Liewald, J. F.; Kay, K.; Watzke, N.; Wood, P. G.; Bamberg, E.; Nagel, G.; Gottschalk, A.; Deisseroth, K., Multimodal Fast Optical Interrogation of Neural Circuitry. *Nature* **2007,** *446* (7136), 633-639.

56. Boyden, E. S.; Zhang, F.; Bamberg, E.; Nagel, G.; Deisseroth, K., Millisecond-Timescale, Genetically Targeted Optical Control of Neural Activity. *Nat Neurosci* **2005,** *8* (9), 1263-1268.

57. Bi, A.; Cui, J.; Ma, Y. P.; Olshevskaya, E.; Pu, M.; Dizhoor, A. M.; Pan, Z. H., Ectopic Expression of a Microbial-Type Rhodopsin Restores Visual Responses in Mice with Photoreceptor Degeneration. *Neuron* **2006,** *50* (1), 23-33.

58. Tomita, H.; Sugano, E.; Fukazawa, Y.; Isago, H.; Sugiyama, Y.; Hiroi, T.; Ishizuka, T.; Mushiake, H.; Kato, M.; Hirabayashi, M.; Shigemoto, R.; Yawo, H.; Tamai, M., Visual Properties of Transgenic Rats Harboring the Channelrhodopsin-2 Gene Regulated by the thy-1.2 Promoter. *PLoS One* **2009,** *4* (11), e7679.

59. Tomita, H.; Sugano, E.; Isago, H.; Hiroi, T.; Wang, Z.; Ohta, E.; Tamai, M., Channelrhodopsin-2 Gene Transduced into Retinal Ganglion Cells Restores Functional Vision in Genetically Blind Rats. *Exp Eye Res* **2010,** *90* (3), 429-436.

60. Zhang, Y.; Ivanova, E.; Bi, A.; Pan, Z. H., Ectopic Expression of Multiple Microbial Rhodopsins Restores ON and OFF Light Responses in Retinas with Photoreceptor Degeneration. *J Neurosci* **2009,** *29* (29), 9186-9196.

61. Greenberg, K. P.; Pham, A.; Werblin, F. S., Differential targeting of optical neuromodulators to ganglion cell soma and dendrites allows dynamic control of center-surround antagonism. *Neuron* **2011,** *69* (4), 713-720.

62. Gaub, B. M.; Berry, M. H.; Holt, A. E.; Isacoff, E. Y.; Flannery, J. G., Optogenetic Vision Restoration Using Rhodopsin for Enhanced Sensitivity. *Mol Ther* **2015,** *23* (10), 1562-1571.

63. Lin, B.; Koizumi, A.; Tanaka, N.; Panda, S.; Masland, R. H., Restoration of Visual Function in Retinal Degeneration Mice by Ectopic Expression of Melanopsin. *Proc Natl Acad Sci U S A* **2008,** *105* (41), 16009-16014.

64. Polosukhina, A.; Litt, J.; Tochitsky, I.; Nemargut, J.; Sychev, Y.; De Kouchkovsky, I.; Huang, T.; Borges, K.; Trauner, D.; Van Gelder, R. N.; Kramer, R. H., Photochemical Restoration of Visual Responses in Blind Mice. *Neuron* **2012,** *75* (2), 271-282.

65. Tochitsky, I.; Polosukhina, A.; Degtyar, V. E.; Gallerani, N.; Smith, C. M.; Friedman, A.; Van Gelder, R. N.; Trauner, D.; Kaufer, D.; Kramer, R. H., Restoring Visual Function to Blind Mice with a Photoswitch that Exploits Electrophysiological Remodeling of Retinal Ganglion Cells. *Neuron* **2014,** *81* (4), 800-813.

66. Stawski, P.; Sumser, M.; Trauner, D., A Photochromic Agonist of AMPA Receptors. *Angew Chem Int Ed Engl* **2012,** *51* (23), 5748-5751.

67. Laprell, L.; Hull, K.; Stawski, P.; Schon, C.; Michalakis, S.; Biel, M.; Sumser, M. P.; Trauner, D., Restoring Light Sensitivity in Blind Retinae Using a Photochromic AMPA Receptor Agonist. *ACS Chem Neurosci* **2016,** *7* (1), 15-20.

68. Lin, Y.; Jones, B. W.; Liu, A.; Vazquez-Chona, F. R.; Lauritzen, J. S.; Ferrell, W. D.; Marc, R. E., Rapid Glutamate Receptor 2 Trafficking During Retinal Degeneration. *Mol Neurodegener* **2012,** *7*, 7.

69. Santos-Ferreira, T.; Volkner, M.; Borsch, O.; Haas, J.; Cimalla, P.; Vasudevan, P.; Carmeliet, P.; Corbeil, D.; Michalakis, S.; Koch, E.; Karl, M. O.; Ader, M., Stem Cell-Derived Photoreceptor Transplants Differentially Integrate Into Mouse Models of Cone-Rod Dystrophy. *Invest Ophthalmol Vis Sci* **2016,** *57* (7), 3509-3520.

70. MacLaren, R. E.; Pearson, R. A.; MacNeil, A.; Douglas, R. H.; Salt, T. E.; Akimoto, M.; Swaroop, A.; Sowden, J. C.; Ali, R. R., Retinal Repair by Transplantation of Photoreceptor Precursors. *Nature* **2006,** *444* (7116), 203-207.

71. Singh, M. S.; Charbel Issa, P.; Butler, R.; Martin, C.; Lipinski, D. M.; Sekaran, S.; Barnard, A. R.; MacLaren, R. E., Reversal of End-Stage Retinal Degeneration and Restoration of Visual Function by Photoreceptor Transplantation. *Proc Natl Acad Sci U S A* **2013,** *110* (3), 1101-1106.

72. Seiler, M. J.; Jones, B. W.; Aramant, R. B.; Yang, P. B.; Keirstead, H. S.; Marc, R. E., Computational Molecular Phenotyping of Retinal Sheet Transplants to Rats with Retinal Degeneration. *Eur J Neurosci* **2012,** *35* (11), 1692-1704.

73. Dorn, J. D.; Ahuja, A. K.; Caspi, A.; da Cruz, L.; Dagnelie, G.; Sahel, J. A.; Greenberg, R. J.; McMahon, M. J.; gus, I. I. S. G., The Detection of Motion by Blind Subjects With the Epiretinal 60-Electrode (Argus II) Retinal Prosthesis. *JAMA Ophthalmol* **2013,** *131* (2), 183-189.

74. da Cruz, L.; Coley, B. F.; Dorn, J.; Merlini, F.; Filley, E.; Christopher, P.; Chen, F. K.; Wuyyuru, V.; Sahel, J.; Stanga, P.; Humayun, M.; Greenberg, R. J.; Dagnelie, G.; Argus, I. I. S. G., The Argus II Epiretinal Prosthesis System Allows Letter and Word Reading and Long-Term Function in Patients with Profound Vision Loss. *Br J Ophthalmol* **2013,** *97* (5), 632-636.

75. Ho, A. C.; Humayun, M. S.; Dorn, J. D.; da Cruz, L.; Dagnelie, G.; Handa, J.; Barale, P. O.; Sahel, J. A.; Stanga, P. E.; Hafezi, F.; Safran, A. B.; Salzmann, J.; Santos, A.; Birch, D.; Spencer, R.; Cideciyan, A. V.; de Juan, E.; Duncan, J. L.; Eliott, D.; Fawzi, A.; Olmos de Koo, L. C.; Brown, G. C.; Haller, J. A.; Regillo, C. D.; Del Priore, L. V.; Arditi, A.; Geruschat, D. R.; Greenberg, R. J.; Argus, I. I. S. G., Long-Term Results from an Epiretinal Prosthesis to Restore Sight to the Blind. *Ophthalmology* **2015,** *122* (8), 1547-1554.

76. Le Meur, G.; Stieger, K.; Smith, A. J.; Weber, M.; Deschamps, J. Y.; Nivard, D.; Mendes-Madeira, A.; Provost, N.; Pereon, Y.; Cherel, Y.; Ali, R. R.; Hamel, C.; Moullier, P.; Rolling, F., Restoration of Vision in RPE65-Deficient Briard Dogs using an AAV Serotype 4 Vector That Specifically Targets the Retinal Pigmented Epithelium. *Gene Ther* **2007,** *14* (4), 292-303.

77. Sahel, J. A.; Roska, B., Gene Therapy for Blindness. *Annu Rev Neurosci* **2013,** *36*, 467-488.

78. Jacobson, S. G.; Cideciyan, A. V.; Roman, A. J.; Sumaroka, A.; Schwartz, S. B.; Heon, E.; Hauswirth, W. W., Improvement and Decline in Vision with Gene Therapy in Childhood Blindness. *N Engl J Med* **2015,** *372* (20), 1920-1926.

79. Acland, G. M.; Aguirre, G. D.; Ray, J.; Zhang, Q.; Aleman, T. S.; Cideciyan, A. V.; Pearce-Kelling, S. E.; Anand, V.; Zeng, Y.; Maguire, A. M.; Jacobson, S. G.; Hauswirth, W. W.; Bennett, J., Gene Therapy Restores Vision in a Canine Model of Childhood Blindness. *Nat Genet* **2001,** *28* (1), 92-95.

80. Cideciyan, A. V.; Hauswirth, W. W.; Aleman, T. S.; Kaushal, S.; Schwartz, S. B.; Boye, S. L.; Windsor, E. A.; Conlon, T. J.; Sumaroka, A.; Pang, J. J.; Roman, A. J.; Byrne, B. J.; Jacobson, S. G., Human RPE65 Gene Therapy for Leber Congenital Amaurosis: Persistence of Early Visual Improvements and Safety at 1 Year. *Hum Gene Ther* **2009,** *20* (9), 999-1004.

81. Cideciyan, A. V.; Hauswirth, W. W.; Aleman, T. S.; Kaushal, S.; Schwartz, S. B.; Boye, S. L.; Windsor, E. A.; Conlon, T. J.; Sumaroka, A.; Roman, A. J.; Byrne, B. J.; Jacobson, S. G., Vision 1 Year After Gene Therapy for Leber's Congenital Amaurosis. *N Engl J Med* **2009,** *361* (7), 725-727.

82. Beltran, W. A.; Cideciyan, A. V.; Iwabe, S.; Swider, M.; Kosyk, M. S.; McDaid, K.; Martynyuk, I.; Ying, G. S.; Shaffer, J.; Deng, W. T.; Boye, S. L.; Lewin, A. S.; Hauswirth, W. W.; Jacobson, S. G.; Aguirre, G. D., Successful Arrest of Photoreceptor and Vision Loss Expands the Therapeutic Window of Retinal Gene Therapy to Later Stages of Disease. *Proc Natl Acad Sci U S A* **2015,** *112* (43), 5844-5853.

83. Jacobson, S. G.; Cideciyan, A. V.; Aguirre, G. D.; Roman, A. J.; Sumaroka, A.; Hauswirth, W. W.; Palczewski, K., Improvement in Vision: a New Goal for Treatment of Hereditary Retinal Degenerations. *Expert Opin Orphan Drugs* **2015,** *3* (5), 563-575.

84. Euler, T.; Schubert, T., Multiple Independent Oscillatory Networks in the Degenerating Retina. *Front Cell Neurosci* **2015,** *9*, 444.

85. Margolis, D. J.; Newkirk, G.; Euler, T.; Detwiler, P. B., Functional Stability of Retinal Ganglion Cells After Degeneration-Induced Changes in Synaptic Input. *J Neurosci* **2008,** *28* (25), 6526-6536.

86. Stasheff, S. F., Emergence of Sustained Spontaneous Hyperactivity and Temporary Preservation of OFF Responses in Ganglion Cells of the Retinal Degeneration (rd1) Mouse. *J Neurophysiol* **2008,** *99* (3), 1408-1421.

87. Menzler, J.; Zeck, G., Network Oscillations in Rod-Degenerated Mouse Retinas. *J Neurosci* **2011,** *31* (6), 2280-2291.

88. Reichenbach, A.; Bringmann, A., Muller Cells in the Healthy Retina. In *Muller Cells in the Healthy and Diseased Retina*, Springer Science+Business Meddia, LLC: New York, 2010; pp 35-299.

89. Bringmann, A.; Grosche, A.; Pannicke, T.; Reichenbach, A., GABA and Glutamate Uptake and Metabolism in Retinal Glial (Muller) Cells. *Front Endocrinol* **2013,** *4*, 1-14.

CHAPTER 2

MATERIALS AND METHODS

The main body of the work presented in this dissertation relies on computational molecular phenotyping (CMP). CMP is a robust method for quantitative small molecule immunohistochemistry combined with cluster analysis to identify cell classes found in normal tissue, and identify metabolic variation in degenerative tissue. This chapter will introduce the animal model predominately used throughout this study. The background associated with the methods and model organism is extensive and presented in greater detail here to aid the reader in understanding the recurrent concepts underlying the body of work in the following chapters.

2.1 Computational Molecular Phenotyping (CMP)

Accurate classification of cells within biological systems is an important basic component of understanding how systems function. For decades the role of metabolism in cellular systems has been predominantly assessed using homogenates, which yields information about total concentrations of small molecules and enzymes across an entire tissue, but cannot divulge information about single cells, let alone interactions between cells. The nervous system is an exceedingly complex heterocellular system, in which small molecules act within cells and on neighboring cells through tightly regulated, cell-specific

mechanisms. Based on early studies in the late 1970s and early 1980s that demonstrated cells had combinations of neurotransmitters and neuropeptides at different levels within single cells,[1-2] it stands to reason that the concentration of small molecules contained within the various cellular compartments might be unique to each morphologically and functionally distinct type of cell. This concept was formalized as the signature hypothesis in the 1980s, which posited that each morphologically and functionally unique type of neuron would also possess distinct neurochemical compositions.[3-6] Computational molecular phenotyping is a robust method for harnessing the quantitative aspects of electron microscopy compatible, postembedding immunocytochemistry,[7] and uses pattern recognition to classify cells into different cellular classes based on their signatures, which are defined by quantitative differences in small molecule concentration mixtures.[8-10]

2.1.1 Molecular Trapping and IgG Labeling

One of the predominant issues with respect to immunohistochemical detection of small molecules is the efficient trapping of small molecules in tissue. Formaldehyde (HCHO) is a 1-carbon small molecule that rapidly penetrates tissue and stops molecular interaction through aldehyde (-CHO) binding to terminal amines on specific proteins and small molecules. Formaldehyde is the traditional aldehyde for immunohistochemistry. However, its ability to cross-link protein amines via the formation of methylene bridges occurs relatively slowly; full formaldehyde cross-linking can take several weeks and even that is very sparse. Glutaraldehyde ($HCO\text{-}(CH_2)_3\text{-}CHO$), on the other hand, is a 5-carbon molecule, with a chain of three methylene groups and two aldehyde groups which rapidly bind with any available amine or imine via nucleophilic attack by N resulting in a Schiff's

base formation. The increased number of carbons greatly increases the potential for cross-linking, which generates a tightly cross-linked protein matrix.[11] The generated matrix of glutaraldehyde conjugated amines can in turn bind to other free aldehydes via imine condensation, efficiently trapping small molecules quickly in cells. A potential complication of using solely glutaraldehyde in fixation is the two aldehyde groups. Assuming each glutaraldehyde molecule has a single aldehyde group binding an amine associated with protein, there will be an equal number of aldehyde groups available for small molecule binding. However, the number of free amines found in a cell is approximately 10 fold less than protein matrix amines, leaving a large number of unbound aldehyde groups. These unbound aldehyde groups will cause an increase in background due to nonspecific binding by antibodies.[11] If solely formaldehyde fixation is used, the slow, and inefficient, cross-linking will cause a large percentage of small molecules to be lost during processing. Therefore, our solution is the use of a mixed aldehyde fixation protocol. By using 1% formaldehyde (333 mM, with 333 mM free aldehyde groups) and 2.5% glutaraldehyde (250 mM, with 500 mM free aldehyde groups), small molecules are still effectively trapped while the total number of free aldehydes is reduced. Using a standard primary amine-secondary amine model[12] of trapping where each amine N can capture two aldehyde carbons leads to a minimum of ≈ 84% capture by glutaraldehyde cross-linking, assuming no glutaraldehyde-formaldehyde exchange. But exchange is quite likely during Schiff's base formation as the nucleophilic attack is strongly affected by water molecules at the condensation site and highly reversible under even neutral conditions. Assuming one switch event during condensation leads to 94% capture and two switches yields 97.5% amino acid capture, this is consistent with radiochemistry estimates

suggesting glutaraldehyde-formaldehyde mixtures lead to >86-95% retention of [3H]-amino acids.[13]

Immunoglobulins (IgGs) have been developed for detection of small molecules for almost a century. In the 1920s and 30s, Karl Landsteiner and colleagues performed pioneering research introducing the concept of haptens.[14] Haptens, whether naturally occurring or synthetic, are small molecules that alone generate no immunological response, but when attached to a carrier molecule form a hapten-carrier adduct that is capable of initiating an immunological response. It is this concept that facilitates the generation of antibodies to small molecules such as amino acids. We harness this principle by using IgGs that have a high specificity to individual amino acid-glutaraldehyde adducts.[15]

The protein matrix generated by glutaraldehyde cross-linking in cells has a mean pore diameter of 2-5nm as calculated simply from the size of glutaraldehyde. IgGs, on the other hand, are approximately 10x7x2nm, which precludes penetration of IgGs into glutaraldehyde-fixed tissue. This limits all epitope detection to the surface and makes small molecule detection proportional to the density presented on the section surface following surface etching to increase epitope mobility and IgG access. IgG binding is largely hydrogen bonding and requires hydrophilic regimes, so it is necessary to remove the plastic epoxide bond matrix. This feature of molecular trapping combined with surface labeling lends itself to direct quantification of small molecules found within a cell independent of section thickness. Tissue penetration by IgGs or ISH probes in frozen section or whole mounts, though helpful in detection of sparse proteins, results in uneven penetration of the antibodies into the various tissue compartments, making quantification impractical. The evaluation of small molecule concentration from these labeled sections is simple because

the available epitope density presenting on the surface of the section scales as a function of concentration (independent calculations‡).[7, 15]

From the accurate small molecule trapping and IgG labeling described above,[7, 9, 15] we have one-dimensional information about the concentrations of amino acids contained within single cells in a tissue sample. The standard method for analysis of multiple antibody labeled cells in immunocytochemistry is by using multiple secondary antibodies conjugated to fluorophores reactive to different wavelengths. A key problem with fluorophores is bleaching, or the progressive decrease in brightness due singlet quenching, largely by intermolecular collision in the aqueous state. This makes fluorescent identification of small molecule concentrations in aqueous mounts nonarchival. Gold-conjugated secondary antibodies or proteins binding to IgGs used in transmission electron microscopy, are archival[16], but have the problem of being too small for easy detection by light microscopy at low density. Reverse-engineering the gold-toning method of photography, chemical reduction of silver nitrate to elemental silver particles plated on to gold particles was first applied to Western blotting techniques[17] and then developed in the Marc lab for immunocytochemistry.[15] In the presence of colloidal gold, the induction phase of hydroquinone reduced silver nitrate is drastically reduced, and the silver particles nucleate around the gold particle in a logarithmic fashion.[18] This feature lends silver-intensification to quantitative immunohistochemistry,[15] allowing the concentration of silver particles to function as a direct logarithmic readout of intercellular small molecule concentrations. Marc et al., directly calibrated the method against HPLC determinations of

‡ http://marclab.org/technologies/cmp/cmp-substrates/

small molecules in retina.[9]

2.1.2 CMP Analysis: Pattern Recognition

The above section describes how we can obtain an archival quantitative measure of small molecules in a single section. Quantitative immunocytochemistry on thin sections allowed a direct test the signature hypothesis.[9, 19-21] To apply these data to test the signature hypothesis, multiple small molecule signatures need to be evaluated simultaneously in single cells. The fact that IgG labeling for CMP is only surface binding, making section thickness irrelevant, lends it to using multiple thin sections through tissue and aligning them computationally. The smallest neuronal soma of the retina is the rod soma, which measures approximately 5μm in diameter (independent measurements from EM data). If the tissue were sectioned at 500nm, as in Ottersen's experiments,[7] 10 IgG labeled sections could fit within a single cell; however, that would assume the first section was perfectly aligned with the edge of the cell, which is improbable. As serial sections are cut thinner, a single cell being able to be stained for up to 12 small molecules becomes increasingly more probable. For this reason, we cut samples (except where otherwise noted) at 100nm throughout this dissertation. Because these are individually cut sections, computational alignment of sections is necessary for multidimensional cell classification algorithms to be effective. Images of all molecular signals are acquired under constant gain and flux to allow for direct comparable quantification between metabolites. Images were aligned into a registered volume using nonlinear thin-plate-spline warping[22] of selected chosen control

points. The primary tool was ir-tweak, available in ir-tools from the NCR[§] toolset.[9-10, 23-26] Once in a registered volume, the multichannel dataset lends itself to pattern recognition via various clustering methods.

By assigning each aligned grayscale image to a red, green, or blue color channel (rgb), we can visually identify the most dramatic differences between the metabolic signatures of major cell types and visualize the retina with more depth than traditional histology. However, this is not a statistical measure, and even with extensive rgb visualization of all possible combinations of all aligned images of IgG concentrations generated, we cannot accurately segment all of the metabolically distinct cells of the retina and one cannot see variance. Computationally, clustering (e.g. K-means or isodata) functions by similar principles: features are extracted from data and used by a classifier to subdivide the large mass of data into smaller data groups that share similar statistical features. These groups are termed *classes*. Rather than handling each IgG labeled registered image in isolation, duplicate, or triplicate, cluster analysis allows us to evaluate all *N* generated images simultaneously.

Of clustering algorithms a popular unsupervised (i.e. no user directed training or sample classes) learning algorithm is *k-means*. K-means is a rapid method of separating input data into *k* clusters (groupings of similar points or data vectors) and has been extensively used in multispectral satellite imaging. We view each *N*-dimensional pixel representation as a data point in Euclidean space (*N* = individual image channels composed of an IgG labeled grayscale image) (Figure 2.1b). In its most common implementation, the

---

[§] http://www.sci.utah.edu/download/ncrtoolset

k-means algorithm randomly assigns a set of *k N*-dimensional center points (centroids) in the data space, and decision boundaries are drawn between the centroids *k* (Figure 2.1c). All of the data points within each decision boundary are grouped, and the new mean of the points is computed, which becomes and new centroid. New boundary lines are computed from the new centroids (Figure 2.1d). The process of computing new centroids and boundaries are iterated until the movement of the centroid falls below a preset threshold, at which point the algorithm is said to converge (Figure 2.1e). The decision boundaries computed when a k-means converges determines the hypervolume containing the data points for each of the *k* regions, each denoting a metabolic class. We then remap the points back into the x,y conformation of a 2D image with colors assigned to its cluster membership, generating a theme map (Figure 2.1f). The theme map is then used as a mask for extracting individual histogram values of each small molecule, revealing its modal concentration in the class. In symmetrical unimodal histograms, the mode, median, and mean are the same. In general we summarize the data as spatial means, but the histogram always exists as the underlying dataset. The list of *N* small molecule means that define a class is termed its signature.

Defining *k* can be a difficult task in the case of biological systems and, in fact, there is no formal method to extract the right *k*, nor is there an ideal clustering algorithm for all problems.[27] We do not know *a priori* how many metabolically distinct cell types are possible, particularily in cases of pathology where the normal metabolic signatures of cells may have disappeared or diverged, but it is simple to compare k-means results using the same initial *k*, eliminating empty classes and comparing different classes. Visualization of cell-classes by representative theme-maps permits the identification of any inappropriate

classes arising from excessively stringent k values (e.g., differentiation of nucleus from cytoplasm within a single cell), and the emergence of over-clustering enables us to determine when the appropriate *k* for the sample has been reached. The classes produced are then tested for significant separability from one another using Bhattacharyya separability, which is a weighted measure of the degree of overlap between two statistical populations in *N*-dimensions. Over the course of this project, we found use of two other unsupervised clustering variants, similar to k-means, to be useful. One is an iteratively masking method, using custom software (CMP, Scientific Computing Institute, Salt Lake City, UT). Though the computational algorithm being run is k-means, it has the option to mask components not relevent to identification of metabolic classes (background, kerf, etc.). All k-means algorithms allow this, but CMP is particularly easy to use. This classification is run iteratively with *k* being incremented by 1 until it converges on statistics consistent with biological classes,[9] that is, no subcellular fractionation. The second is the use of the isodata algorithm first used in neural classification by Marc and Jones, 2002.[10] Isodata starts out with a defined *k* and then merges or splits them based their mutual variances. Isodata is known as a heuristic or self-adjusting algorithm. In practice, data analysis starts CMP as a first screen, then switches to formal k-means (which has more parameter flexibility), and then switches to isodata if necessary.

2.2 P347L Transgenic Rabbit Model of Retinitis Pigmentosa

The Tg P347L rabbit is a rabbit model of initially cone-sparing autosomal dominant retinitis pigmentosa (adRP) originally developed in the Kondo laboratory.[28] Although there are a large number of animal models of retinal degeneration in drosophila,[29-30] zebrafish,[31]

mouse,[32-35] rat,[36] chicken,[37] cat,[38-39] dog,[40-41] and pig.[42] medium sized animals with large eyes are extremely important for the development and testing of therapeutic interventions for retinal degenerative diseases. Testing surgical interventions, such as epi- or subretinal implants, particularly require a large eye model, and the costs of maintaining cats, dogs, or pigs can be prohibitively expensive. Rabbits provide a potential model organism of medium size, with an eye only ~25% smaller than that of a human.[43-44] Harnessing the technology of bacterial artificial chromosomes (BACs), Kondo et al., generated a rabbit with a proline to leucine mutation caused by a C-to-T transition at proline 347 in exon 5 of the rabbit rhodopsin gene.[28] This Tg P347L rabbit presents with a rod-dominant progressive photoreceptor degeneration, where rod photoreceptors display signs of degeneration and die prior to the degeneration and loss of cones. Like most transgenic models, the Tg P347L rabbit is an overexpression model with ≈ 6 copies of the defective gene.[28] By 12 postnatal weeks, ERGs demonstrate a 72% reduction in scotopic a-wave (rod-response) amplitudes, and 95% reduction by 48 weeks. Under photopic conditions, a-wave (cone-response) amplitudes persisted, though they did show a 65% reduction in amplitude.[28] CMP combined with TEM demonstrated, in randomly selected regions, the P347L Tg rabbit has a profound loss of rod photoreceptors by 16 weeks, and a subsequent loss of cones by 40 weeks.[23] At 40 weeks TEM reveals regional fluctuations in Müller cell polyribosome and protein levels, while CMP demonstrates glial seal formation, neurite outgrowth, glutamate receptor phenotype switching, and metabolic alterations.[23] All of these changes are found in human RP.[23-24]

Based on these previous studies detailing the early changes in the retina following rod loss and cone outer segment degeneration, the rabbit model is a likely candidate for

determining long-term consequences of photoreceptor degeneration and analyzing the potential for retinas to sustain therapeutic interventions long-term.

Figure 2.1 K-means generation of theme maps. (b) *N*-dimensional pixel representation as a data point in Euclidean space. (c) K center points (centroids) are randomly placed in data and boundary lines are drawn. (d) All vectors within boundaries are averaged, and the centroids are moved to the average means. (e) The process is repeated until the centroids no longer move beyond a threshold in the averaging means step. (f) The clusters are then overlaid on top of the image stack and the clusters are used as masks to extract the underlying histograms.

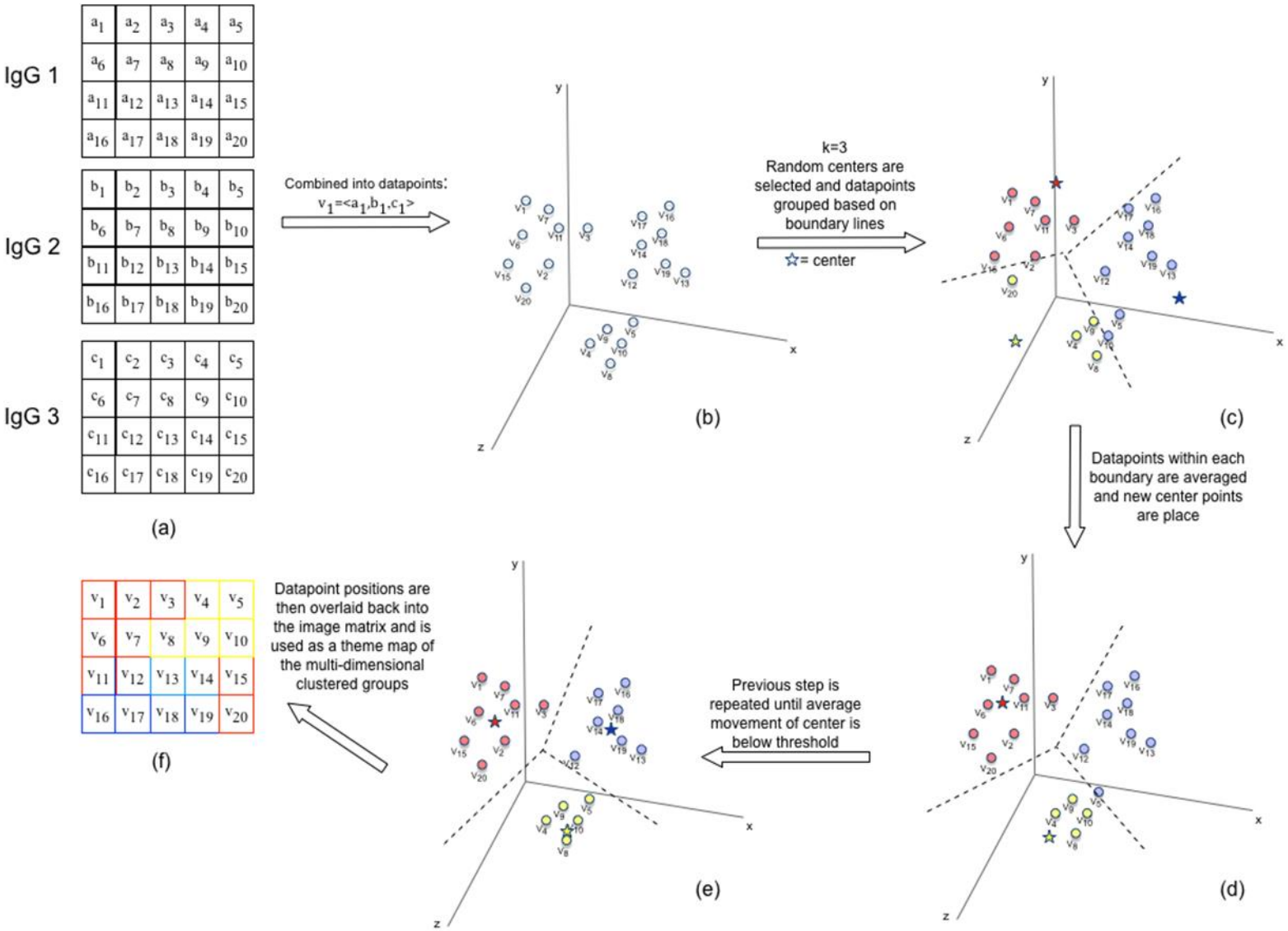
IgG 1
IgG 2
IgG 3
(a)
Combined into datapoints:
$v_1=<a_1,b_1,c_1>$
(b)
k=3
Random centers are selected and datapoints grouped based on boundary lines
☆= center
(c)
Datapoints within each boundary are averaged and new center points are place
(d)
Previous step is repeated until average movement of center is below threshold
(e)
Datapoint positions are then overlaid back into the image matrix and is used as a theme map of the multi-dimensional clustered groups
(f)

2.3 References

1. Watt, C. B.; Su, Y. Y.; Lam, D. M., Interactions Between Enkephalin and GABA in Avian Retina. *Nature* **1984,** *311* (5988), 761-763.

2. Burnstock, G., Do Some Nerve Cells Release More than one Transmitter? *Neuroscience* **1976,** *1* (4), 239-248.

3. Lam, D. M.; Li, H. B.; Su, Y. Y.; Watt, C. B., The Signature Hypothesis: Co-Localizations of Neuroactive Substances as Anatomical Probes for Circuitry Analyses. *Vision Res* **1985,** *25* (10), 1353-1364.

4. Lam, D. M.; Hollyfield, J. G., Localization of Putative Amino Acid Neurotransmitters in the Human Retina. *Exp Eye Res* **1980,** *31* (6), 729-732.

5. Watt, C. B.; Li, H. B.; Lam, D. M., The Presence of Three Neuroactive Peptides in Putative Glycinergic Amacrine Cells of an Avian Retina. *Brain Res* **1985,** *348* (1), 187-191.

6. Hokfelt, T.; Millhorn, D.; Seroogy, K.; Tsuruo, Y.; Ceccatelli, S.; Lindh, B.; Meister, B.; Melander, T.; Schalling, M.; Bartfai, T.; et al., Coexistence of Peptides with Classical Neurotransmitters. *Experientia* **1987,** *43* (7), 768-780.

7. Ottersen, O. P., Postembedding Immunogold Labelling of Fixed Glutamate: An Electron Microscopic Analysis of the Relationship Between Gold Particle Density and Antigen Concentration. *J Chem Neuroanat* **1989,** *2* (1), 57-66.

8. Kalloniatis, M.; Fletcher, E. L., Immunocytochemical Localization of the Amino Acid Neurotransmitters in the Chicken Retina. *J Comp Neurol* **1993,** *336* (2), 174-193.

9. Marc, R. E.; Murry, R. F.; Basinger, S. F., Pattern Recognition of Amino Acid Signatures in Retinal Neurons. *J Neurosci* **1995,** *15* (7 Pt 2), 5106-5129.

10. Marc, R. E.; Jones, B. W., Molecular Phenotyping of Retinal Ganglion Cells. *J Neurosci* **2002,** *22* (2), 413-427.

11. Kiernan, J. A., Formaldehyde, Formalin, Paraformaldehyde and Glutaraldehyde: What They Are and What They Do. *Microsc Today* **2000,** *08* (01), 8-12.

12. Carey, F. A.; Giuliano, R. M., *Organic Chemistry*. Tenth ed.; McGraw Hill Education: New York, NY, 2017; Vol. 10.

13. Peters, T., Jr.; Ashley, C. A., An Artefact in Radioautography due to Binding of Free Amino Acids to Tissues by Fixatives. *J Cell Biol* **1967,** *33* (1), 53-60.

14. Landsteiner, K., *The Specificity of Serological Reactions*. Dover Publications: New York, NY, 1936.

15. Marc, R. E.; Wei-Ley, S.; Kalloniatis, M.; Raiguel, S. F.; Van Haesendonck, E., Patterns of Glutamate Immunoreactivity in the Goldfish Retina. *J Neurosci* **1990,** *10* (12), 4006-4034.

16. Evans, N. R.; Webb, H. E., Comparison of Protein A-Gold and Ferritin Immunoelectron Microscopy of Semliki Forest Virus in Mouse Brain Using a Rapid Processing Technique. *J Histochem Cytochem* **1984,** *32* (4), 372-378.

17. Daneels, G.; Moeremans, M.; De Raeymaeker, M.; De Mey, J., Sequential Immunostaining (Gold/Silver) and Complete Protein Staining (AuroDye) on Western Blots. *J Immunol Methods* **1986,** *89* (1), 89-91.

18. James, T., The Reduction of Silver Ions by Hydroquinone. *Am Chem Soc* **1939,** *61* (3), 648-652.

19. Marc, R. E.; Jones, B. W., Retinal Remodeling in Inherited Photoreceptor Degenerations. *Mol Neurobiol* **2003,** *28* (2), 139-147.

20. Marc, R. E.; Cameron, D., A Molecular Phenotype Atlas of the Zebrafish Retina. *J Neurocytol* **2001,** *30* (7), 593-654.

21. Kalloniatis, M.; Marc, R. E.; Murry, R. F., Amino Acid Signatures in the Primate Retina. *J Neurosci* **1996,** *16* (21), 6807-6829.

22. Bookstein, F. L., Principal Warps - Thin-Plate Splines and the Decomposition of Deformations. *IEEE Trans Pattern Anal and Mach Intell* **1989,** *11* (6), 567-585.

23. Jones, B. W.; Kondo, M.; Terasaki, H.; Watt, C. B.; Rapp, K.; Anderson, J.; Lin, Y.; Shaw, M. V.; Yang, J. H.; Marc, R. E., Retinal Remodeling in the Tg P347L Rabbit, a Large-Eye Model of Retinal Degeneration. *J Comp Neurol* **2011,** *519* (14), 2713-27133.

24. Jones, B. W.; Pfeiffer, R. L.; Ferrell, W. D.; Watt, C. B.; Marmor, M.; Marc, R. E., Retinal Remodeling in Human Retinitis Pigmentosa. *Exp Eye Res* **2016,** *150*, 149-165.

25. Jones, B. W.; Pfeiffer, R. L.; Ferrell, W. D.; Watt, C. B.; Tucker, J. F.; Marc, R. E., Retinal Remodeling And Metabolic Alterations in Human AMD. *Front Cell Neurosci* **2016,** *10*, 103.

26. Marc, R. E., Mapping Glutamatergic Drive in the Vertebrate Retina with a Channel-Permeant Organic Cation. *J Comp Neurol* **1999,** *407* (1), 47-64.

27. Meyer, D.; Leisch, F.; Hornik, K., The Support Vector Machine Under Test. *Neurocomputing* **2003,** *55* (1-2), 169-186.

28. Kondo, M.; Sakai, T.; Komeima, K.; Kurimoto, Y.; Ueno, S.; Nishizawa, Y.; Usukura, J.; Fujikado, T.; Tano, Y.; Terasaki, H., Generation of a Transgenic Rabbit Model of Retinal Degeneration. *Invest Ophthalmol Vis Sci* **2009,** *50* (3), 1371-1377.

29. Griciuc, A.; Aron, L.; Ueffing, M., Looking Into Eyes: Rhodopsin Pathologies in Drosophila. *Adv Exp Med Biol* **2012,** *723*, 415-423.

30. Chow, C. Y.; Kelsey, K. J.; Wolfner, M. F.; Clark, A. G., Candidate Genetic Modifiers of Retinitis Pigmentosa Identified by Exploiting Natural Variation in Drosophila. *Hum Mol Genet* **2015,** *25* (4), 651-659.

31. Brockerhoff, S. E.; Hurley, J. B.; Janssen-Bienhold, U.; Neuhauss, S. C.; Driever, W.; Dowling, J. E., A Behavioral Screen for Isolating Zebrafish Mutants with Visual System Defects. *Proc Natl Acad Sci U S A* **1995,** *92* (23), 10545-10549.

32. Keeler, C. E., The Inheritance of a Retinal Abnormality in White Mice. *Proc Natl Acad Sci U S A* **1924,** *10* (7), 329-333.

33. Pittler, S. J.; Keeler, C. E.; Sidman, R. L.; Baehr, W., PCR Analysis of DNA from 70-Year-Old sections of Rodless Retina Demonstrates Identity with the Mouse rd Defect. *Proc Natl Acad Sci U S A* **1993,** *90* (20), 9616-9619.

34. Chang, B.; Hawes, N. L.; Hurd, R. E.; Davisson, M. T.; Nusinowitz, S.; Heckenlively, J. R., Retinal Degeneration Mutants in the Mouse. *Vision Res* **2002,** *42* (4), 517-525.

35. Han, J.; Dinculescu, A.; Dai, X.; Du, W.; Smith, W. C.; Pang, J., Review: The History and Role of Naturally Occurring Mouse Models with Pde6b Mutations. *Mol Vis* **2013,** *19*, 2579-2589.

36. Bourne, M. C.; Campbell, D. A.; Tansley, K., Hereditary Degeneration of the Rat Retina. *Br J Ophthalmol* **1938,** *22* (10), 613-623.

37. Semple-Rowland, S. L.; Lee, N. R., Avian Models of Inherited Retinal Disease. *Methods Enzymol* **2000,** *316*, 526-536.

38. Narfstrom, K., Hereditary Progressive Retinal Atrophy in the Abyssinian Cat. *J Hered* **1983,** *74* (4), 273-276.

39. Barnett, K. C.; Curtis, R., Autosomal Dominant Progressive Retinal Atrophy in Abyssinian Cats. *J Hered* **1985,** *76* (3), 168-170.

40. Aguirre, G., Retinal Degenerations in the Dog. I. Rod Dysplasia. *Exp Eye Res* **1978,** *26* (3), 233-253.

41. Suber, M. L.; Pittler, S. J.; Qin, N.; Wright, G. C.; Holcombe, V.; Lee, R. H.; Craft, C. M.; Lolley, R. N.; Baehr, W.; Hurwitz, R. L., Irish Setter Dogs Affected with Rod/Cone Dysplasia Contain a Nonsense Mutation in the Rod cGMP Phosphodiesterase Beta-Subunit Gene. *Proc Natl Acad Sci U S A* **1993,** *90* (9), 3968-3972.

42. Petters, R. M.; Alexander, C. A.; Wells, K. D.; Collins, E. B.; Sommer, J. R.; Blanton, M. R.; Rojas, G.; Hao, Y.; Flowers, W. L.; Banin, E.; Cideciyan, A. V.;

Jacobson, S. G.; Wong, F., Genetically Engineered Large Animal Model for Studying Cone Photoreceptor Survival and Degeneration in Retinitis Pigmentosa. *Nat Biotechnol* **1997,** *15* (10), 965-970.

43. Silver, D.; Csutak, A., Human Eye Dimensions for Pressure-Volume Relations. *Invest Ophthalmol Vis Sci* **2010,** *51* (13), 5019.

44. Park, J.; Bungay, P. M.; Lutz, R. J.; Augsburger, J. J.; Millard, R. W.; Sinha Roy, A.; Banerjee, R. K., Evaluation of Coupled Convective-Diffusive Transport of Drugs Administered by Intravitreal Injection and Controlled Release Implant. *J Control Release* **2005,** *105* (3), 279-295.

CHAPTER 3

MÜLLER CELL METABOLIC CHAOS DURING RETINAL DEGENERATION

Reprinted with Permission from Elsevier Ltd

Pfeiffer, R.L.; Marc, R.E.; Kondo, M.; Terasaki, H.; Jones, B.W., Müller Cell Metabolic Chaos During Retinal Degeneration. *Exp Eye Res* **2016,** *150,* 62-70.

Experimental Eye Research 150 (2016) 62–70

Contents lists available at ScienceDirect

Experimental Eye Research

journal homepage: www.elsevier.com/locate/yexer

Research article

Müller cell metabolic chaos during retinal degeneration

Rebecca L. Pfeiffer [a, b, *], Robert E. Marc [a, b], Mineo Kondo [c], Hiroko Terasaki [d], Bryan W. Jones [a, b]

[a] Dept of Ophthalmology, Moran Eye Center, University of Utah, Salt Lake City, UT, USA
[b] Interdepartmental Program in Neuroscience, University of Utah, Salt Lake City, UT, USA
[c] Department of Ophthalmology, Mie University Graduate School of Medicine, Tsu, Japan
[d] Department of Ophthalmology, Nagoya University, Graduate School of Medicine, Nagoya, Japan

ARTICLE INFO

Article history:
Received 1 October 2015
Received in revised form
21 April 2016
Accepted in revised form 25 April 2016
Available online 30 April 2016

Keywords:
Retinal degeneration
Müller cell
Retinal remodeling
Retina
Computational molecular phenotyping (CMP)
Retinitis pigmentosa (RP)

ABSTRACT

Müller cells play a critical role in retinal metabolism and are among the first cells to demonstrate metabolic changes in retinal stress or disease. The timing, extent, regulation, and impacts of these changes are not yet known. We evaluated metabolic phenotypes of Müller cells in the degenerating retina.

Retinas harvested from wild-type (WT) and rhodopsin Tg P347L rabbits were fixed in mixed aldehydes and resin embedded for computational molecular phenotyping (CMP). CMP facilitates small molecule fingerprinting of every cell in the retina, allowing evaluation of metabolite levels in single cells.

CMP revealed signature variations in metabolite levels across Müller cells from TgP347L retina. In brief, neighboring Müller cells demonstrated variability in taurine, glutamate, glutamine, glutathione, glutamine synthetase (GS), and CRALBP. This variability showed no correlation across metabolites, implying the changes are functionally chaotic rather than simply heterogeneous. The inability of any clustering algorithm to classify Müller cell as a single class in the TgP347L retina is a formal proof of metabolic variability in the present in degenerating retina.

Although retinal degeneration is certainly the trigger, Müller cell metabolic alterations are not a coherent response to the microenvironment. And while GS is believed to be the primary enzyme responsible for the conversion of glutamate to glutamine in the retina, alternative pathways appear to be unmasked in degenerating retina. Somehow, long term remodeling involves loss of Müller cell coordination and identity, which has negative implications for therapeutic interventions that target neurons alone.

1. Introduction

1.1. Retinal degeneration and remodeling

Retinal degenerations such as Usher Syndrome, retinitis pigmentosa (RP), and age-related macular degeneration (AMD) cause irreversible vision impairment. These disorders ultimately cause the death of all photoreceptors in large retinal areas, often triggered by rod degeneration. During and following photoreceptor degeneration, the neural retina undergoes progressive remodeling, including ectopic neuritogenesis, microneuroma formation, loss of distinct layer lamination, Müller cell hypertrophy, metabolic alterations of neurons and glia, and progressive neuronal loss (Kolb and Gouras, 1974; Strettoi et al., 2002; Fisher and Lewis, 2003; Jones et al., 2003; Marc and Jones, 2003; Marc et al., 2003; Strettoi et al., 2003; Jones and Marc, 2005; Jones et al., 2005, 2011, 2012).

Abbreviations: adRP, autosomal dominant retinitis pigmentosa; AMD, age-related macular degeneration; CDF, cumulative distribution function; CMP, computational molecular phenotyping; CRALBP, cellular Retinaldehyde binding protein 1; EAAT, excitatory amino acid transporter; GABA, γ-aminobutyric acid; GFAP, glial fibrillary acidic protein; GS, glutamine synthetase; KS test, Kolmogorov-Smirnov test; mdCMP, morphology driven CMP; RPE, retinal pigmented epithelium; RP, retinitis pigmentosa; rgb, red green blue; SNAT, sodium-coupled neutral amino acid transporter; Tg P347L, rabbit rhodopsin proline 347 → leucine transgenic model of autosomal dominant RP.

* Corresponding author. University of Utah, Moran Eye Center, 65 Mario Capecchi, Dr., Salt Lake City, UT 84132, USA.
E-mail address: R.Pfeiffer@utah.edu (R.L. Pfeiffer).

http://dx.doi.org/10.1016/j.exer.2016.04.022

The mechanisms of these alterations are not fully characterized and their impacts on the long-term viability of therapeutic interventions are uncertain (Marc et al., 2014).

1.2. Müller glia in degenerating retina

Müller glia are among the first to show metabolic changes in retinal degenerations. Müller cells support many neuronal metabolic processes including (but not limited to) glucose transport, removal of NH_3^+ byproducts, CO_2, redistribution of K^+, and recycling amino acids (Newman et al., 1984; Wilson, 2002; Reichenbach and Bringmann, 2010; Bringmann et al., 2013; Hurley et al., 2015). Müller cell morphology varies subtly between aerobic and anaerobic retinas, but no major functional differences in metabolic support have been described (Dreher et al., 1992), except for the absence of GABA transport and recycling in non-mammalians (Marc, 1992, 2004). Müller cells are thought to be a homogenous class in all vertebrates. Though there has been some indication of Müller cell heterogeneity based on previous genetic and cell culture experiments, functional and metabolic subclasses have never been observed (Rowan and Cepko, 2004; Roesch et al., 2012). Müller cells display a characteristic normal small molecule signature high in taurine and glutamine and very low in all other markers including glutamate across all vertebrate classes (Marc, 2004). Indeed these signatures are indistinguishable despite vast differences in systemic biology across vertebrates, including avascular ectotherms such as teleost fishes (Marc et al., 1995; Marc and Cameron, 2001), avascular non-mammalian endotherms such as avians (Kalloniatis and Fletcher, 1993), avascular mammals (Marc, 1992), and a range of vascular mammals such as mouse, rat, cat, and primate (Kalloniatis et al., 1996; Jones et al., 2003; Marc et al., 1998a,b, 2008). Mammalian Müller cells display a definitive protein signature with elevated glutamine synthetase (GS) and cytosolic retinaldehyde binding protein (CRALBP) and respond to stress (e.g. reactive oxygen species stress) with massive upregulation of glial fibrillary acidic protein (GFAP) levels (Bignami and Dahl, 1979; Erickson et al., 1987; Fisher and Lewis, 2003; Luna et al., 2010).

1.3. Müller glia functions and homogeneity

Müller cells are thought to be an essential component of glutamate recycling in the retina (Pow and Robinson, 1994) by importing extracellular glutamate via high-affinity Na^+-dependent transporters (e.g. EAAT1) and rapidly amidating it to glutamine via GS (Riepe and Norenburg, 1977). Müller cells then export glutamine via a Na^+-dependent transporter (SNAT3) into the extracellular compartment where neurons can import it via SNAT1 and other mechanisms for synthesis of neurotransmitters and other metabolites. Due to rapid amidation by GS, glutamate is only found at $\approx$0.1–0.6 mM in Müller cells, in contrast to bipolar or ganglion cells where it may be as high as 10 mM (Marc et al., 1990; Marc and Jones, 2002; Marc, 2004). Retinal glutamate synthesis is commonly thought to be predominantly dependent on the glutamine/glutamate cycle (Marc, 2004) and, therefore, GS activity (Pow and Robinson, 1994). It has been presumed, that the homogeneity of Müller cell metabolic signatures is shaped by the microenvironment created by neurons surrounding the Müller column, including cone photoreceptors (Reichenbach and Bringmann, 2010). Data from previous work in our lab (Jones et al., 2011) and the results presented here indicate this may not be the case.

1.4. Transgenic P347L rabbit model of autosomal-dominant retinitis pigmentosa (adRP)

Numerous animal models have been developed for studying retinitis pigmentosa, including fruit fly (Griciuc et al., 2012; Chow et al., 2016), zebrafish (Brockerhoff et al., 1995), mouse (Keeler, 1924; Pittler et al., 1993; Chang et al., 2002; Han et al., 2013), rat (Bourne et al., 1938), chicken (Semple-Rowland and Lee, 2000), pig (Petters et al., 1997), cat (Narfstrom, 1983; Barnett and Curtis, 1985), and dog (Aguirre, 1978; Suber et al., 1993). Of these animal models, the large eye models have proven to be especially useful for analyzing retinal degenerations (Jones et al., 2011) and testing new treatments (Chader, 2002), though larger animals can be expensive, slow to mature and breed. To address this problem a transgenic rabbit model with a primary rod degeneration caused by a human rhodopsin proline 347 → leucine mutation characteristic of a human variant of adRP was developed by the Kondo laboratory (Kondo et al., 2009). We have previously characterized the progression of degeneration in this rabbit model over the first year of degeneration, demonstrating that it progresses through cone-sparing retinal degeneration analogous to that seen in humans. In brief, the degeneration presents initially with loss of rod photoreceptors, which may survive up to 12–16 weeks; subsequently, cone photoreceptors will also degenerate by around 40 weeks of age. During this time the neural retina becomes deafferented and undergoes a series of remodeling events including massive rewiring through microneuromas, changes in cell types and numbers, and Müller cell hypertrophy and metabolic changes. For a more comprehensive description of the remodeling associated with this model see previous publications (Jones et al., 2011, 2012).

1.5. Computational molecular phenotyping

This study focuses on the metabolic changes in Müller cells during degeneration and quantifies the changes across Müller cells as a class and within individual cells. The technique used for this study is computational molecular phenotyping (CMP), which allows for quantitative evaluation of metabolite levels within single cells (Marc et al., 1995; Kalloniatis et al., 1996; Marc and Cameron, 2001). This is unique to our approach as it obviates dissociation and/or homogenization required for biochemical assays and uniquely allows visualization of metabolic diversity. Indeed, the key finding enabled by CMP is that Müller cells in degenerating retinas slowly lose the ability to uniformly regulate their metabolomes.

2. Methods

2.1. Model systems

The heterozygous Transgenic (Tg) P347L rabbit is a model of human adRP, originally generated in the Kondo laboratory (Kondo et al., 2009). In brief, these rabbits express a mutated rhodopsin gene with a C-to-T transition at proline 347, causing a proline to leucine replacement. This mutation causes degeneration of the photoreceptors phenotypically similar to other adRP mutations and to human cone-sparing RP (Jones et al., 2011). Control rabbits used in these experiments are the transgene negative unaffected littermates of the TgP347L rabbits (WT). Two TgP347L rabbits, ages 2 years and 2 years 5 months, were selected to evaluate late stage adRP degenerating retina. Two WT rabbits were selected for illustrative comparison ($\approx$6–12 months and 3 year 8 month rabbit). For additional statistical analysis, we compared these to Müller cell datasets from diverse vertebrates in our library including samples from 150 goldfish; 13 primates; 65 rats including 25 with fetal retinal transplants and 30 from early phase retinal degenerations that show no Müller cell changes; and over 1450 separate assays from 90 rabbits, most 6–12 months old but some as old as 2 years. We also have very aged human samples that show no Müller cell variations (Jones et al., 2016a, 2016b). In total we have at least 559

retinal samples from 319 individual animals.

2.2. Tissue processing

Retinal samples were harvested as previously described (Marc et al., 1990; Marc, 1999). Rabbits were tranquilized with intramuscular ketamine/xylazine followed by deep anesthesia with 2-3 doses of 15% aqueous intraperitoneal urethane, followed by bilateral thoracotomy. All animal experiments were conducted according to the ARVO Statement for the Use of Animals in Ophthalmic and Vision Research, with the approval of the Institutional Animal Care and Use Committee at the University of Utah. Following euthanasia, both eyes were removed and hemisected. Retinas were cut into smaller pieces and placed in 2.5% glutaraldehyde, 1% formaldehyde, 0.1 M cacodylate (pH 7.4), 1 mM $MgSO_4$, 3% sucrose fixation solution. After 24 h fixation, tissues were dehydrated through graded methanols to acetone and embedded in an epoxide resin (Marc et al., 1995). Tissue stacks (Marc et al., 1990) were serially sectioned at 100 nm onto 12-well array slides.

2.3. CMP and nomenclature

We used CMP to identify cell classes and quantify the effects of retinal degeneration on core retinal metabolism (Marc et al., 1995; Marc and Cameron, 2001; Jones et al., 2003). Each well of the array slide was probed with an IgG selective for one of seven small molecules denoted by single letter codes as described in previous publications (D aspartate, E glutamate, G glycine, J glutathione, Q glutamine, τ taurine, γ GABA), CRALBP, or GS and visualized with a secondary antibody conjugated to a 1.4 nm gold granule, followed by silver intensification (Marc et al., 1995; Marc and Jones, 2002) (Table 1). CMP yields quantitative measures of small molecules, enables computational classification of cells, and defines a signature for each class. When we refer to a molecule's signal, we will use protein amino acid notation, e.g. E for glutamate (Marc et al., 1995). A triplet mapping refers to the assignment of a molecule to a color channel, e.g. γGE → rgb (Marc and Cameron, 2001). Finally, a signature refers to the pattern of signal strengths associated with set of molecules that define a cell class (Marc and Jones, 2002) and can be several molecules long depending on the number of channels we use. But in practice, Müller cells are defined by a four-channel signature with high taurine and glutamine (τ^+ and Q^+), moderate glutathione levels J, and low glutamate we denote by E^0. Normal Müller cells also have very low alanine, arginine, aspartate, glycine and GABA levels (Marc et al., 1995, 1998a,b). Thus when we refer to the Müller cell "τQE" signature, we imply the $\tau^+Q^+JE^0$ complex signature.

2.4. Analysis

We used K-means clustering (Marc et al., 1995) to identify all natural cellular compartments, all molecular signals were captured as 8 bit images using a cooled QImaging Retiga CCD camera (Surrey, BC) under constant gain and flux. The channels were then computationally aligned using ir-tweak (Anderson et al., 2009), generating a registered volume of individual grayscale images of each metabolite. To generate a cluster theme map all channels were loaded into custom software (CMP, Scientific Computing Institute, Salt Lake City UT), which facilitated k-means clustering with a masking option to remove background and kerf. This classification was run iteratively with k increased by 1 until it converged on statistics consistent with known biological classes (Marc et al., 1995). From these data, we can determine absolute metabolite levels in all cell classes, visualized as univariate histograms (CellKit, © Robert E. Marc, 2003).

Due to the high variability in Müller cell signals observed in late phase III advanced phases of retinal degeneration, a modified classification was developed. Sections were clustered using the same K-means classification as in normal retina, but this yielded many different classes for individual Müller cells across the retina. We grouped the Müller cell subclasses into a single artificial class by metabolic exclusion of neurons (e.g. subtraction of γ+, G+ or E+ neurons) and summation of remaining subclasses until they matched the morphology of Müller cells as defined by unique signals such as GS, τQE, and CRALBP in normal retina. This means of clustering is morphology-driven computational metabolic phenotyping (mdCMP). Finally, we used both binomial probability calculations and the single-sample methods of Crawford and Howell (1998) and Crawford and Garthwaite (2012) to determine population significances.

Image J (Schneider et al., 2012) and CellKit were used for histogram visualization, Microsoft Excel was used for cumulative distribution function (CDF) generation and statistical tests (e.g. Kolmogorov-Smirnov, KS), and Adobe Photoshop was used for final image creation. For ease of visualization of metabolite signals, channels are mapped to rgb images: τ, GS γ → red; Q and G → green; and E → blue. Thus a triplet of metabolites is mapped, for example, as γGE → rgb. The displayed images are max-min linearly stretched for human visualization. All statistics, clustering, and metabolic quantification were run on raw image data.

3. Results

During late stage (phase III) remodeling of the Tg P347L retina, after the loss of the sensory retina and global remodeling has

Table 1
Immunocytochemistry reagents.

Reagent	SKU	RRID	Source	Dilution
anti-L-alanine IgG	A100R	AB_2532052	Signature Immunologics	1:100
anti-agmatine IgG	B100R	AB_2532053	Signature Immunologics	1:100
anti-agmatine IgY	B100C	AB_2532054	Signature Immunologics	1:100
anti-L-aspartate IgG	D100R	AB_2341093	Signature Immunologics	1:100
anti-L-glutamate IgG	E100R	AB_2532055	Signature Immunologics	1:100
anti-L-glutamate IgY	E100C	AB_2532056	Signature Immunologics	1:100
anti-glycine IgG	G100R	AB_2532057	Signature Immunologics	1:100
anti-glutathione IgG	J100R	AB_2532058	Signature Immunologics	1:100
anti-L-glutamine IgG	Q100R	AB_2532059	Signature Immunologics	1:100
anti-taurine IgG	TT100R	AB_2532060	Signature Immunologics	1:100
anti-GABA IgG	YY100R	AB_2532061	Signature Immunologics	1:100
anti-GABA IgY	YY100C	AB_2532062	Signature Immunologics	1:100
anti-GS IgG	610517	AB_397879	BD Biosciences	1:50
anti-CRALBP IgG	NA	AB_2314227	Gift of Dr. Jack Saari	1:400

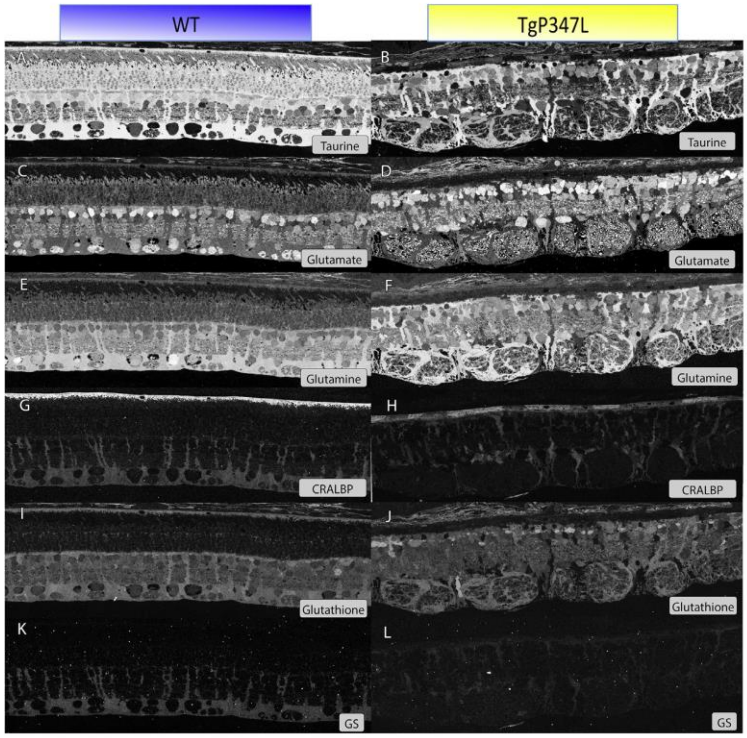

Fig. 1. Comparison of WT amino acid levels to that of Tg P347L. All images are the inverted silver density images of molecular immunoreactivity in serial 100 nm sections so that higher intensity = higher concentration. (Left) Registered WT small molecule channels. (Right) Registered TgP347L retina of the same channels as WT.

initiated (Marc et al., 2003; Jones et al., 2012), Müller cell metabolism changes more radically than we had ever seen. We sought to define the extent of metabolic variation in Müller cell small molecule and protein levels CMP examination of CMP signatures (Fig. 1), K-means clustering (Fig. 2) and quantitative histogramming (Fig. 3) and statistical analysis.

3.1. CMP signatures

During degeneration, Müller cell taurine content displays both dysregulation and intercellular variation in phase III remodeling (Fig. 1A,B). Some survivor Müller cells display higher taurine levels than normal while others display much lower levels. This variation is not regional, as vastly different Müller cells can be immediate neighbors. In contrast, glutamate (the core metabolite of neuronal signaling) appears to be quite high in survivor neurons and only slightly depressed in Müller cells (Fig. 1C,D). Given the near uniformity of glutamate signals in both WT and Tg P347L retinas, we expected a small uniform increase in Müller cell glutamine content as had been previously observed in retinal degenerations. But the phase III Tg P347L rabbit displays both strong glutamine elevation and as much intercellular variation as taurine (Fig. 1E,F). Another molecule linked to glutamate levels (as least as a sink for glutamate) is glutathione. In degenerate retina, the population mean of glutathione in Müller cells is similar to age-matched healthy controls, but intercellular levels are much more variable (Fig. 1I,J). Given these variations in small molecules, we explored whether characteristic protein markers of Müller cells were altered in any way. Even though CRALBP is not functionally linked to the glutamate-glutamine cycle, putative taurine osmoregulation, or the behavior of redox molecules like glutathione, CRALBP is also remarkably variable in remodeling Müller cells (Fig. 1G,H). The RPE of degenerating retina also has dramatically decreased and patchy CRALBP expression. Simultaneously, some Müller cells lack detectable CRALBP, while others upregulate content to match some remnant RPE cells. The high levels of CRALBP, in addition to similar levels of other metabolites, makes certain Müller cell metabolic signatures similar to RPE cells in remodeling. Finally, we see that GS is also severely reduced in phase III remodeling, but not uniformly. Like the other signatures, GS varies considerably between neighboring Müller cells in the same region of degenerate retina. But considering this change, it is also remarkable that Tg P347L rabbit glutamate signals in Müller cells rise above WT Müller cells in only a few instances, and even cells with low GS do not show large increases in glutamate content.

3.2. Clustering, histograms and analysis

The nature of Müller cell homogeneity in normal retina and variation the Tg P347L rabbit retina is far better visualized by combining single quantitative channels into classic τQE → rgb maps (Fig. 2A,C). Every Müller cell across the retina forms a single homogeneous class (Fig. 2A). By using all six channels to create a theme map of all statistically separable cell classes, it is easily demonstrated that a single class emerges for Müller cells (Fig. 2B). In normal retina, a τQE signature always separates the entire Müller

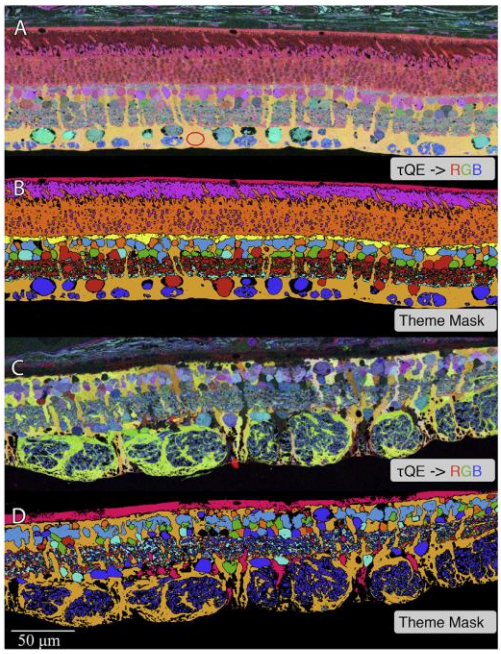

Fig. 2. Representative τQE and theme maps of WT retina vs degenerate retina. A and C are registered images of amino acid immunoreactivity in serial 100 nm sections. Both have been clustered using K-Means (k = 12) in which all classes of cells are separated by metabolic signature. Metabolic signatures used for generating maps: E,Q, J, τ, G, γ, GS, and CRALBP. 1A) τQE → rgb of a WT rabbit retina. The Müller cells (endfeet highlighted by red oval) are clearly identifiable by their characteristic shape and signature, which appears yellowish orange in this configuration. 1B) Clustering theme map of WT retina using 7 metabolic signatures. The orange theme class clearly identifies the Müller cells and makes them completely separable from all other cell types of the retina. 1C) τQE → rgb of TgP347L degenerate rabbit retina. The Müller cells have less pronounced endfeet in part due to hypertrophy that may include redistribution of volume from the endfeet to more apical locations within the retina. Müller cells display a range of colors. 1D) Theme map of the TgP347L retina. Simple K-means clustering does not extract Müller cells. By using the mCMP method the orange theme class was generated by fusing non-neuronal glial signatures into a single artificial class, demonstrating the location of the remaining Müller cells, with the exception of the pink group that has a signature metabolically similar to the RPE, due to a pronounced loss of typical Müller cell amino acids.

cell cohort from all other retinal cells. This is a formal proof, substantiated by direct measures, that metabolite levels and fluxes are highly conserved with low variance.

The Müller cell τQE signature of the phase III Tg P347L retina is an array of molecular mixtures. While variability is qualitatively evident in the τQE signature (Fig. 2C), the Müller cell cohort is proven to be inhomogenous when no clustering algorithm was capable of grouping all Müller cell variants into a class (not shown). But to provide a statistical test of the cohort as a whole, we had to fuse the many individual Müller cells into two major classes (Fig. 2D) as described in the methods.

Using the theme classes as a mask, we could then extract the histograms for normal and Tg P347L retinal Müller cells. In all cases, small molecule signals of Tg P347L rabbit Müller cells are much more variable than normal Müller cells (Fig. 3A–D). In addition, both proteins CRALBP and GS have essentially collapsed to very low levels (Fig. 3E,F).

How do we statistically assess individual Müller cell differences? First, the homogeneity in WT retina is so profound that borders between Müller cells are indistinguishable by optical microscopy. Using transmission electron microscope images from rabbit retinal connectome RC1 (Anderson et al., 2011) we evaluated the size of the endfeet of 301 neighboring Muller cells in the ganglion cell layer. This analysis revealed that the mean endfoot diameter is 5.2 ± 0.75 μm. By using a sampling area of 4 × 4 μm we ensured that each signal patch represents one or two (rarely three) Müller cells in WT retina. Horizontal sections through the endfeet of Müller cells in the ganglion cell layer were probed for τQE and their distributions evaluated for collections of individual Müller cells in WT and Tg retinas. The distributions were compared using a two-sample Kolmogorov-Smirnov (KS) test, which showed the distributions of the two populations were significantly different $p < 0.001$ (Fig. 4). It is obvious that from both the univariate histograms and the cumulative distribution functions (CFDs) that the variances of the Müller cell population sample in the Tg P347L retina are abnormally high.

To further stress that the variability is intercellular and not intracellular, we analyzed the CDFs of ten 4 × 4 μm samples, taken at separate locations to be indicative of separate Müller cells. These CDF's were compared to the normal distribution of the entire Müller cell population (Tg: ~817 Müller cells, WT: ~1053 Müller cells) in horizontal sections (Figs. 4 and 5). The CDFs from the individual endfeet in the WT section overlay closely with the total population indicating that there is low variability between individual cells and that they have consistent amino acid concentrations. In the Tg section, the CDF of the total population is much broader than the WT population and, remarkably, the CDFs from the endfeet of 10 individual remodeling Müller cells vary by as much as a log unit.

Finally, we have to address the problem of sample size. Rare clinical samples or expensive experiments that take long times to evolve are problematic but can be managed with classical combinatorial and parametric methods. First, while it is beyond the scope of this paper to produce hundreds of images, we nevertheless have τQE signatures for literally thousands of Müller cells from over a dozen species and hundreds of individual retinas and animals. All τQE signatures from non-mammalians and mammals are identical, except for very small shifts in amino acid means and all form a single class with extremely low variances (e.g. Marc et al., 1995, 1998a; Kalloniatis et al., 1996; Marc and Jones, 2003; etc.). All of these samples are archival and still exist in our libraries; they also include 2 year old rabbits, 27 year old macaques and a 78 year old human, all having the same single-class τQE signature. These older retinas are indistinguishable from juvenile retinas of any mammal. If we sample 100 Müller cells from each of 559 retinas and find only a single class, by clustering or visually, that sets the probability of success for repeating that conclusion in the next sample at no less than 0.9998. Using the binomial distribution one would argue that a sample from two Tg P347L rabbit retinas failing to form single Müller cell classes has a probability of 1×10^{-6}. This means that late phase III remodeling creates a state unlike any known retina and solves the rare case problem. More aggressively, we can use the approach developed for single-case research (Crawford and Howell, 1998; Crawford and Garthwaite, 2012) and use the histogram half-width of data from rabbit, goldfish and monkey as representative for the control half-width of all species. This has three important features. First, the half width is largely independent of the histogram mean. Second, we can pick the worst case data set based on the oldest cameras, noisiest immunocytochemistry and earliest technology (Marc et al., 1995) and show that newer histograms are narrower. Thus using the worst case control data biases against a type I error. Third, the half-width of each case is itself the average of many Müller cells, and so represents a measure of a single retina's variability. Using Marc et al. (1995) the half-width for the Müller

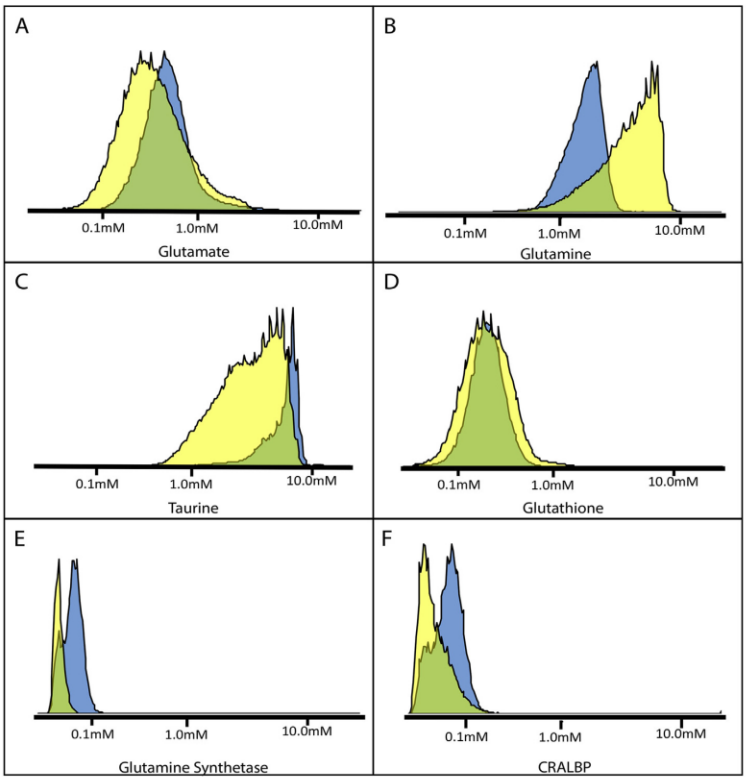

Fig. 3. Univariate amino acid probability density distributions (histograms) for each of the amino acids displayed in Fig. 2. (Yellow) Tg P347L retina; (Blue) WT retina. The histograms each represent aggregate signals from 15 to 20 Müller cells as described in Marc and Jones (Marc and Jones, 2002) and displayed as normalized probability density versus pixel values scaled as concentration.

cell taurine signal is 60 PV in an 8-bit image capture. Although the mean for taurine in the primate retina is lower than goldfish, the half-width is ≈50 PV. In the WT rabbit using low noise cameras, thinner sections and far better image registration the half-width is ≈PV 40. So we can safely assume that the mean half-width (x) is 50 PV or less with a range of 10 PV. If we conservatively call the range the standard deviation (s), and assume that the taurine half-width (x_{tg} ≈ 100 PV) of the Tg P347L rabbit is the mean of an equivalent population, the formula for Student's $t_{n-1} = (x_{tg}-x)/(s \times (n + 1/n)^{1/2}) \geq 4$ over a range of n values and achieves $p < 0.01$ for any $n \geq 5$. So merely taking the three published half-widths and the two control widths shown here demonstrates that the rare outcome of these two Tg P347L rabbit retinas is not simply an outlier on the normal distribution.

4. Discussion

K-means clustering identifies all major cell classes and allows profiling of normal metabolite levels and variation in Müller cells of normal retina. The very fact that k-means fails to classify all Müller cells in the degenerating retina is a formal proof that Müller cell metabolism is highly variable in disease. We used mdCMP to reconstitute the entire Müller cell population and generated a theme map of cell types in the degenerate state (Fig. 2C–D).

This shows the metabolic revisions in retinal degenerations are more complex than previously believed. In every observed species, Müller cells show high homogeneity in their metabolic signatures in healthy retinas (Marc et al., 1990; Kalloniatis and Fletcher, 1993; Kalloniatis et al., 1996; Marc et al., 1998b; Marc and Cameron, 2001). However, in degenerating retina, Müller cells lose their remarkably precise metabolic homogeneity and become variable early in degeneration, with persistent changes throughout subsequent remodeling. It has been noted previously that much of the neural cell death and remodeling associated with photoreceptor loss can be delayed as long as cone photoreceptors are present, though other aspects of remodeling continue to occur (Jones et al., 2011, 2012). Previous publications also demonstrate that early in adRP degeneration, while cones are still present, Müller cells begin to slightly alter their metabolic signatures in respect to one another (Jones et al., 2011). We show that this early variability increases throughout later remodeling. If microenvironments shaped Müller cell signatures we would expect patchy signatures with neighboring Müller cells showing similar signatures. This never happens. Rather, signature variations appear to be independent of any geographic property. The variation appears more extensive in later stage remodeling retina than shown by Jones et al., 2011, further indicating a lack of predictability of metabolic variation during the course of adRP.

The probable impacts of these variations on retinal function are unclear, particularly as the mechanisms by which these alterations

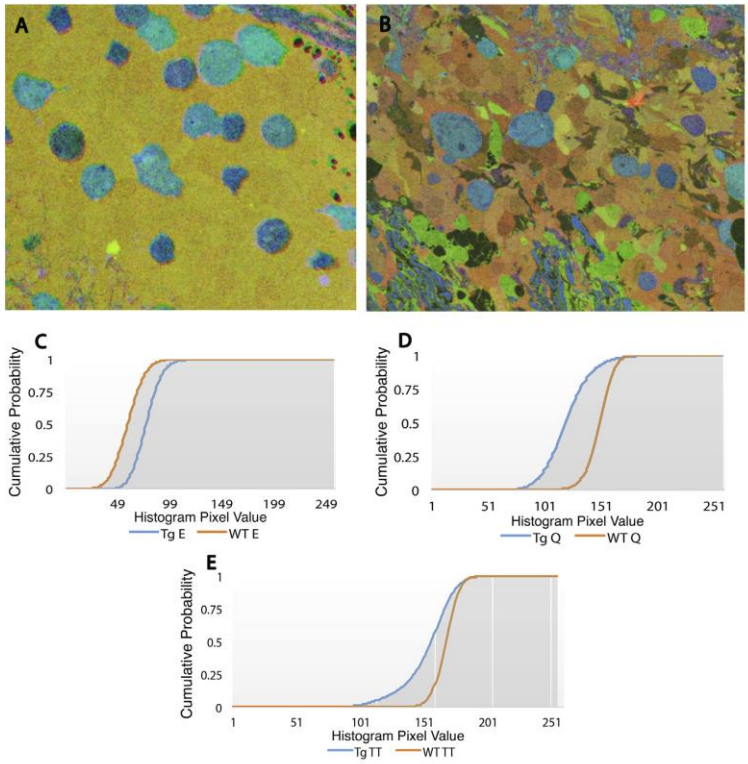

Fig. 4. 4A+B) τQE → rgb mappings of registered of amino acid signals in serial 100 nm sections. Color variation in an individual cells indicates varying differing ratios of τQE. (A) WT retina. (B) TgP347L retina C–E) Normal distributions of glutamate, glutamine, and taurine levels across entire Muller cell population of Tg P347L (blue) and WT retinas (red). All Tg distributions are significantly separable from WT distributions based on K-S test with a $p < 0.001$.

arise are unknown. Possible mechanisms and precipitating factors leading to the chaotic of signatures seen here in late stage remodeling retina will require further experimentation. These signatures may reflect transporter deficiencies of the Müller cells, unknown enzyme expression, or Müller cells entering altered cellular states reflecting division or progression towards cell death. One such striking altered mechanism is that the simple E → Q conversion by GS no longer defines Müller cell signatures. Remarkably, Müller cells appear to be able to both metabolize E and synthesize Q by yet unknown pathways. The nature of the signature variability is also unclear. It is possible that it is part of a common degeneration response pathway (which all Müller cells enter) where they are no longer synchronized with one another. This possibility will require the ability to track the changes in a group of cells over time. But the precision of normal Müller cell signatures is equally mysterious, as we know of no homeostatic synchronizer for cellular metabolism.

Extensive metabolic variation in remodeling retina is confounded by the fact that the changes do not follow patterns predicted by our current understanding of amino acid recycling. While the nonstoichiometric variation of E, Q, and GS is perplexing, it is not without possible explanation. It has been previously pointed out that GS is the not the only enzyme that uses E as a substrate, nor is there a known enzymatic cluster that exclusively controls E levels (Marc, 2004; McKenna, 2007). E is a primary carbon skeleton for a host of biochemical processes. A possible route for E metabolism in the absence of GS is the TCA cycle (Poitry et al., 2000). Previous studies in brain have shown that under acute increases in extracellular E (>200 μM) as much as 25% of extracellular E is metabolized via the TCA cycle generating lactate and aspartate (McKenna et al., 1996). This may provide a mechanism to supply energy demands of a pathologic system given the increase in the production of stress marker proteins (e.g. GFAP), Müller cell hypertrophy, and neuronal neuritegenesis. Other pathways that may explain the Q accumulation and E metabolism are alternate transaminases that could become expressed, activated or simply unmasked under conditions of degeneration (Michal, 1999; Reichenbach and Bringmann, 2010). One such aminotransferase is alanine aminotransferase (ALAT or ALT), which catalyzes the formation of alanine and alpha-ketoglutarate (αKG) from glutamate. These products combined with lactate may synthesize Q, either in the Müller cells, or may be transported to neurons as a precursor for glutamate. Further investigation into the accumulation of Q in some Müller cells, in the absence of GS, will be required.

The other signature characteristics observed in the late stage degenerating retina have numerous possible pathways and mechanisms by which they arise. One such mechanism is an alteration of taurine transport, because no cell of the neural retina synthesizes taurine (Marc et al., 1998b). Since the outer retina collapses in retinal remodeling with the ultimate emergence of a glial seal between the neural retina and any remaining RPE cells (Jones and Marc, 2005; Jones et al., 2011), it may be that some Müller cells

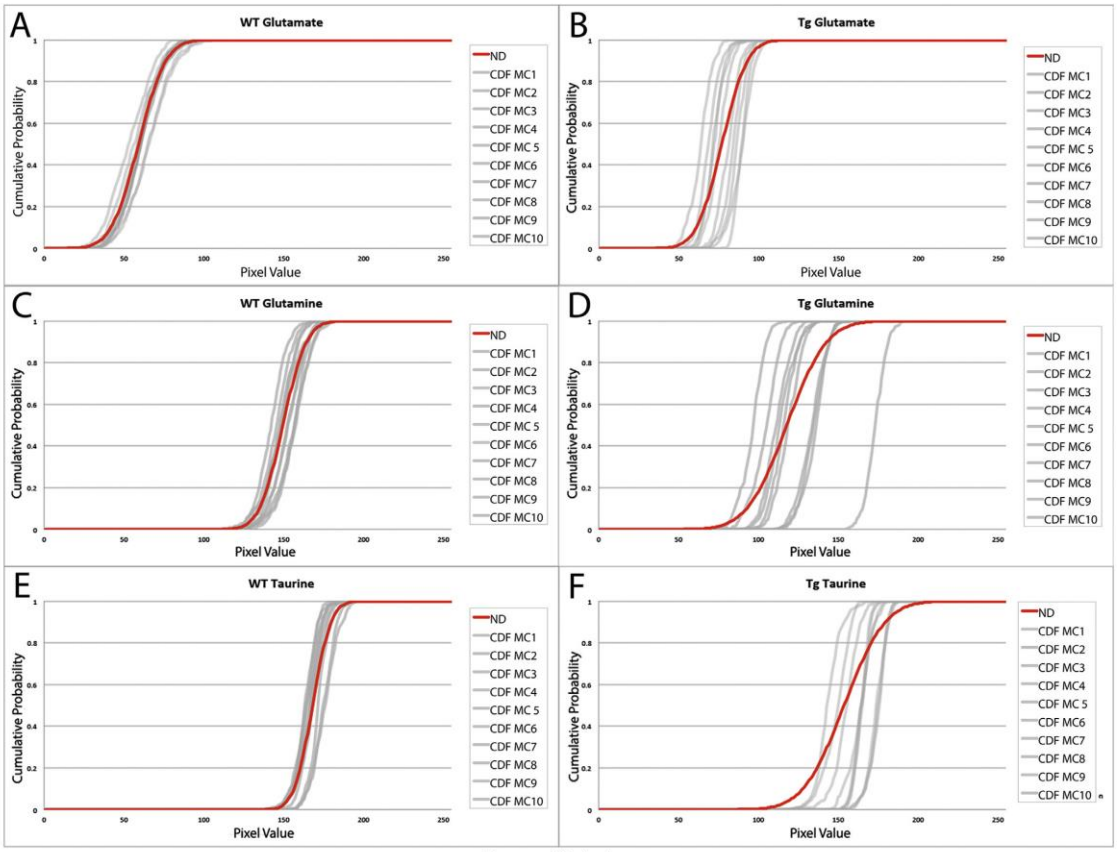

Fig. 5. Cumulative distribution frequencies (CDFs) of the entire Müller cell cohorts in the regions displayed in 4C–F (red Normal Distribution (ND) line) in addition to 10 4 × 4 μm regions from WT and degenerate retina (MC1-10 CDFs) as gray lines. On the left is the WT retina in which the CDFs align closely with the normal distribution. On the right is a horizontal section from a TgP347L rabbit. The CDFs from 4 × 4 μm regions of those Müller cells result in widely varying CDFs that coincide with the normal distribution only in rare cases.

are buried beneath layers of other Müller cell processes and any transport of taurine from the subretinal space may vary across Müller cells. The varied levels of glutathione is consistent with previous and ongoing studies of retinal degeneration and injury in multiple models and is also found in human RP (Marc et al., 2007, 2008; Jones et al., 2016a, Jones et al., 2016b). Glutathione increase in Müller cells is likely associated with oxidative stress and one of the multiple pathways glutamate is metabolized by in the absence of GS. This however, cannot account for the total concentration of glutamate being metabolized. The continued variation of protein and small molecules demonstrates that remodeled Müller cells do not correlate their metabolomes with their neighbors.

These observations illustrate and quantify chaotic metabolic variations across Müller cells in the degenerating retina. Clearly, Müller cells have the capacity to independently respond variably to retinal stress, driving wide deviation from the robust, precise metabolic profile of the Müller cell cohort in healthy retina. The ability to deviate so widely from healthy Müller cells without showing signs of Müller cell death raises the intriguing question of what maintains the homogeneity of Müller cells in the non-pathologic state? Also, once metabolic chaos is initiated, can we reverse it and restore Müller cells to a uniform support network? The understanding of these fundamental questions will be essential to the development of robust therapeutic interventions for retinal degeneration since a lack of consistent metabolic support by Müller cells will make sustainable neurotransmission unlikely.

Acknowledgements:

Supported by: EY015128 (RM), NIH EY02576 (RM), EY014800 Vision Core, an unrestricted grant from Research to Prevent Blindness to the Moran Eye Center; Edward N. and Della L. Thome Memorial Foundation grant for Age-Related Macular Degeneration Research (BWJ), a Research to Prevent Blindness Career Development Award (BWJ), Moran Eye Center Tiger Team Translational Medicine Award (BWJ).

References

Aguirre, G., 1978. Retinal degenerations in the dog. I. Rod dysplasia. Exp. Eye Res. 26, 233–253.

Anderson, J.R., Jones, B.W., Watt, C.B., Shaw, M.V., Yang, J.H., Demill, D.,

Lauritzen, J.S., Lin, Y., Rapp, K.D., Mastronarde, D., Koshevoy, P., Grimm, B., Tasdizen, T., Whitaker, R., Marc, R.E., 2011. Exploring the retinal connectome. Mol. Vis. 17, 355–379.
Anderson, J.R., Jones, B.W., Yang, J.H., Shaw, M.V., Watt, C.B., Koshevoy, P., Spaltenstein, J., Jurrus, E., Kannan, U.V., Whitaker, R.T., Mastronarde, D., Tasdizen, T., Marc, R.E., 2009. A computational framework for ultrastructural mapping of neural circuitry. PLoS Biol. 7, e1000074.
Barnett, K.C., Curtis, R., 1985. Autosomal dominant progressive retinal atrophy in Abyssinian cats. J. Hered. 76, 168–170.
Bignami, A., Dahl, D., 1979. The radial glia of Müller in the rat retina and their response to injury. An immunofluorescence study with antibodies to the glial fibrillary acidic (GFA) protein. Exp. Eye Res. 28, 63–69.
Bourne, M.C., Campbell, D.A., Tansley, K., 1938. Hereditary degeneration of the rat retina. Br. J. Ophthalmol. 22, 613–623.
Bringmann, A., Grosche, A., Pannicke, T., Reichenbach, A., 2013. GABA and glutamate uptake and metabolism in retinal glial (Muller) cells. Front. Endocrinol. 4, 48.
Brockerhoff, S.E., Hurley, J.B., Janssen-Bienhold, U., Neuhauss, S.C., Driever, W., Dowling, J.E., 1995. A behavioral screen for isolating zebrafish mutants with visual system defects. Proc. Natl. Acad. Sci. U. S. A. 92, 10545–10549.
Chader, G.J., 2002. Animal models in research on retinal degenerations: past progress and future hope. Vis. Res. 42, 393–399.
Chang, B., Hawes, N.L., Hurd, R.E., Davisson, M.T., Nusinowitz, S., Heckenlively, J.R., 2002. Retinal degeneration mutants in the mouse. Vis. Res. 42, 517–525.
Chow, C.Y., Kelsey, K.J., Wolfner, M.F., Clark, A.G., 2016. Candidate genetic modifiers of retinitis pigmentosa identified by exploiting natural variation in Drosophila. Hum. Mol. Genet. 25 (4), 651–659.
Crawford, J.R., Garthwaite, P.H., 2012. Single-case research in neuropsychology: a comparison of five forms of t-test for comparing a case to controls. Cortex 48, 1009–1016 a journal devoted to the study of the nervous system and behavior.
Crawford, J.R., Howell, D.C., 1998. Comparing an individual's test score against norms derived from small samples. Clin. Neuropsychol. 12, 482–486.
Dreher, Z., Robinson, S.R., Distler, C., 1992. Müller cells in vascular and avascular retinae: a survey of seven mammals. J. Comp. Neurol. 323, 59–80.
Erickson, P.A., Fisher, S.K., Guerin, C.J., Anderson, D.H., Kaska, D.D., 1987. Glial fibrillary acidic protein increases in Muller cells after retinal detachment. Exp. Eye Res. 44, 37–48.
Fisher, S.K., Lewis, G.P., 2003. Muller cell and neuronal remodeling in retinal detachment and reattachment and their potential consequences for visual recovery: a review and reconsideration of recent data. Vis. Res. 43, 887–897.
Griciuc, A., Aron, L., Ueffing, M., 2012. Looking into eyes: rhodopsin pathologies in Drosophila. Adv. Exp. Med. Biol. 723, 415–423.
Han, J., Dinculescu, A., Dai, X., Du, W., Smith, W.C., Pang, J., 2013. Review: the history and role of naturally occurring mouse models with Pde6b mutations. Mol. Vis. 19, 2579–2589.
Hurley, J.B., Lindsay, K.J., Du, J., 2015. Glucose, lactate, and shuttling of metabolites in vertebrate retinas. J. Neurosci. Res. 93, 1079–1092.
Jones, B.W., Kondo, M., Terasaki, H., Lin, Y., McCall, M., Marc, R.E., 2012. Retinal remodeling. Jpn. J. Ophthalmol. 56, 289–306.
Jones, B.W., Kondo, M., Terasaki, H., Watt, C.B., Rapp, K., Anderson, J., Lin, Y., Shaw, M.V., Yang, J.H., Marc, R.E., 2011. Retinal remodeling in the Tg P347L rabbit, a large-eye model of retinal degeneration. J. Comp. Neurol. 519, 2713–2733.
Jones, B.W., Marc, R.E., 2005. Retinal remodeling during retinal degeneration. Exp. Eye Res. 81, 123–137.
Jones, B.W., Watt, C.B., Frederick, J.M., Baehr, W., Chen, C.K., Levine, E.M., Milam, A.H., Lavail, M.M., Marc, R.E., 2003. Retinal remodeling triggered by photoreceptor degenerations. J. Comp. Neurol. 464, 1–16.
Jones, B.W., Watt, C.B., Marc, R.E., 2005. Retinal remodeling. Clin. Exp. Optom. 88, 282–291.
Jones, B.W., Pfeiffer, R.L., Ferrell, W.D., Watt, C.B., Marmor, M., Marc, R.E., 2016a. Retinal remodeling in human retinitis pigmentosa. Exp. Eye Res. 150, 149–165. http://www.ncbi.nlm.nih.gov/pubmed/27020758.
Jones, B.W., Pfeiffer, R.L., Ferrell, W.D., Watt, C.B., Tucker, J.F., Marc, R.E., 2016b. Retinal remodeling and metabolic alterations in human AMD. Front. Cell. Neurosci. (in press) http://journal.frontiersin.org/article/10.3389/fncel.2016.00103/full.
Kalloniatis, M., Fletcher, E.L., 1993. Immunocytochemical localization of the amino acid neurotransmitters in the chicken retina. J. Comp. Neurol. 336, 174–193.
Kalloniatis, M., Marc, R.E., Murry, R.F., 1996. Amino acid signatures in the primate retina. J. Neurosci. Off. J. Soc. Neurosci. 16, 6807–6829.
Keeler, C.E., 1924. The inheritance of a retinal abnormality in white mice. Proc. Natl. Acad. Sci. U. S. A. 10, 329–333.
Kolb, H., Gouras, P., 1974. Electron microscopic observations of human retinitis pigmentosa, dominantly inherited. Investig. Ophthalmol. 13, 487–498.
Kondo, M., Sakai, T., Komeima, K., Kurimoto, Y., Ueno, S., Nishizawa, Y., Usukura, J., Fujikado, T., Tano, Y., Terasaki, H., 2009. Generation of a transgenic rabbit model of retinal degeneration. Investig. Ophthalmol. Vis. Sci. 50, 1371–1377.
Luna, G., Lewis, G.P., Banna, C.D., Skalli, O., Fisher, S.K., 2010. Expression profiles of nestin and synemin in reactive astrocytes and Müller cells following retinal injury: a comparison with glial fibrillar acidic protein and vimentin. Mol. Vis. 16, 2511–2523.
Marc, R., Pfeiffer, R., Jones, B., 2014. Retinal prosthetics, optogenetics, and chemical photoswitches. ACS Chem. Neurosci. 5, 895–901.
Marc, R.E., 1992. The structure of GABAergic circuits in ectotherm retinas. In: Mize, R., Marc, R.E., Sillito, A. (Eds.), GABA in the Retina and Central Visual System. Elsevier, Amsterdam, pp. 61–92.
Marc, R.E., 1999. Mapping glutamatergic drive in the vertebrate retina with a channel-permeant organic cation. J. Comp. Neurol. 407, 47–64.
Marc, R.E., 2004. Retinal neurotransmitters. In: Chalupa, L.M., Werner, J. (Eds.), The Visual Neurosciences. MIT Press, Cambridge MA, pp. 315–330.
Marc, R.E., Cameron, D., 2001. A molecular phenotype atlas of the zebrafish retina. J. Neurocytol. 30, 593–654.
Marc, R.E., Jones, B.W., 2002. Molecular phenotyping of retinal ganglion cells. J. Neurosci. Off. J. Soc. Neurosci. 22, 413–427.
Marc, R.E., Jones, B.W., 2003. Retinal remodeling in inherited photoreceptor degenerations. Mol. Neurobiol. 28, 139–147.
Marc, R.E., Jones, B.W., Anderson, J.R., Kinard, K., Marshak, D.W., Wilson, J.H., Wensel, T., Lucas, R.J., 2007. Neural reprogramming in retinal degeneration. Investig. Ophthalmol. Vis. Sci. 48, 3364–3371.
Marc, R.E., Jones, B.W., Watt, C.B., Strettoi, E., 2003. Neural remodeling in retinal degeneration. Prog. Retin. Eye Res. 22, 607–655.
Marc, R.E., Jones, B.W., Watt, C.B., Vazquez-Chona, F., Vaughan, D.K., Organisciak, D.T., 2008. Extreme retinal remodeling triggered by light damage: implications for age related macular degeneration. Mol. Vis. 14, 782–806.
Marc, R.E., Murry, R.F., Basinger, S.F., 1995. Pattern recognition of amino acid signatures in retinal neurons. J. Neurosci. Off. J. Soc. Neurosci. 15, 5106–5129.
Marc, R.E., Murry, R.F., Fisher, S.K., Linberg, K.A., Lewis, G.P., 1998a. Amino acid signatures in the detached cat retina. Investig. Ophthalmol. Vis. Sci. 39, 1694–1702.
Marc, R.E., Murry, R.F., Fisher, S.K., Linberg, K.A., Lewis, G.P., Kalloniatis, M., 1998b. Amino acid signatures in the normal cat retina. Investig. Ophthalmol. Vis. Sci. 39, 1685–1693.
Marc, R.E., Wei-Ley, S., Kalloniatis, M., Raiguel, S.F., Van Haesendonck, E., 1990. Patterns of glutamate immunoreactivity in the goldfish retina. J. Neurosci. 10, 4006–4034.
McKenna, M.C., 2007. The glutamate-glutamine cycle is not stoichiometric: fates of glutamate in brain. J. Neurosci. Res. 85, 3347–3358.
McKenna, M.C., Sonnewald, U., Huang, X., Stevenson, J., Zielke, H.R., 1996. Exogenous glutamate concentration regulates the metabolic fate of glutamate in astrocytes. J. Neurochem. 66, 386–393.
Michal, G., 1999. Amino acids and derivatives. In: Biochemical Pathways: an Atlas of Biochemistry and Molecular Biology, vol. 1. John Wiley & Sons Inc., New York, pp. 46–58.
Narfstrom, K., 1983. Hereditary progressive retinal atrophy in the Abyssinian cat. J. Hered. 74, 273–276.
Newman, E.A., Frambach, D.A., Odette, L.L., 1984. Control of extracellular potassium levels by retinal glial cell K+ siphoning. Science 225, 1174–1175.
Petters, R.M., Alexander, C.A., Wells, K.D., Collins, E.B., Sommer, J.R., Blanton, M.R., Rojas, G., Hao, Y., Flowers, W.L., Banin, E., Cideciyan, A.V., Jacobson, S.G., Wong, F., 1997. Genetically engineered large animal model for studying cone photoreceptor survival and degeneration in retinitis pigmentosa. Nat. Biotechnol. 15, 965–970.
Pittler, S.J., Keeler, C.E., Sidman, R.L., Baehr, W., 1993. PCR analysis of DNA from 70-year-old sections of rodless retina demonstrates identity with the mouse rd defect. Proc. Natl. Acad. Sci. U. S. A. 90, 9616–9619.
Poitry, S., Poitry-Yamate, C., Ueberfeld, J., MacLeish, P.R., Tsacopoulos, M., 2000. Mechanisms of glutamate metabolic signaling in retinal glial (Muller) cells. J. Neurosci. Off. J. Soc. Neurosci. 20, 1809–1821.
Pow, D.V., Robinson, S.R., 1994. Glutamate in some retinal neurons is derived solely from glia. Neuroscience 60, 355–366.
Reichenbach, A., Bringmann, A., 2010. Muller cells in the healthy retina. In: Muller Cells in the Healthy and Diseased Retina. Springer Science+Business Media, LLC.
Riepe, R.E., Norenburg, M.D., 1977. Muller cell localisation of glutamine synthetase in rat retina. Nature 268, 654–655.
Roesch, K., Stadler, M.B., Cepko, C.L., 2012. Gene expression changes within Müller glial cells in retinitis pigmentosa. Mol. Vis. 18, 1197–1214.
Rowan, S., Cepko, C.L., 2004. Genetic analysis of the homeodomain transcription factor Chx10 in the retina using novel multifunctional BAC transgene mouse reporter. Dev. Biol. 271, 388–402.
Schneider, C.A., Rasband, W.S., Eliceiri, K.W., 2012. NIH image to image J: 25 years of image analysis. Nat. Methods 9, 671–675.
Semple-Rowland, S.L., Lee, N.R., 2000. Avian models of inherited retinal disease. Methods Enzymol. 316, 526–536.
Strettoi, E., Pignatelli, V., Rossi, C., Porciatti, V., Falsini, B., 2003. Remodeling of second-order neurons in the retina of rd/rd mutant mice. Vis. Res. 43, 867–877.
Strettoi, E., Porciatti, V., Falsini, B., Pignatelli, V., Rossi, C., 2002. Morphological and functional abnormalities in the inner retina of the rd/rd mouse. J. Neurosci. Off. J. Soc. Neurosci. 22, 5492–5504.
Suber, M.L., Pittler, S.J., Qin, N., Wright, G.C., Holcombe, V., Lee, R.H., Craft, C.M., Lolley, R.N., Baehr, W., Hurwitz, R.L., 1993. Irish setter dogs affected with rod/cone dysplasia contain a nonsense mutation in the rod cGMP phosphodiesterase beta-subunit gene. Proc. Natl. Acad. Sci. U. S. A. 90, 3968–3972.
Wilson, D.J., 2002. 2-deoxy-d-glucose uptake in the inner retina: an in vivo study in the normal rat and following photoreceptor degeneration. Trans. Am. Ophthalmol. Soc. 100, 353–364.

CHAPTER 4

EVALUATION OF EXCITOTOXICITY AS A MECHANISM OF RETINAL DEGENERATION

4.1 Introduction

Müller cells are well known to play important roles in structural and metabolic processes of the retina. They provide central metabolic support to the surrounding cells, particularly in the glutamate cycle.[1-2] Müller cells are the only cells of the retina which possess glutamine synthetase.[2] In the primary glutamate cycle, glutamate is released from excitatory neurons and perisynaptic Müller cell processes transport the extra cellular glutamate into Müller cells, primarily via EAAT1 (excitatory amino acid transporter 1), also referred to as GLAST (glutamate/aspartate transporter).[3] Upon entering the Müller cell, glutamine synthetase rapidly converts glutamate to glutamine by amidation. Following the conversion to glutamine within the Müller cell, glutamine is exported into the extracellular space by glial SN1.[4-5] In all neurons, but especially in GABAergic and glutamatergic neurons, glutamine can be converted back to glutamate by glutaminase (EC 3.5.1.2). Glutamate can now be loaded into vesicles via vesicular glutamate transporters (VGLUT) and released upon depolarization or converted to GABA by glutamate decarboxylase (EC 4.1.1.15) and loaded into vesicles via VGAT (which transports both GABA and glycine). The role of Müller glia is integral to both the extracellular glutamate

clearance and the synthesis of glutamate and GABA within the retina.

Given this central role of Müller cells and glutamine synthetase in retinal glutamate metabolism, it is reasonable to expect that any disruption of this system could be detrimental to the maintenance of glutamate homeostasis in the retina. However, the role of Müller glia during retinal degeneration and whether the changes observed in the glutamate cycle are a cause or result of the degeneration are unclear and current topics of investigation. One popular hypothesis is the possibility of glutamate excitotoxicity in the retina contributing to neuronal degeneration of distressed retina.[6-8]

4.1.1 Excitotoxicity Hypothesis

One proposed mechanism of retinal degeneration is excitotoxicity-mediated degeneration. This concept was originally introduced by Lucas and Newhouse in 1957, where they demonstrated high levels of glutamate can be toxic to neural systems.[9] Excitotoxicity as a mechanism of not only brain injury, but as a factor contributing to neural death during retinal degeneration, has been supported by other studies.[6-7, 10-11] A study that proposed a possible mechanism of excitotoxic injury was by Szatkowski, Barbour, and Attwell in 1990.[12] They demonstrated that under conditions of high extracellular potassium, and high intracellular sodium and glutamate, a nonvesicular mechanism of glutamate release could be evoked from retinal Müller cells, indicating that Müller cells could potentially lose their capacity to adequately sequester glutamate away from neurons, which would be a likely component contributing to the development of an excitotoxic environment.

Another study investigating the potential role of excitotoxicity in retinal

degeneration was conducted on the *rd1* mouse.[13] The *rd1* mouse is a model of retinitis pigmentosa in which the mouse has early onset retinal degeneration, beginning with the loss (actually a failure to completely develop followed by cell death) of rod photoreceptors.[14] Delyfer et al. used a chemiluminescence detection system to analyze the ratio of given amino acids to the total amino acid concentration.[13] They found that the levels of glutamate, glutamine, and glycine were all significantly higher in the *rd1* mouse than in the control. These data indicate a deficiency in the metabolism of core amino acids as degeneration progresses. Of importance to the question of glutamate-meditated excitotoxicity: Could the significant increase in the levels of glutamate within the degenerate retina could be contributing to the phase 2 photoreceptor degeneration or phase 3 neuronal seen in the *rd1* mouse?

In addition to the aforementioned papers, which are primarily focused on the Müller glia's ability to properly sequester glutamate, much of the excitotoxicity argument is based on ionotropic glutamate receptor associated toxicity. Ionotropic glutamate receptors (iGluRs) are postsynaptic ligand-gated ion channels, divided into three classes: N-methyl-D-aspartate (NMDA), α-amino-3-hydroxy-5-methyl-4-isoxazolepionic acid (AMPA), and kainate (KA) receptors. AMPA and NMDA receptors are both calcium permeable when bound by glutamate (KA receptors are less Ca-permeant), and excessive calcium following sustained glutamate activation is thought to be the primary mechanism causing neural death in excitotoxicity.[15] AMPA and KA receptors are often lumped together as ionotropic non-NMDA receptors, as NMDA is an agonist at neither while KA and AMPA are agonists both, as is quisqualate. The effects of persistent AMPAR activation have been evaluated via KA administration. KA is a selective ionotropic glutamate receptor agonist, which

binds to KA receptors with high affinity and activates currents with fast desensitization, and binds with lower affinity to more prevalent receptors, but does not desensitize, producing a sustained cation current. Previous studies demonstrate that when KA is applied to the retina it greatly outcompetes glutamate for the AMPARs available on a large number of cell types within the retina, including but not limited to: starburst amacrine cells, AII amacrine cells, bipolar cells, and ganglion cells; sustained AMPAR sensitization can trigger apoptotic mechanisms.[16] In addition to the studies into AMPARs potential role in mediating excitotoxicity, NMDARs have been implicated in contributing to neural death.[17] The sustained sensitization of NMDARs or AMPARs can lead to a prolonged increase in intracellular calcium within the cell, leading to cell death.

4.1.2 Evidence Disputing Excitotoxicity

The role of glutamine synthetase in the glutamate cycle of the neural retina was clearly shown by Pow and Robinson[18] in which they used the suicide inhibitor D,L-methionine D,L-sulphoximine (MSO) to inhibit glutamine synthetase (GS) activity in a normal rabbit retina. This demonstrated that following the inhibition of glutamine synthetase, bipolar and ganglion cells of the neural retina no longer exhibit any glutamate immunoreactivity (although the Marc lab has somewhat conflicting unpublished results). In contrast, Müller cells are extremely immunoreactive for glutamate as they no longer possess active GS to convert glutamate to glutamine. Of special interest to the question of excitotoxicity, they also tested the effect of increasing the extracellular levels of glutamate 5 fold (35µM), and this also failed to elicit an increase in glutamate levels in bipolar or ganglion cells.

Marc et al. examined the role of the glutamate cycle in injury models of retinal degeneration using amino acid signatures of detached cat retina.[19] Following detachment, Müller cells quickly lose their ability to convert glutamate to glutamine as seen by a decrease in Müller cell levels of glutamine and increases in glutamate. Consistent with the results of Pow and Robinson, this loss of apparent glutamine synthetase activity leads to a large increase in levels of intracellular glutamate in Müller cells (~5mM). Although glutamate concentration does later recover in neurons between days 6-30 of detachment, it is still substantially less glutamate than is found in neurons of the healthy retina and never regains normal levels.

In addition to the alterations in glutamate-glutamine cycle in an injury model of retinal degeneration and remodeling, many immunocytochemical studies of metabolic changes have been performed on a variety of gene defect models of retinal degeneration.[20-22] In all of these studies there is a stereotypic pattern to the degeneration of the retina and the responses of the Müller cells, which are extremely similar to those seen in the injury induced model. Pfeiffer et al., showed a rise in the glutamine and glutamine synthetase levels in Müller cells.[23] This rise in glutamine synthetase and glutamine subsequently dissipated as the retina continued to degenerate and remodel.[24] Glutamate levels have been reported to either increase[20] in Müller cells, or decrease.[22] This inconsistency between studies is probably the result of variation in time points in addition to the large variability in amino acid signatures that can be observed between individual Müller cells in degenerated retina.[20, 23, 25] The overall trend in the degenerate retina is a decline in neuronal glutamate and glutamine as the retina degenerates, however, it appears that following the initial decline there is some recovery, but it never again reaches normal levels. This

variability between Müller cells of glutamine, glutamate, and glutamine synthetase and its metabolic impact on surrounding retina warrants further investigation, however, none of these studies indicate excitotoxicity as a component of the degeneration.

In this paper we examine the response of Müller cells to retinal degeneration over time, and whether the Müller cell metabolism alterations found in RP are likely to contribute to an excitotoxic mechanism of degeneration. Primarily identifying how the levels of glutamate and glutamine respond to the loss of glutamine synthetase during phase 3 remodeling and degeneration, and how glutamate transport capabilities of Müller cells are affected.

4.2 Materials and Methods

4.2.1 Model Systems

The transgenic rabbit model of autosomal dominant retinitis pigmentosa (Tg P347L), described in Chapters 2 and 3,[24] was used for the assessment of metabolic variability using quantitative glutamine synthetase immunocytochemistry, quantitative CMP for glutamine, glutamate comparison analysis, and quantitative D-Aspartate loading. Six Tg rabbits spanning in ages from 1.5 years to 6+ years were used, with 3 wild-type (wt) littermates spanning 1.5 to 8 years used as controls. All animal experiments were conducted according to the ARVO Statement for the use of animals in ophthalmic and vision research with the supervision and approval of the Institutional Animal Care and Use Committee (IACUC) at the University of Utah. In addition, two human specimens, aged 21 and 77, diagnosed with RP were collected within 5 hours post mortem. RP tissues were obtained from two sources: The Foundation Fighting Blindness Retina Donor Program at Stanford

University and the University of Utah Lions Eye Bank. Genotyping of donors was not available and the mutations involved are unknown. Institutional approval for use of human eyes was obtained from the University of Utah and Stanford University and followed the tenets of the Declaration of Helsinki. All retinal tissues and data were de-identified in accordance with HIPPA Privacy Rules. These specimens were processed for CMP and used for analysis of variability.

4.2.2 Tissue Processing

Rabbit and human tissues were processed identically to those in Chapter 3, utilizing mixed aldehyde fixation for small molecules and proteins. In addition to the immediate fixation of many retinal samples, some retinas were processed for D-Aspartate (D-Asp) transport capabilities. In these cases, retinal chips ≈ 10-30 mm^2 were transferred to cellulose acetate filter discs and bathed in 35°C Ames medium[26] equilibrated with 95% O_2/5% CO_2 for 2-5 min. Following equilibration, some chips were then transferred to Ames media containing D-Aspartate (D-Asp) at 5 mM (a saturating level for EAATs), to evaluate the transport functions of Müller cells in the intact retina[27] prior to fixation. All other chips were immediately transferred to mixed aldehyde fixation buffers.

4.2.3 CMP Analysis

CMP analysis of retinas was conducted as described in Chapter 3, which yields quantitative immunohistochemistry allowing us to directly compare levels of metabolites between samples. The previous chapters have described using k-means and isodata unsupervised classification to track the variability of Müller cells in representative fields.

In this study we sought to better understand the extent of the metabolic variability in degenerate retina. To fully characterize the metabolic changes occurring in Müller cells during degeneration, we argue it is necessary to quantify the number of Müller cell metabolic states in a selected sample. To perform this type clustering, a fusion version of unsupervised and supervised classification methods called intraclass separability analysis was used. First, the clusters of distinct Müller cell metabolic states generated from ISODATA classification were used to gain an idea of the total number of metabolic subclasses within the Müller cell class. Using this map, supervised classification using PCI Geomatica (Richmond Hill, Ontario, Canada) was performed as follows: Between 20-25 seed points were set in the training component of supervised classification using raster seeding in which 6 input theme map channels were used (Taurine (τ), Glutamine Synthetase (GS), Glutamine (Q), Glutamate (E), Glutathione (J), and retinaldehyde-binding protein 1 (CRALBP)). The pixel tolerance was set at 12 with an 8-connected neighborhood, allowing enough brightness variability to account for pixelation. From these seed points a Bhattacharyya Distance statistic was run on all seed points and any points with a separability of >1.9 were merged into a single metabolic class. A Bhattacharyya Distance of greater than 1.9 is equivalent to a *p*-value of <0.01. From this training channel, a maximum likelihood with a NULL class classification was run on the entire sample generating a theme map of the Müller cells and their separable metabolic variability.

4.3 Results

Previous studies have shown Müller cells diverge from one another in an increasingly chaotic fashion,[20, 24-25] however, the impact of this chaotic divergence and its

impact on the glutamate cycle is currently unknown. First, we demonstrate that the chaotic divergence of Müller cell metabolic signatures of rabbit retina is also present in human retinal degenerations (Figure 4.1). Levels of taurine, glutamine, and glutamate (red, green, and blue respectively), vary dramatically between Müller cells, including neighboring Müller cells as seen indicated by the red circle (Figure 4.1A). This variability continues throughout degeneration in rabbits (Figure 4.1B). It is also observed relatively early in humans (Figure 4.1C, 21 year old affected by recessive RP), and continues throughout RP progression (Figure 4.1D, 77 year old affected by unknown but likely dominant RP). This demonstrates that the variability found in rabbits is not unique.

The observed variety of metabolic signatures in Müller cells led us to further classify the variability between Müller cell signatures within small regions of degenerate retina. Using intraclass separability analysis (see Section 4.2.3), Müller cells within a representative vertical region of intact retina classify into 6 metabolic states (Figure 4.2). This metabolic state separability is further distinguishable by Bhattacharyya distance (>1.9). The observed subclass separability is never found across the superclass of Müller cells in a normal retina, where only one class is known. It is of interest to note that these variable states do not occur as a continuum, which is expected if microenvironmental factors cause the variation. Rather all of the observed Müller cell subclasses appear independently of the metabolic states of their neighbors.

As noted in previous descriptions of the metabolic alterations occurring during degeneration.[23-25] GS levels are drastically lower throughout the degenerate retina (albeit to varying extents). This paradoxically occurs simultaneously with the observed global increase in glutamine and stable global concentration of Müller cell glutamate.[24] This is in

stark contrast to the classic model that glutamate and glutamine levels in the retina are stoichiometrically related to the available GS activity. To determine whether this fundamental relationship is maintained despite the degeneration induced heterogeneity observed in Müller cells, we sampled n =5 Müller cells across both healthy and degenerate retinas and evaluated the relative amounts of glutamate, glutamine, and GS. In the healthy retinas, the levels of all three (and thus their ratios) remain constant. In the degenerate retinas, all three metabolites vary widely and independently of one another, conflicting with the standard model of glutamate-glutamine metabolism (Figure 4.3).

It has been previously hypothesized that the decrease in GS is related to a loss in EAAT1 (the main E transporter found on Müller cells) found by the Reichenbach laboratory.[28-29] To test this hypothesis we performed D-Aspartate loading both WT and TgP347L rabbit retinas. Until extremely late stages of degeneration, D-Asp loading, presumably by EAAT1, was fully functional in the degenerate retinas and capable of transporting any extracellular glutamate into Müller cells (Figure 4.4). In aged and neurodegenerate rabbit retinas (Figure 4.4D), some Müller cells appear to have lost glutamate transport capabilities (white arrows). We cannot yet explain the mechanisms allowing for the continued metabolism of glutamate and the increase in Müller cell glutamine, though it is probable that Müller cells with depressed GS activity unmask less commonly observed metabolic pathways. One potential unmasked mechanism is amidation of glutamate into glutamine through transaminase activity.

4.4 Conclusions and Discussion

Three main conclusions may be drawn from this study. First, over the course of retinal degeneration, the chaotic phenotypes that appear in Müller cells not only vary with respect to one another, but diverge into multiple statistically separable metabolic classes. The impact of these states on the surrounding neurons warrants further study. Second, although GS is variably reduced in Müller cells across the retina in degeneration, its level appears to have minor impact on the levels of glutamate or glutamine within the same Müller cells. This implies the existence of a network-based metabolic homeostasis. Third, we see no evidence that Müller cell glutamate transport is drastically altered in response to the metabolic variability observed throughout degeneration, until the degeneration has advanced to a point in which it is unlikely there is a very high quantity of glutamate being released to need sequestration. Previous suggestions that Müller cell glutamate transport fails early in retinal degenerations[6-7] are unsupported by our data. Importantly, our analyses sample hundreds to thousands of adjacent Müller cells and there is no variation in glutamate transport until very late degeneration. Thus the conflicting results are not likely due to sampling differences.

These observations have several implications for retinal degeneration, particularly that arising from retinitis pigmentosa. As levels of GS have no correlated impact in glutamate or glutamine, concentrations within the Müller cells indicates GS is likely not the primary enzyme responsible for glutamate metabolism in the degenerated retina. Based on previous studies in the brain, this is not particularly surprising. This also conflicts with the acute studies of Pow,[18] but it is important to recall that retinal degenerations are chronic steady states. Glutamate is a primary carbon skeleton that may be generated from multiple

enzymatic pathways and contributes to multiple other pathways. We argue that the glutamate-glutamine cycle should be considered less of a stoichiometric biochemical pathway and more of an intersection with many other metabolic pathways.[30] The amount glutamate contributes to one pathway over another is likely to change depending on the metabolic demands of a cell, and in the case of glia, the requirements of the surrounding tissue. There is the caveat of the highly variable metabolic signatures found between Müller cells in close proximity to one another, which indicates a lack of microenvironmental influence over Müller cell metabolism. We do not know what drives the Müller cells to adopt such variability in their metabolic signatures, however to this end, we don't know what causes the metabolism of Müller cells to be so homogeneous in the first place. This question will require further investigation of both healthy retinas and degenerate retinas.

A primary question this study sought to address is whether glutamate excitotoxicity is a likely mechanism contributing to the neurodegeneration observed in the inner retina following the loss of photoreceptors. In a more prosaic sense we ask whether the deaths of photoreceptors and any associated bursts of extracellular glutamate cells pose a challenge to cells that express iGluRs, that is, horizontal, OFF cone bipolar, amacrine and ganglion cells. Based on quantitative immunocytochemical methods of determining levels of glutamate within the intact retina, combined with the D-Asp transport results reported in this chapter, we do not find evidence that levels of extracellular glutamate are likely to rise for a sustained period of time. Although the traditional view of excitotoxicity has been largely regarded as a component of retinal degeneration, more recent studies,[22] combined with ours, have largely called this view into question. For excitotoxicity to cause cell stress and death, sustained activity by high levels of glutamate are required, as well as expression

of iGluRs. Our results indicate that Müller cells continue to transport glutamate with no apparent change in Vmax long after neurodegeneration has greatly reduced the neural population of the retina. Although it is possible that there are local spikes in glutamate due to photoreceptor death, any downstream neuronal death would have to occur in minutes (rather than the reported days in the fastest models[31]) to potentially overwhelm functional Müller cell transport.[32] Therefore we conclude glutamate-mediated excitotoxicity is not likely to significantly contribute to the neuronal death observed in retinal degenerative diseases.

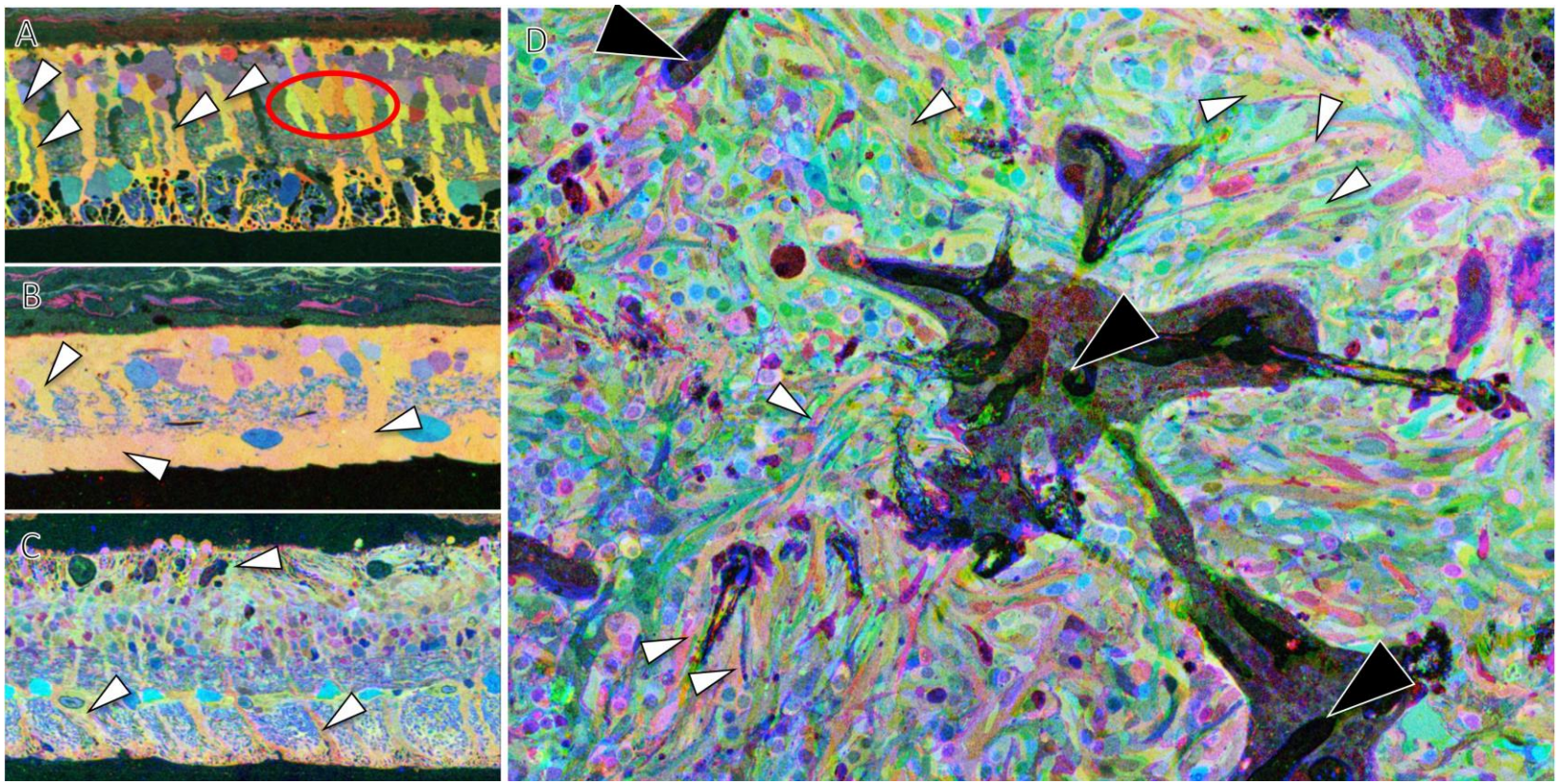

Figure 4.1 Müller cell metabolic variation across retinal regions and species. All are RGB registered projections of adjacent images of amino acid immunoreactivity; red = T, green = Q, and blue = E. Color variance in an individual image indicates varying ratios of TQE, and variance in concentration. A) Vertical section through central portion of rabbit retina. Arrows indicate select Müller cells demonstrating high variability. Ellipse highlights 5 Müller cells directly adjacent to one another all with varying metabolic profiles in comparison to their direct neighbor. B) Vertical section through peripheral region of TgP347L degenerate rabbit retina that has undergone massive remodeling and cell death. Arrows indicate Müller cells with varying metabolic profiles. C) Vertical section from a deceased 21yo male affected by early onset retinitis pigmentosa. Arrows indicate Müller cells, with varying levels of metabolites. D**)** Horizontal section of retina from 77 yo male affected by retinitis pigmentosa. Black arrows indicate blood vessels. White arrows indicate select Müller cells with drastically varying levels of metabolites

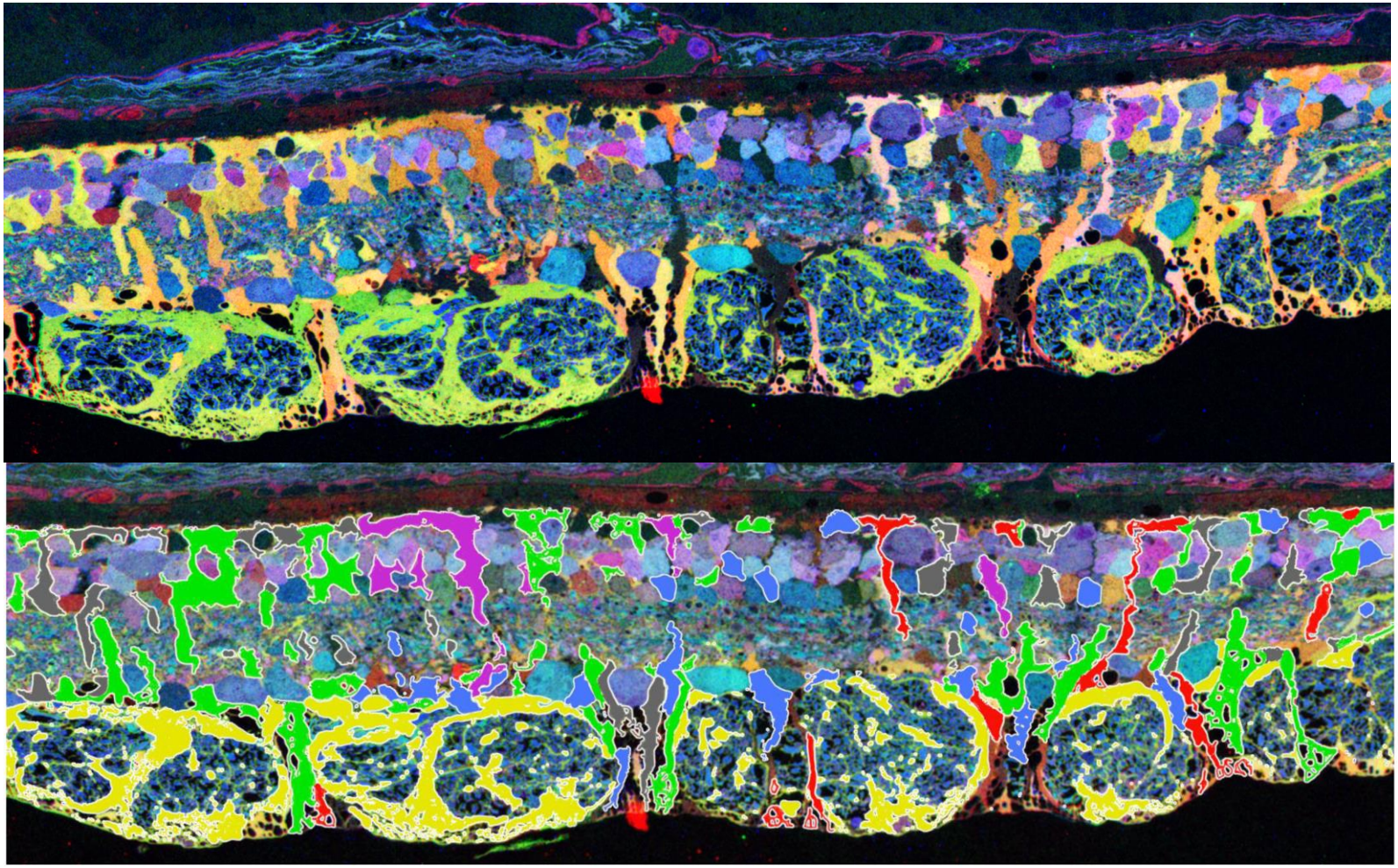

Figure 4.2: Müller cell metabolic variation within Müller cells. Base image is RGB registered projections of amino acid immunoreactivity with red = T, green = Q, and blue = E. Overlaid colors outlined in white are a representative mask based on the 6 Müller cell metabolic states a vertical section of Tg P347L retina. The mask was formed as described in the Methods section by intraclass separability analysis. Masks of similar color indicate metabolic states that are not highly separable from one another. Masks of differing color indicate that the metabolic states of the underlying Müller cell are significantly separable from one another via Bhattacharyya distance analysis

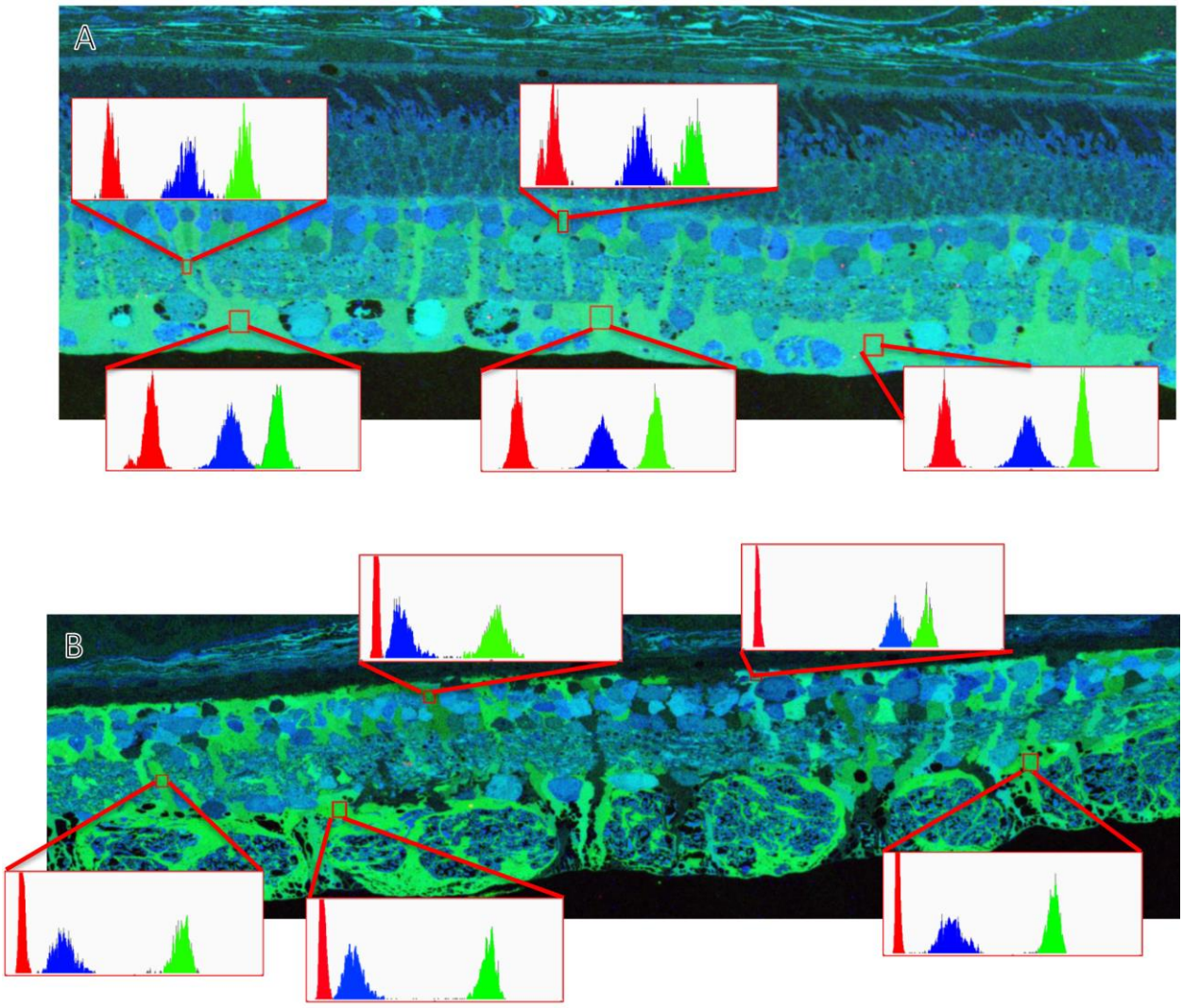

Figure 4.3 GS/Q/E variability in WT compared to degenerate retina. Images are RGB registered images of molecular immunoreactivity with red = GS, green = Q, and blue = E. Images are inverted to display intensity, similar to that of fluorescence. Colors in histogram plots are indicative of the same channel as in the RGB image. A) WT retina with 5 selected Müller cell regions. Pixel values for the sampled regions vary slightly, but the location of the individual peaks remains relatively constant indicating consistent concentrations of GS, Q, and E. B) Degenerate retina with 5 selected Müller cell regions. GS (in red) varies only slightly because the quantity of GS in this region of degenerate retina is extremely low. Despite the overall low concentrations of GS, the levels of E (blue) and Q (green) vary dramatically. Both may be higher or lower than is found in WT Müller cells, but variance does not appear to correlate with each other in any consistent way.

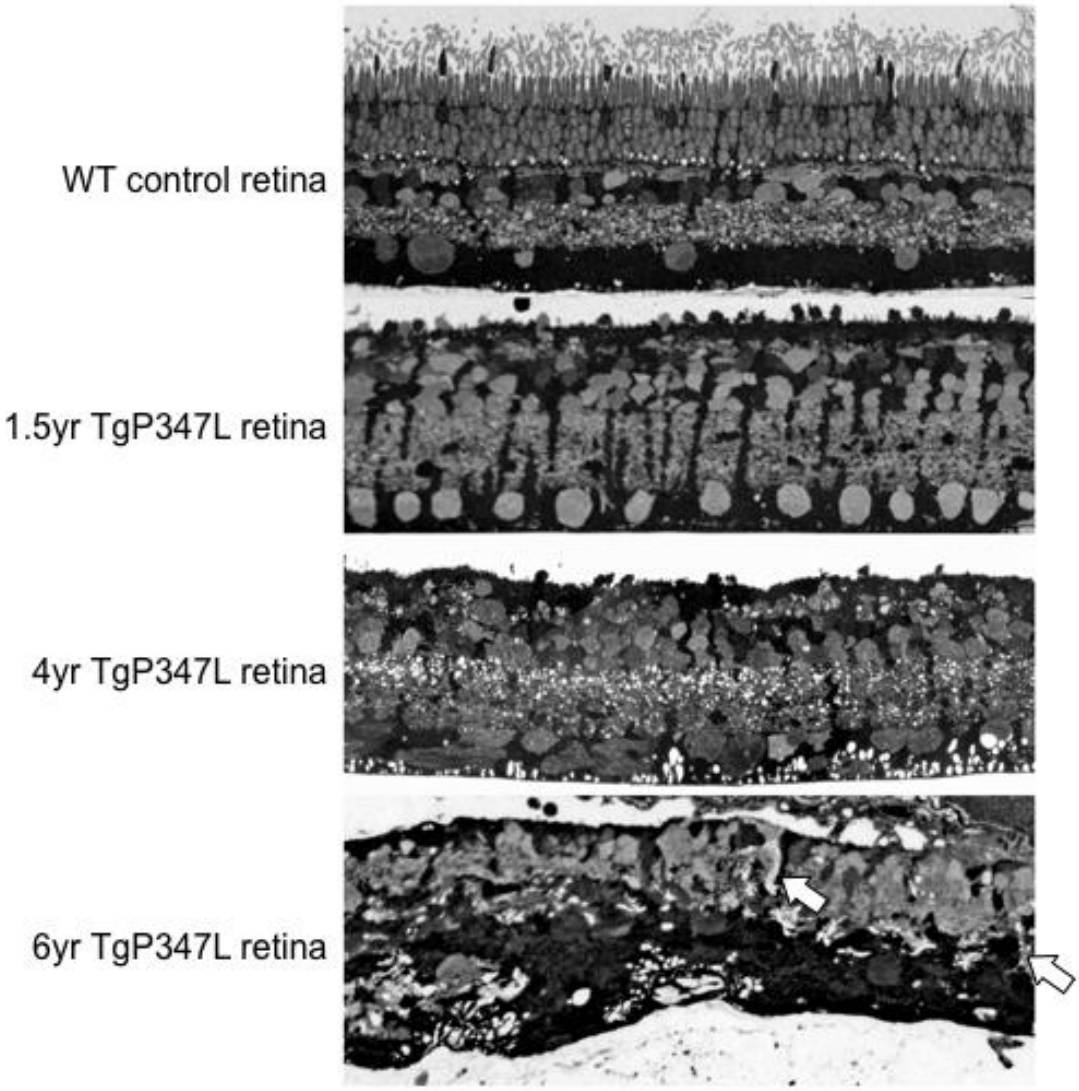

Figure 4.4 D-Aspartate loading in retinal chips. Amino acid immunoreactivity from 100nm sections of retina loaded in vitro by incubating immediately post-mortem with 5mM D-Asp and subsequently fixing with 2.5% glutaraldehyde. Images are density scaled, meaning darker areas are indicative of greater D-Asp immunoreactivity and thereby greater D-Asp transport prior to fixation. White arrows indicate Müller cells with deficient D-Asp loading, indicating deficient glutamate transport.

4.5 References

1. Reichenbach, A.; Bringmann, A., Muller Cells in the Healthy Retina. In *Muller Cells in the Healthy and Diseased Retina*, Springer Science+Business Meddia, LLC: New York, 2010; pp 35-299.

2. Riepe, R. E.; Norenburg, M. D., Muller Cell Localisation of Glutamine Synthetase in Rat Retina. *Nature* **1977,** *268* (5621), 654-655.

3. Rauen, T.; Rothstein, J. D.; Wassle, H., Differential Expression of Three Glutamate Transporter Subtypes in the Rat Retina. *Cell Tissue Res* **1996,** *286* (3), 325-336.

4. Chaudhry, F. A.; Reimer, R. J.; Krizaj, D.; Barber, D.; Storm-Mathisen, J.; Copenhagen, D. R.; Edwards, R. H., Molecular Analysis of System N Suggests Novel Physiological Roles in Nitrogen Metabolism and Synaptic Transmission. *Cell* **1999,** *99* (7), 769-780.

5. Umapathy, N. S.; Li, W.; Mysona, B. A.; Smith, S. B.; Ganapathy, V., Expression and Function of Glutamine Transporters SN1 (SNAT3) and SN2 (SNAT5) in Retinal Muller Cells. *Invest Ophthalmol Vis Sci* **2005,** *46* (11), 3980-3907.

6. Bringmann, A.; Grosche, A.; Pannicke, T.; Reichenbach, A., GABA and Glutamate Uptake and Metabolism in Retinal Glial (Muller) Cells. *Front Endocrinol* **2013,** *4*, 1-14.

7. Reichenbach, A.; Bringmann, A., New Functions of Muller Cells. *Glia* **2013,** *61* (5), 651-678.

8. Izumi, Y.; Kirby, C. O.; Benz, A. M.; Olney, J. W.; Zorumski, C. F., Muller Cell Swelling, Glutamate Uptake, and Excitotoxic Neurodegeneration in the Isolated Rat Retina. *Glia* **1999,** *25* (4), 379-389.

9. Lucas, D. R.; Newhouse, J. P., The Toxic Effect of Sodium L-Glutamate on the Inner Layers of the Retina. *AMA Arch Ophthalmol* **1957,** *58* (2), 193-201.

10. Olney, J. W., Glutamate-Induced Retinal Degeneration in Neonatal Mice. Electron Microscopy of the Acutely Evolving Lesion. *J Neuropathol Exp Neurol* **1969,** *28* (3), 455-474.

11. Olney, J. W., The Toxic Effects of Glutamate and Related Compounds in the Retina and the Brain. *Retina* **1982,** *2* (4), 341-359.

12. Szatkowski, M.; Barbour, B.; Attwell, D., Non-Vesicular Release of Glutamate from Glial Cells by Reversed Electrogenic Glutamate Uptake. *Nature* **1990,** *348* (6300), 443-446.

13. Delyfer, M. N.; Forster, V.; Neveux, N.; Picaud, S.; Leveillard, T.; Sahel, J. A., Evidence for Glutamate-Mediated Excitotoxic Mechanisms During Photoreceptor Degeneration in the rd1 Mouse Retina. *Mol Vis* **2005,** *11*, 688-696.

14. Chang, B.; Hawes, N. L.; Hurd, R. E.; Davisson, M. T.; Nusinowitz, S.; Heckenlively, J. R., Retinal Degeneration Mutants in the Mouse. *Vision Res* **2002,** *42* (4), 517-525.

15. Choi, D. W., Glutamate Neurotoxicity in Cortical Cell Culture is Calcium Dependent. *Neurosci Lett* **1985,** *58* (3), 293-297.

16. Park, Y. H.; Mueller, B. H., 2nd; McGrady, N. R.; Ma, H. Y.; Yorio, T., AMPA Receptor Desensitization is the Determinant of AMPA Receptor Mediated Excitotoxicity in Purified Retinal Ganglion Cells. *Exp Eye Res* **2015,** *132*, 136-150.

17. Choi, D. W.; Koh, J. Y.; Peters, S., Pharmacology of Glutamate Neurotoxicity in Cortical Cell Culture: Attenuation by NMDA Antagonists. *J Neurosci* **1988,** *8* (1), 185-196.

18. Pow, D. V.; Robinson, S. R., Glutamate in Some Retinal Neurons is Derived Solely from Glia. *Neuroscience* **1994,** *60* (2), 355-366.

19. Marc, R. E.; Murry, R. F.; Fisher, S. K.; Linberg, K. A.; Lewis, G. P., Amino Acid Signatures in the Detached Cat Retina. *Invest Ophthalmol Vis Sci* **1998,** *39* (9), 1694-1702.

20. Jones, B. W.; Kondo, M.; Terasaki, H.; Watt, C. B.; Rapp, K.; Anderson, J.; Lin, Y.; Shaw, M. V.; Yang, J. H.; Marc, R. E., Retinal Remodeling in the Tg P347L Rabbit, a Large-Eye Model of Retinal Degeneration. *J Comp Neurol* **2011,** *519* (14), 2713-27133.

21. Ross, J. W.; Fernandez de Castro, J. P.; Zhao, J.; Samuel, M.; Walters, E.; Rios, C.; Bray-Ward, P.; Jones, B. W.; Marc, R. E.; Wang, W.; Zhou, L.; Noel, J. M.; McCall, M. A.; DeMarco, P. J.; Prather, R. S.; Kaplan, H. J., Generation of an Inbred Miniature Pig Model of Retinitis Pigmentosa. *Invest Ophthalmol Vis Sci* **2012,** *53* (1), 501-507.

22. Gibson, R.; Fletcher, E. L.; Vingrys, A. J.; Zhu, Y.; Vessey, K. A.; Kalloniatis, M., Functional and Neurochemical Development in the Normal and Degenerating Mouse Retina. *J Comp Neurol* **2013,** *521* (6), 1251-1267.

23. Pfeiffer, R. L.; Marc, R. E.; Kondo, M.; Terasaki, H.; Jones, B. W., Muller Cell Metabolic Chaos During Retinal Degeneration. *Exp Eye Res* **2016,** *150*, 62-70.

24. Pfeiffer, R. L.; Marc, R. E.; Jones, B. W., Muller cell metabolic chaos during retinal degeneration. *Exp Eye Res* **2016**.

25. Jones, B. W.; Pfeiffer, R. L.; Ferrell, W. D.; Watt, C. B.; Marmor, M.; Marc, R. E., Retinal Remodeling in Human Retinitis Pigmentosa. *Exp Eye Res* **2016,** *150*, 149-165.

26. Ames, A., 3rd; Nesbett, F. B., In Vitro Retina as an Experimental Model of the Central Nervous System. *J Neurochem* **1981,** *37* (4), 867-877.

27. Marc, R. E.; Murry, R. F.; Basinger, S. F., Pattern Recognition of Amino Acid Signatures in Retinal Neurons. *J Neurosci* **1995,** *15* (7 Pt 2), 5106-5129.

28. Ishikawa, M.; Yoshitomi, T.; Zorumski, C. F.; Izumi, Y., Downregulation of Glutamine Synthetase via GLAST Suppression Induces Retinal Axonal Swelling in a Rat Ex Vivo Hydrostatic Pressure Model. *Invest Ophthalmol Vis Sci* **2011,** *52* (9), 6604-6616.

29. Rauen, T.; Wiessner, M., Fine Tuning of Glutamate Uptake and Degradation in Glial Cells: Common Transcriptional Regulation of GLAST1 and GS. *Neurochem Int* **2000,** *37* (2-3), 179-189.

30. McKenna, M. C., The Glutamate-Glutamine Cycle is not Stoichiometric: Fates of Glutamate in Brain. *J Neurosci Res* **2007,** *85* (15), 3347-3358.

31. Sahaboglu, A.; Paquet-Durand, O.; Dietter, J.; Dengler, K.; Bernhard-Kurz, S.; Ekstrom, P. A.; Hitzmann, B.; Ueffing, M.; Paquet-Durand, F., Retinitis Pigmentosa: Rapid Neurodegeneration is Governed by Slow Cell Death Mechanisms. *Cell Death Dis* **2013,** *4*, e488.

32. Sarthy, V. P.; Pignataro, L.; Pannicke, T.; Weick, M.; Reichenbach, A.; Harada, T.; Tanaka, K.; Marc, R., Glutamate Transport by Retinal Muller Cells in Glutamate/Aspartate Transporter-Knockout Mice. *Glia* **2005,** *49* (2), 184-196.

CHAPTER 5

LONG-TERM RETINAL DEGENERATION LEADS TO EXTENSIVE NEURODEGENERATION AND ALPHA SYNUCLEIN AGGREGATION

5.1 Effects of Long-Term Remodeling on Therapeutic Interventions

Retinal degenerations encompass many disorders that manifest with the death of photoreceptors leading to a loss of vision due to lack of sensory retinal input. Though some retinal degenerations are age-related, others may be early onset. In either case the affected individual is likely to suffer severe vision impairment for years or decades. Vision rescue of this population is an audacious goal, which many groups are pursuing through a variety of mechanisms. Cell replacement, genetic alteration, bionic implants, optogenetics, and stem cell therapy have all been proposed as possible mechanisms to restore vision following the loss of photoreceptors.[1-6] However, the long-term impact and potential of each of these interventions cannot be adequately predicted without a full understanding of retinal remodeling of the inner retina following deafferentation.[7]

There have been a number of proposed mechanisms contributing to remodeling and neuronal cell death in the inner retina associated with the loss of photoreceptors, including metabolic alterations,[8-11] retinoic acid synthesis,[12] changes in protein homeostasis,[13] oxidative stress, and changes in glucose metabolism.[14] Protein aggregates are associated

with neurodegenerative diseases in the brain and have also been correlated to some retinal diseases where age is a primary risk factor (age-related macular degeneration and glaucoma).[15] Although it is likely that a combination of the above mechanisms ultimately contribute to retinal remodeling, pathologic protein aggregation or proteinopathy is a probable central component of pathogenesis in retinal remodeling.

5.2 Animal Models of Retinal Remodeling and Possible Caveats

Retinal remodeling is associated with loss of retinal input in both humans and animal models. A caveat in the current knowledge of retinal remodeling is that primarily short-lived animal models have been employed to evaluate the extent and components of remodeling.[16] This causes a distinct disconnect between the experimental models of vision rescue and the ultimate goal of restoring sight in individuals who have severely remodeled inner retinas following years to decades of vision loss. In contrast to mouse or rat models of retinal degeneration (with mean lifespans of 700-800 days), the rhodopsin transgenic (Tg) P347L rabbit permits evaluation of retinal remodeling over many years (7-8y), recapitulating the remodeling observed in humans (see section 5.3.1).[17] Using this model we evaluate late stage remodeling and mechanisms active long after the degeneration of photoreceptors is complete using computational molecular phenotyping (CMP),[18] electron microscopy (EM), and immunohistochemical (IHC) analysis of proteins found to aggregate in other neuropathies.

5.3 Materials and Methods

5.3.1 Model Systems

The Tg P347L rabbit is a rabbit model of cone sparing autosomal dominant retinitis pigmentosa (adRP) originally developed in the Kondo laboratory. It contains a rhodopsin proline 347 to leucine mutation that causes primary rod degeneration.[17] Control rabbits were the unaffected littermates of Tg P347L rabbits (WT) (n = 7). We have previously characterized the progression of degeneration found in this rabbit, demonstrating the progression of degeneration in this rabbit follows the same trajectory of degeneration and subsequent remodeling seen in humans.[9, 19-21] In brief, the P347L rabbit presents initially with rod photoreceptor degeneration and loss, though some rods survive up to 12-16 weeks, followed subsequently by progressive cone photoreceptor loss. By 40 weeks the majority of photoreceptors have degenerated and the inner retina is in varying states of phase 2 and 3 remodeling. We expanded on the previous work by evaluating 10 Tg P347L rabbits spanning ages 3 mo to 6+ years for protein and metabolic changes.

5.3.2 Tissue Processing

Retinal samples were collected as previously described.[22-23] All animal experiments were conducted according to the ARVO Statement for the use of animals in ophthalmic and vision research with the supervision and approval of the institutional animal care and use committee (IACUC) at the University of Utah. Animals were euthanized with urethane, isoflurane, or pentobarbital (depending on USDA guidelines at the time of experiment), followed by bilateral thoracotomy. Following euthanasia, tissues were cut into smaller pieces and split between 3 fixative solutions:

1. 2.5% glutaraldehyde solution (2.5%FGMg) used for quantification: 2.5% glutaraldehyde, 1% formaldehyde, 0.1M phosphate buffer (pH 7.4), 1 mM $MgSO_4$, 3% sucrose.
2. 4% formaldehyde solution (4%F) used for initial antibody testing and protein expression pattern identification: 4% formaldehyde, 0.1M phosphate buffer (pH 7.4), 1 mM $MgSO_4$, 3% sucrose.
3. Cacodylate glutaraldehyde solution (2.5%Cac) for ultrastructural analysis by transmission electron microscopy (TEM). 2.5% glutaraldehyde, 1% formaldehyde, 0.1M cacodylate buffer (pH 7.4), 1 mM $MgSO_4$, 3% sucrose.

All tissues for CMP and TEM were processed as previously described.[18, 24-25] In addition to the small molecules used for CMP described below in section 5.3.3, we used glutaraldehyde tolerant antibodies to full protein α-synuclein (α-syn), phosphorylated α-synuclein (P-α-syn), Ubiquitin (Ubi), phosphorylated tau protein (tau), and β-amyloid. For a full list of antibodies used see Table 1.

5.3.3 Computational Molecular Phenotyping (CMP)

We used CMP for the identification of cell classes and quantified the changes in protein levels of the inner retina.[18, 25-26] Each well of the array slide was probed for an IgG for 1 of 6 small molecules: aspartate (D), glutamate (E), glycine (G), glutamine (Q), taurine (τ), or GABA (γ). All primary antibodies were probed with a gold conjugated secondary then silver intensified for 6.5mins on a 30°C plate.[18, 27] Slides were then captured as 8-bit images using a QImaging Retina CCD camera (Surrey, BC) under constant gain and offset. The grayscale images were then computationally aligned using ir-tweak,[28] generating a

registered volume where each grayscale image is an individual metabolite. We used computational clustering (isodata) to define class signatures (PCI Geomatica), which allows cells to be separated into metabolically relevant cell classes according to small molecule signals.[27, 29] Cell classes are then represented as a theme map, in which each color represents a single statistical cell class. These theme maps can then be used for masking all but a single cell type and evaluating the associated protein expression, or can be overlaid on traditional TEM images.[10, 25] In addition to theme maps, molecular signals are also viewed in triplicate combinations using red, green, and blue (rgb). For example, τQE→rgb assigns taurine, glutamine, and glutamate to red, green, and blue channels, respectively.

5.3.4 Protein Variation Quantification

In addition to the small molecules used for identifying cell classes present in tissue, we used a number of antibodies for the identification, localization, and relative concentration of proteins. Proteins probed for were: glutamine synthetase (GS), GFAP, phosphorylated ser129 alpha-synuclein (Pα-syn), alpha-synuclein (α-syn), ubiquitin (ubi), tau, beta-amyloid (β-amy), rhodopsin (1D4), and tomato-lectin (TL). Relative protein concentrations were calculated by probing the tissue stacks with monoclonal rhodopsin antibody 1D4 in addition to proteins of interest. Based on our experience using CMP with small molecules, we extended the approach to also include proteins, by using the known concentration of rhodopsin (5 mM) and the known efficacy of 1D4[30] to estimate the levels of each of the proteins over time. In addition, we performed Western blot analysis to further validate our observations of increases in α-syn in Tg retinas. Briefly, dissected retinas were homogenized, and then solubilized in lysis buffer.[31-32] After sonication, homogenates were

centrifuged for 15min at 12000 rpm, supernatant transferred to new tubes, and total protein content was measured by the Bio-Rad Bradford protein assay. 20µg of protein was incubated at room temperature for at least 30 mins with Laemmli sample buffer [50mM Tris-HCL, 2% SDS, 100mM DTT, and 10% glycerol], separated on a 15% SDS gel and transferred to a PVDF membrane in transfer buffer. Blots were blocked using 5% dried milk, 0.1% Tween diluted in TBS (TBST). Blots were probed using anti-α-syn (1:2000) and anti-actin (1:2000) overnight at 4°C. Membranes were washed 3x in 5% dried milk in TBST (~5 mins each) and incubated in either goat-anti-mouse or goat-anti-chicken IgGs at a concentration of 1:2000 for 1 hr at room temperature. Membranes were washed 2x in 5% dried milk in TBST followed by 3x in TBST (~5min each). The blots were exposed to film after SuperSignal chemiluminescent substrate treatment (Pierce, Rockford IL) and imaged by FluorChem Q with AlphaInnotech AlphaView software (Cell Biosciences, Inc., Santa Clara, CA, USA).

5.4 Characterization of Aged P347L Rabbit

By 40 weeks of age the Tg P347L rabbit retina is largely devoid of rod and cone outer segments and has an extremely depressed ERG (80% scotopic a- and b-wave reduction, and 70% photopic a and b wave reduction.[17] During years 2-4 the retina manifests a total loss of photoreceptor nuclei in a patchy fashion. Ultimately, with the loss of cones, the retina enters into phase 3 remodeling (Figure 5.1A-C). Although it was previously assumed (with little evidence) that the retina would enter into a state of equilibrium at this level of remodeling, CMP analysis of retinas from 2-, 4-, 5-, and 6-year-old degenerate retinas show pronounced loss of glutamine synthetase (GS) (Figure 5.2

A,D,G,J,M), high levels of metabolic heterogeneity between neighboring Müller cells, and increased levels of anatomical remodeling most notably in their endfeet (Figure 5.2 B,E,H,K,N). This continuum of metabolic revision and structural remodeling continues until the Müller cells have no recognizable metabolic signature or form, but are transformed into thick, overlapping blocks of glia or replaced by a debris-like assemblies filling large areas of the remnant retina (Figure 5.2 C,F,I,L,O). In tandem with the Müller cell alterations and ultimate degeneration in aged Tg P347L rabbits, neurons of all types have been lost, exceeding 90% in some areas. Though a large number of neurons were absent by 6 years, some identifiable neurons remained and these were of particular interest. To evaluate their potential to be long term survivors despite the breakdown of the surrounding retina, we combined CMP with TEM imaging which allows us to map the main molecular classes of cell types in TEM images (see materials and methods). In these zones we examined, virtually all of the remnant ganglion cell somas and processes displayed severe cytoplasmic pathologies, apparent proteins aggregates and/or massive internal vesicle accumulations (Figure 5.3). This led us to explore some of the possible molecular markers of similar pathologies found in CNS neurodegenerations.

5.5 Ubiquitin Expression in Retinal Degeneration

The severe late-stage remodeling in the Tg P347L rabbit, including pronounced cell death, metabolic variation, and debris accumulation, is reminiscent of protein aggregation associated with neurodegenerative diseases. For initial evaluation we assessed ubiquitin levels and localization as a measure of protein degradation and aggregation. Soon after the onset of outer segment stress and degeneration levels of ubiquitin are increased in nuclei

of the ONL, with focal patchy increases within ganglion cells (Figure 5.4B). Following the loss of the outer segments, but prior to the complete loss of the ONL (~2yr), ubiquitin levels appear stable, with continued low expression in remnant cones, some cells of the INL, focal expression in ganglion cells, and the beginnings of expression in the optic fiber (Figure 5.4C). By 3-4 years, along with the complete loss of the ONL, ubiquitin expression is dramatically increased in neurons of the inner retina (Figure 5.4D). At 5 years the ubiquitin is found to be patchy in its expression. Some cells have low levels, but regional aggregates appear, which are difficult to assign to intracellular or extracellular compartments (Figure 5.4E). At 6 years the ubiquitin localization remains patchy, similar to that seen at 5 years (Figure 5.4F).

5.6 Alpha Synuclein Aggregation in Older Transgenic Retina

Given these variations in ubiquitin expression and localization, we hypothesized some other proteins were likely involved in remodeling, perhaps those found in slow CNS neurodegenerations. We evaluated the location and expression of α-synuclein (α-syn), β-amyloid, tau phosphorylated at T231, and α-synuclein phosphorylated at locus at S129 (Pα-syn), which is associated with oligomerization. Evaluation of transgenic retinas spanning in age from 3 months through 6 years using protein CMP revealed no aggregation or specialized localization of phosphorylated tau or β-amyloid in the P347L rabbit (data not shown). In contrast, α-syn and Pα-syn showed marked changes in expression and localization as remodeling progressed (Figure 5.5). In WT tissues α-syn is found throughout the retina, with higher levels found in rod outer segments[33] and the ONL, than in neurons or the IPL of the inner retina. Pα-syn is found at low levels distributed in neurons

of the ONL and the INL, along with some signals in fibers and nuclei of the ganglion cell layer. In Tg retinas, the levels of both α-syn and Pα-syn vary with age and level of remodeling present in the retina. Although the signals may vary depending on the level of remodeling in a given region, the basic pattern is as follows: Early in degeneration (3mo-1.5yrs) levels of α-syn are roughly equal to that found in WT, with higher levels found in the outer segments of degenerating rods and lower levels throughout neurons of the outer and inner retina. Pα-syn is dramatically increased in horizontal cells, along with a more subtle uniform increase in the INL, IPL, and GCL. By ~2yrs the thinned ONL shows high levels of α-syn, with increased concentrations in the inner retina as well. Of note, at this stage the α-syn in ganglion cells appears to no longer be uniformly distributed, but rather is aggregated along the outer cell membrane. Extracellular aggregation of Pα-syn around and within some ganglion cells emerges. At ~4yrs degeneration the ONL is largely absent and α-syn is found solely distributed in the nuclei of the inner retina, with some punctate staining distributed within the IPL, presumable at large synapses. Pα-syn levels are two-fold higher than α-syn throughout neurons of the inner retina. Pα-syn has also begun to aggregate inside cells, particularly ganglion cells. At 5yrs the Pα-syn continues to aggregate within ganglion cells, in addition to displaced neurons found within the IPL, and at high concentrations in many INL soma. α-syn is found highly expressed in all remaining cells and is predominantly colocalized with high levels of Pα-syn, with an exception of punctate levels in the IPL as IPL staining is unique to the full protein. By 6-7yrs the structure of the retina is severely decimated. α-syn is distributed widely throughout remnant cells and processes of the retina. Pα-syn is not only ubiquitous in the remaining neurons but is also found in aggregates in the cellular debris making up much of the

remnant retina. Combined, these data indicate α-syn overall increases throughout degeneration while there is a pronounced increase and eventual aggregation of Pα-syn. In support of these data, Western blot analysis reveals a two-fold increase in monomeric α-syn at 4 years of degeneration in P347L rabbit retina, and continual increase to five-fold by 5 years, which is consistent with data from Parkinson's disease suggesting that native cytosolic multimers shift to a monomeric form as a mechanism of disease initiation.[34] In contrast, there is no increase in a-syn in wt rabbit even at 8 years of age, indicating this increase in α-syn is not age-dependent (Figure 5.6). In order to confirm the effects seen in our Western Blot and histological analysis, we performed a blocking experiment, which demonstrated that the antibodies are specific for Pα-syn and α-syn (Figure 5.7).

5.7 Discussion

By evaluating structural, ultrastructural, metabolic, and protein alterations in advanced age TgP347L rabbit retinas we characterize late retinal remodeling as a neurodegenerative proteinopathy. Based on these data we conclude that the previously reported plateau of remodeling in experimental animals and its extrapolation to humans is incorrect and due to incomplete data produced by the short lifespan of rodents.

This development in our understanding of retinal remodeling presents both new hurdles and opportunities to the vision community and neuroscience as a whole. Progressive neurodegeneration and glial deconstruction after the complete loss of photoreceptors suggests that optogenetic and photoswitch interventions are destined to fail in all patients long term, regardless of their initial mechanism of photoreceptor loss. Similarly, cell regenerative approaches using stem cells or differentiated cellular

replacement are also futile because proteinopathy, as in the CNS, likely does not respect cellular origins. A particularly potent example of this the accumulation of pathologic levels of a-syn in some fetal nigral transplants in Parkinson's disease.[35]

Our discovery of retinal remodeling as a neurodegenerative proteinopathy also affords a number of opportunities to the neurodegeneration community. The retina is unrivaled by any other area of the CNS in its accessibility and our understanding of the associated metabolism and circuitry. These factors combined make the remodeled retina an attractive candidate organ for the discovery of pathways leading to α-synuclein aggregation and ways to prevent or reverse it[36] in Parkinson's disease, Lewy-body dementia, multiple-system atrophy, and other α-synuclein associated neurodegenerations.

In the short term this has two primary impacts on research: First, groups interested in success in treating retinal degenerations need to devote more resources to generating interventions that prevent or delay the onset of remodeling, such as blocking retinoic acid activation of neuritogenesis.[12] Second, it is imperative that at least as many resources are devoted to basic research understanding the development of proteinopathies and neurodegeneration as translational therapeutics. Without basic research understanding all of the primary components leading to diseases like neurodegeneration, the vast majority of the developed therapeutics will have small odds of long-term success.

Table 1. Immunocytochemistry reagents

Reagent	RRID	Source	Dilution
anti-D-aspartate IgG	NA	Signature Immunologics	1:100
anti-L-aspartate IgG	AB_2341093	Signature Immunologics	1:100
anti-L-glutamate IgG	AB_2532055	Signature Immunologics	1:100
anti-glycine IgG	AB_2532057	Signature Immunologics	1:100
anti-glutathione IgG	AB_2532058	Signature Immunologics	1:100
anti-L-glutamine IgG	AB_2532059	Signature Immunologics	1:100
anti-taurine IgG	AB_2532060	Signature Immunologics	1:100
anti-GABA IgG	AB_2532061	Signature Immunologics	1:100
anti-GABA IgY	AB_2532062	Signature Immunologics	1:100
anti-GS IgG	AB_397879	BD Biosciences	1:50
anti-CRALBP IgG	AB_2314227	Gift of Dr. Jack Saari	1:400
anti-GFAP	AB_10013382	Dako	1:400
Anti-α-syn pS129	NA	AbCam ab184674	1:500
Anti-α-syn (pan)	NA	AbCam ab190376	1:2000
Anti-ubiquitin	AB_305802	AbCam ab7254	1:200

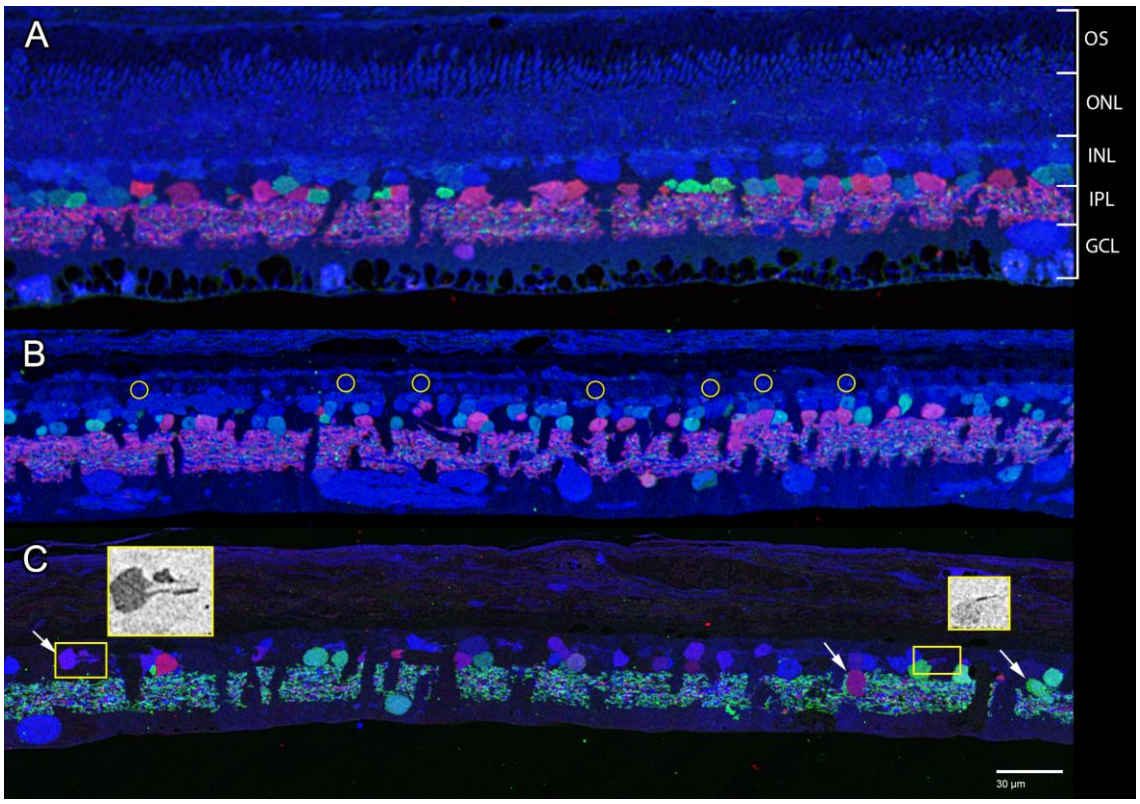

Figure 5.1 Representative registered images of amino acid immunoreactivity in 100nm sections of WT, Phase 2, and Phase 3 remodeling in rabbit retinas. 1A) γGE→ rgb of a WT rabbit retina. The lamination of outer segments (OS), outer nuclear layer (ONL), inner nuclear layer (INL), inner plexiform layer (IPL), and ganglion cell layer (GCL) are all clearly laminated. 1B) γGE→ rgb of a TgP347L degenerate rabbit retina currently in phase 2 remodeling. The yellow circles demonstrate examples of remaining cone cell bodies, although the majority of the OS and ONL is absent. 1C) γGE→ rgb of a TgP347L degenerate rabbit retina in phase 3 remodeling. White arrows indicate amacrine cells, which have translocated from their appropriate position either into the IPL, or have moved apically towards the remnant RPE. Inlaid density scaled images demonstrate aberrant horizontal direction of some GABAergic processes, indicated by boxes.

Figure 5.2 Representative images from WT rabbit (A-C), 2yr (D-F), 4yr (G-I), 5yr (J-L), and 6yr (M-O) Tg P347L rabbit retina. 2A) WT retina stained for glutamine synthetase (GS) showing strong staining throughout Müller cell and their endfeet 2B) WT retina stained for tomato lectin (TL) stains the extra cellular matrix (ECM) allowing the inference of cellular compartments. 2C) τQE → rgb sCMP of a WT rabbit retina. This combination of amino acid facilitates the visualization of most major cell types in the retina. Müller cells appear yellowish-orange in this configuration (indicated by the oval). Ganglion cells appear teal (upward white arrow). Amacrine cells are pink or green immediately adjacent to the IPL (examples demonstrated by black upward arrows). Bipolar cells are the cells of varying shades of pink above the amacrine cells (black horizontal arrows). Horizontal cells are the dull green cells at the border between the ONL and INL (downward white arrows). 2D) GS staining of a 2yr P347L rabbit retina. GS staining shows a global decrease in GS levels, but a nonuniform pattern of decrease between neighboring Müller cells. 2E) TL staining of 2yr Tg P347L rabbit retina. The extra cellular matrix stain visualizes the increase in the fingerlike projections of the Müller cell endfeet. Also there is a thinning in the external limiting membrane and the predicted decrease in nuclei in the outer nuclear layer following the loss of outer segments. 2F) τQE → rgb sCMP of a 2yr Tg P347L rabbit retina. The outer segments and outernuclear layer have degenerated, though a few cone cell bodies remain (examples indicated by yellow circles). Müller cells, although similar, have diverged in metabolic profile as indicated by the varying colors of orangeish-yellow (brackets). Müller cell hypertrophy is also visible at this stage (oval). 2G) GS staining of 4yr Tg P347L rabbit retina. At this stage of degeneration GS has dropped to almost undetectable levels. It is likely that using conventional fluorescent staining, this level of GS would be indistinguishable from background fluorescence. 2H) TL staining of a 4yr P347L rabbit retina. The majority loss of the outernuclear layer is now leading to more aberrant architecture of the Müller glial endfeet. In addition to the continual development of finger-like projections the Müller cell endfeet appear to have become intertwined with some large stalks pushing the IPL out of its normal lamination. The outer limiting membrane has also continued to break down. 2I) τQE → rgb sCMP of a 4yr Tg P347L rabbit retina. Müller cells demonstrate a complete loss of metabolic homogeneity, as demonstrated by the range of colors. The IPL is pushed apically in some regions (white arrows) while it is pushed basally in others (black arrows). 2J) GS staining of a 5yr Tg P347L rabbit retina. GS levels remain markedly lower than WT, with more prominent staining along apical region of retina. 2K) TL staining of a 5yr Tg P347L rabbit retina. ECM staining continues to show the elaboration of intertwined Müller cell projections throughout the GCL, where endfeet once resided. Indicated by a circle is a point in which the basement membrane appears to be breached by some components of the inner retina. 2L) τQE → rgb sCMP of a 5yr Tg P347L rabbit retina. The endfoot region of the Müller glia has expanded to double its original size, while the metabolism has not returned to a homogeneous population as evident by the range of orange, brown, and green. Holes have begun to form in some regions, likely due to compromised aquaporin access to the vitreous. The number of neuronal nuclei has decreased, and lamination in the INL is unclear. 2M) GS staining of a 6yr Tg P347L rabbit retina. GS expression is still at an almost undetectable level. 2N) TL staining of a 6yr Tg P347L rabbit retina. The ECM staining demonstrates a lack of identifiable retinal structure beyond a few cell nuclei. 2O) τQE → rgb sCMP of a 6-7yr Tg P347L rabbit retina. The former GCL has now tripled in size, but has only remnants of processes likely to have arisen from ganglion cells. The sole remaining ganglion cell in this region has migrated into the IPL. Some glial-like signatures remain, but they appear

drastically altered from those found in WT retina. Intermixed with the glia, there are regions largely devoid of any signature, which are being termed debris.

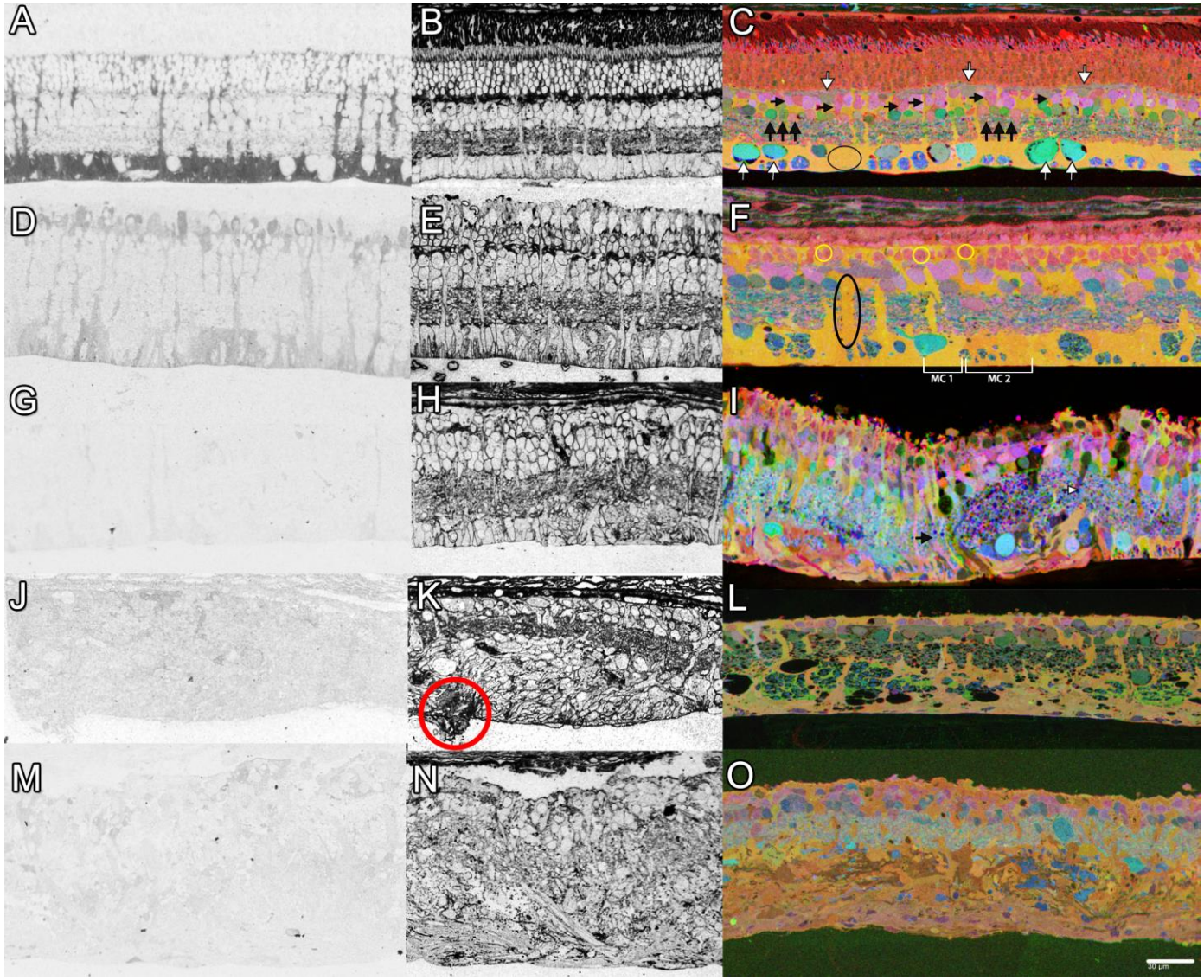
A
B
C
D
E
F
MC 1
MC 2
G
H
I
J
K
L
M
N
O

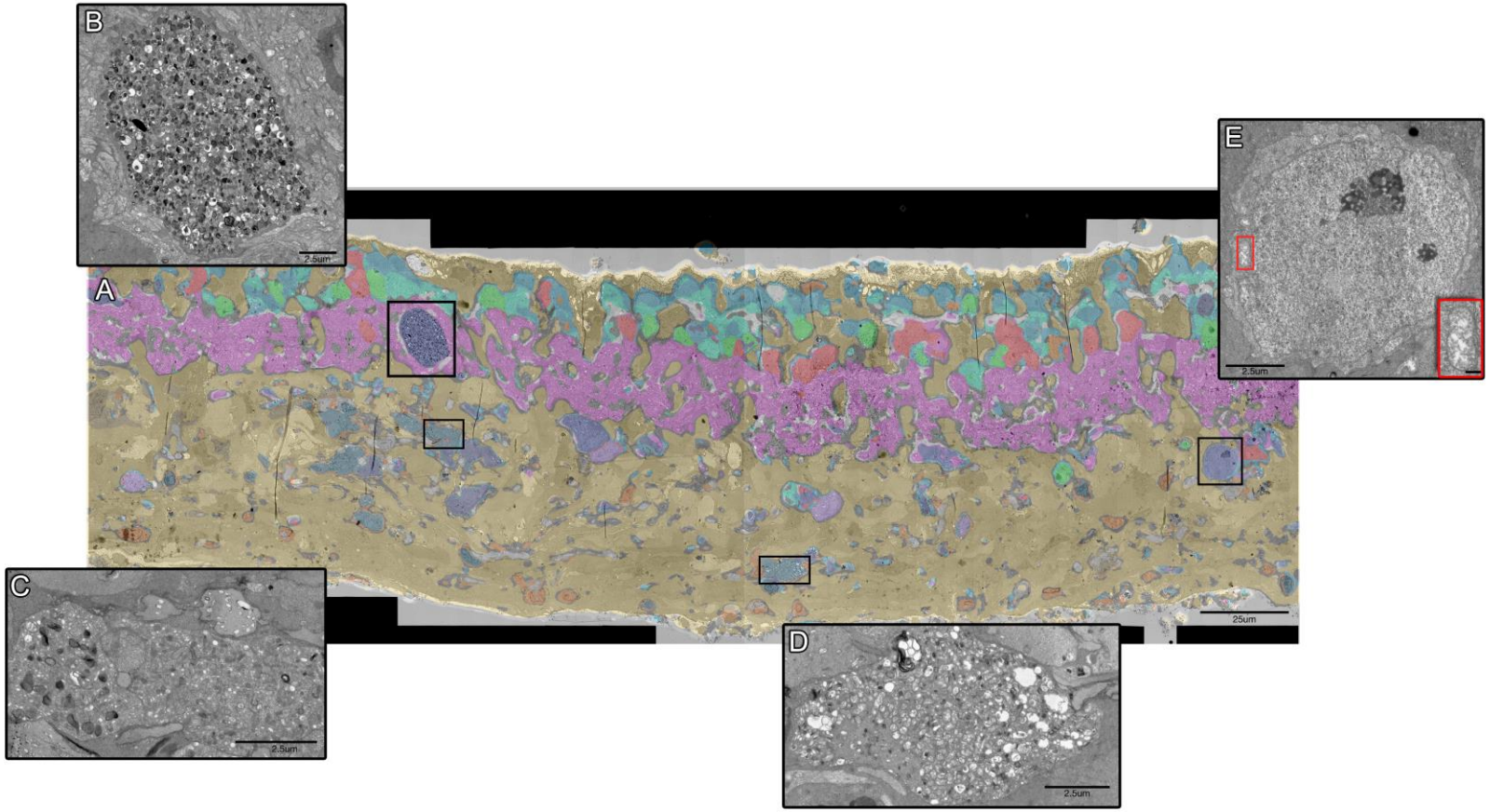

Figure 5.3 Theme map overlay of TEM image of retina. 3A) Theme map generated via k-means clustering of a 6-7yr Tg P347L rabbit retina. Metabolic signatures used for clustering: E, Q, J, D, G, γ, τ, and GS. Purple theme class indicates ganglion cells (GCs), while dark blue in the GCL layer indicates the theme class containing ganglion cell processes. 3B) TEM close-up of large ganglion cell found in the middle of the IPL. Swirl structures are indicative of autophagy. 3C) Magnified TEM image of multiple GC processes in intermediate stage of autophagy. 3D) Magnified TEM image of another GC process almost entirely filled with autophagy-associated swirl structures. 3E) Magnified TEM image of another GC without autophagic swirl structures. Inset magnified mitochondrion demonstrates significant swelling and breakdown of cristae indicating cell stress.

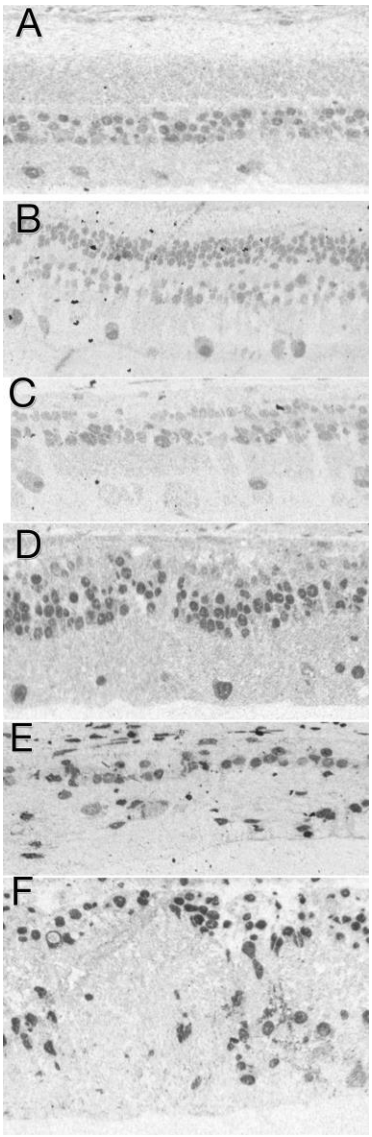

Figure 5.4: Grayscale ubiquitin labeling in rabbit retinas. 4A) WT P347L littermate control demonstrating light ubiquitin immunoreactivity distributed around Müller cells. 4B) 3mo Tg P347L rabbit retina demonstrating increased expression in ONL and some ganglion cells. 4C) 2yr Tg P347L rabbit retina with moderate levels in nuclei of inner retina. 4D) 4yr Tg P347L rabbit retina. Levels of ubiquitin have risen in soma of the INL and GCL.4E) 5yr Tg P347L rabbit retina, demonstrating variable level of ubiquitin across all cell types. 4F) 6yr Tg P347L rabbit retina. Levels of ubiquitin in probable debris is patchy. The remaining somas have varying levels of ubiquitin, but all above baseline levels.

Figure 5.5 Endogenous signaling of phosphorylated α-synuclein (Pα-syn), full protein α-synuclein (α-syn), and GFAP. 5A-C) WT rabbit retina. A) Pα-syn, α-syn, GFAP → RGB mapped B) grayscale Pα-syn and C) grayscale Pα-syn, demonstrating normal expression pattern of Pα-syn and α-syn in the absence of significant stress (indicated by absence of GFAP). 5D-F) 3mo Tg P347L rabbit retina. D) Pα-syn, α-syn, GFAP → RGB mapped E) grayscale Pα-syn and F) grayscale Pα-syn, during early phase 1 retinal remodeling. The largest change is the presence of Pα-syn in the horizontal cells (HCs) indicated by black arrows. 5G-I) 2yr Tg P347L rabbit retina. G) Pα-syn, α-syn, GFAP → RGB mapped H) grayscale Pα-syn and I) grayscale Pα-syn, during early phase 2. The largest change is the emergence of Pα-syn outside of ganglion cells (GCs) indicated by a red circle. 5J-L) 4yr Tg P347L rabbit retina. J) Pα-syn, α-syn, GFAP → RGB mapped K) grayscale Pα-syn and L) grayscale Pα-syn, during late phase 2 retinal remodeling (prior to loss of remnant cones). As the ONL disappears, levels of Pα-syn begin to dramatically increase in the INL and GCL with more diffuse phosphorylated aggregates being found throughout the GCL (downward facing arrows). 5M-O) 5yr Tg P347L rabbit retina. M) Pα-syn, α-syn, GFAP → RGB mapped N) grayscale Pα-syn, during phase 3 retinal remodeling (no remnant photoreceptors). Increased Pα-syn in cells of INL and GCL. In GCs Pα-syn begins to strongly aggregate along outer cell membrane. 5P-R) 6yr Tg P347L rabbit retina. P) Pα-syn, α-syn, GFAP → RGB mapped Q) grayscale Pα-syn and R) grayscale Pα-syn, during the most advanced phase 3 retinal remodeling seen to date. Increased Pα-syn in all remaining cells, and aggregates dispersed throughout previous GCL.

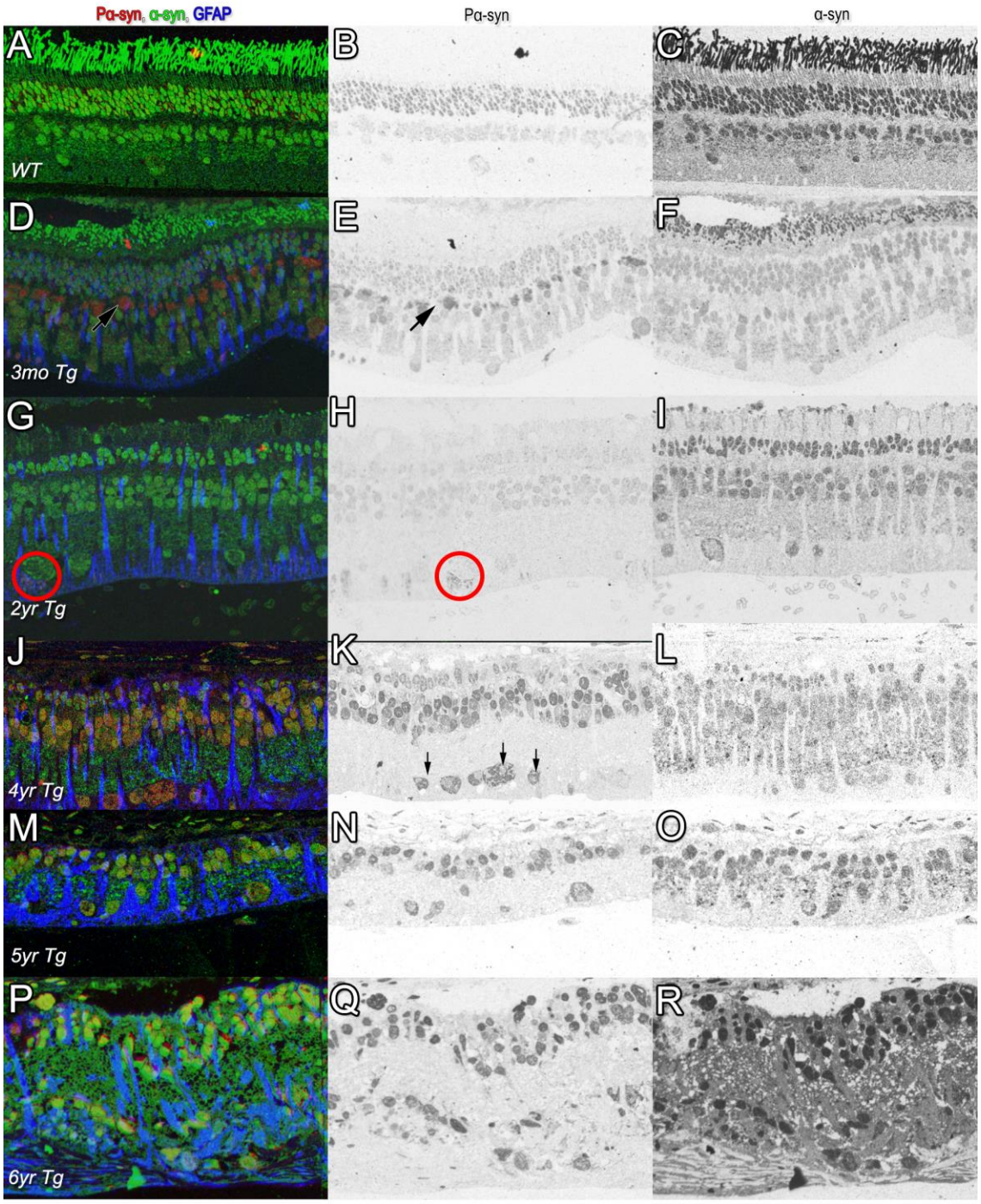
Pα-syn, α-syn, GFAP
Pα-syn
α-syn
A
B
C
WT
D
E
F
3mo Tg
G
H
I
2yr Tg
J
K
L
4yr Tg
M
N
O
5yr Tg
P
Q
R
6yr Tg

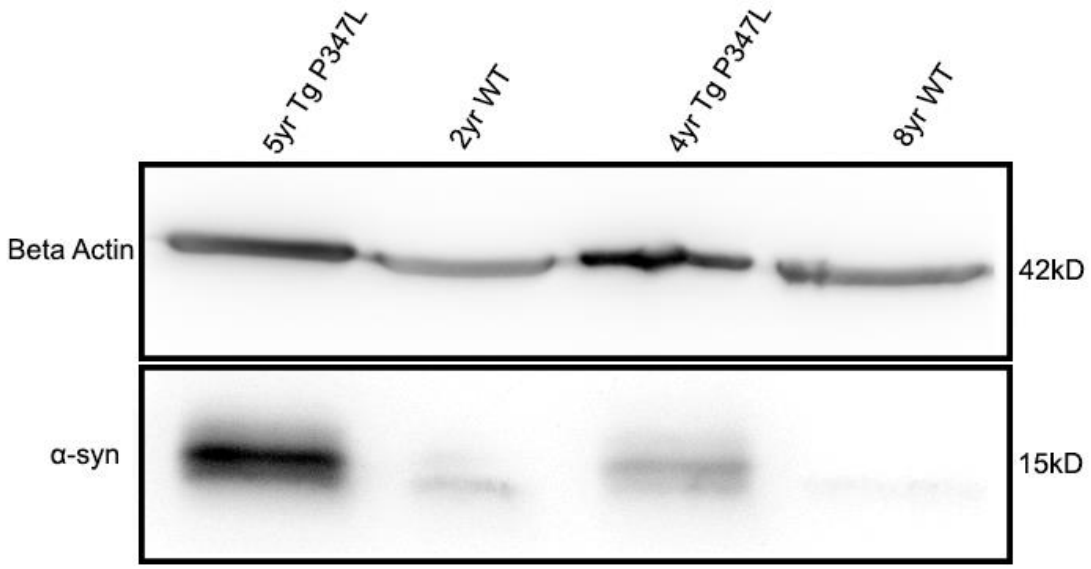

Figure 5.6 Western Blot: Beta actin demonstrated some increase in Tg retinas when compared to WT. α-synuclein demonstrated 2-fold increase at the 4 year time point and increased to 5-fold by 5 years of degeneration.

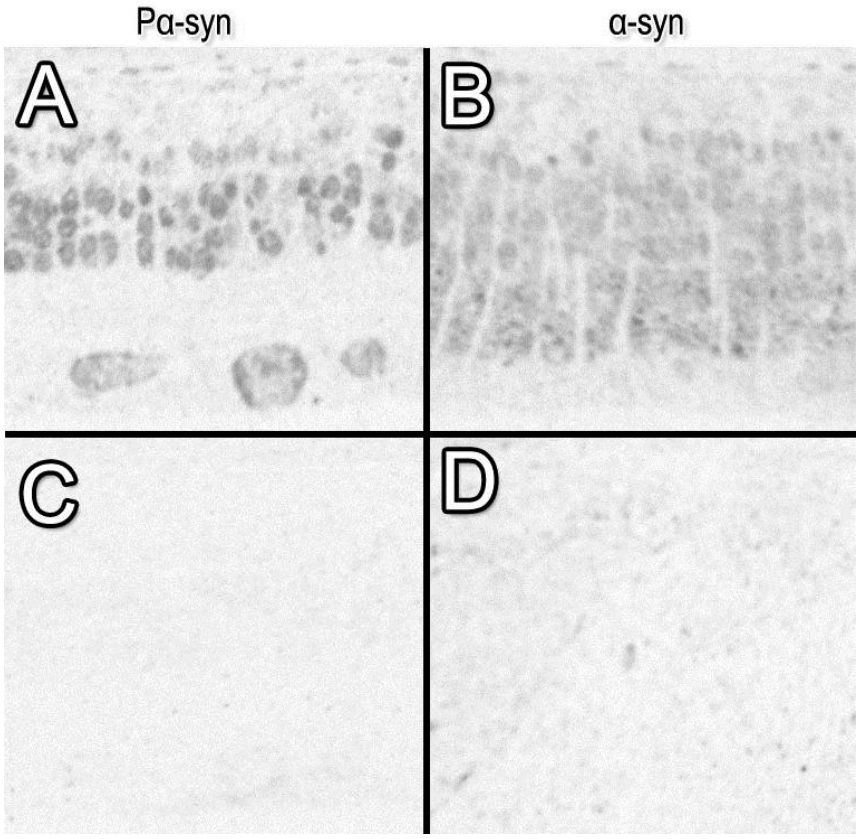

Figure 5.7 Antibody inhibition experiment. A) Pα-syn, without block. B) α-syn without block. C) Pα-syn inhibited by Pα-syn protein fragment. D) α-syn inhibited by full α-syn protein.

5.8 References

1. Busskamp, V.; Picaud, S.; Sahel, J. A.; Roska, B., Optogenetic Therapy for Retinitis Pigmentosa. *Gene Ther* **2012,** *19* (2), 169-175.

2. Petrs-Silva, H.; Linden, R., Advances in Gene Therapy Technologies to Treat Retinitis Pigmentosa. *Clin Ophthalmol* **2014,** *8*, 127-136.

3. Seiler, M. J.; Aramant, R. B., Cell Replacement and Visual Restoration by Retinal Sheet Transplants. *Prog Retin Eye Res* **2012,** *31* (6), 661-687.

4. Lamba, D. A.; Karl, M. O.; Reh, T. A., Strategies for Retinal Repair: Cell Replacement and Regeneration. *Prog Brain Res* **2009,** *175*, 23-31.

5. Weiland, J. D.; Cho, A. K.; Humayun, M. S., Retinal Prostheses: Current Clinical Results and Future Needs. *Ophthalmology* **2011,** *118* (11), 2227-2237.

6. Weitz, A. C.; Behrend, M. R.; Lee, N. S.; Klein, R. L.; Chiodo, V. A.; Hauswirth, W. W.; Humayun, M. S.; Weiland, J. D.; Chow, R. H., Imaging the Response of the Retina to Electrical Stimulation with Genetically Encoded Calcium Indicators. *J Neurophysiol* **2013,** *109* (7), 1979-1988.

7. Marc, R.; Pfeiffer, R.; Jones, B., Retinal Prosthetics, Optogenetics, and Chemical Photoswitches. *ACS Chem Neurosci* **2014,** *5* (10), 895-901.

8. Fletcher, E. L.; Kalloniatis, M., Neurochemical Architecture of the Normal and Degenerating Rat Retina. *J Comp Neurol* **1996,** *376* (3), 343-360.

9. Jones, B. W.; Kondo, M.; Terasaki, H.; Watt, C. B.; Rapp, K.; Anderson, J.; Lin, Y.; Shaw, M. V.; Yang, J. H.; Marc, R. E., Retinal Remodeling in the Tg P347L Rabbit, a Large-Eye Model of Retinal Degeneration. *J Comp Neurol* **2011,** *519* (14), 2713-27133.

10. Marc, R. E.; Jones, B. W., Retinal Remodeling in Inherited Photoreceptor Degenerations. *Mol Neurobiol* **2003,** *28* (2), 139-147.

11. Pfeiffer, R. L.; Marc, R. E.; Jones, B. W., Muller cell metabolic chaos during retinal degeneration. *Exp Eye Res* **2016**.

12. Lin, Y.; Jones, B. W.; Liu, A.; Tucker, J. F.; Rapp, K.; Luo, L.; Baehr, W.; Bernstein, P. S.; Watt, C. B.; Yang, J. H.; Shaw, M. V.; Marc, R. E., Retinoid Receptors Trigger Neuritogenesis in Retinal Degenerations. *FASEB J* **2012,** *26* (1), 81-92.

13. Lewis, G. P.; Erickson, P. A.; Guerin, C. J.; Anderson, D. H.; Fisher, S. K., Changes in the Expression of Specific Muller Cell Proteins During Long-Term Retinal Detachment. *Exp Eye Res* **1989,** *49* (1), 93-111.

14. Hurley, J. B.; Lindsay, K. J.; Du, J., Glucose, Lactate, and Shuttling of Metabolites in Vertebrate Retinas. *J Neurosci Res* **2015,** *93*, 1079-1092.

15. Ohno-Matsui, K., Parallel Findings in Age-Related Macular Degeneration and Alzheimer's Disease. *Prog Retin Eye Res* **2011,** *30* (4), 217-238.

16. Chang, B.; Hawes, N. L.; Hurd, R. E.; Davisson, M. T.; Nusinowitz, S.; Heckenlively, J. R., Retinal Degeneration Mutants in the Mouse. *Vision Res* **2002,** *42* (4), 517-525.

17. Kondo, M.; Sakai, T.; Komeima, K.; Kurimoto, Y.; Ueno, S.; Nishizawa, Y.; Usukura, J.; Fujikado, T.; Tano, Y.; Terasaki, H., Generation of a Transgenic Rabbit Model of Retinal Degeneration. *Invest Ophthalmol Vis Sci* **2009,** *50* (3), 1371-1377.

18. Marc, R. E.; Murry, R. F.; Basinger, S. F., Pattern Recognition of Amino Acid Signatures in Retinal Neurons. *J Neurosci* **1995,** *15* (7 Pt 2), 5106-5129.

19. Pfeiffer, R. L.; Marc, R. E.; Kondo, M.; Terasaki, H.; Jones, B. W., Muller Cell Metabolic Chaos During Retinal Degeneration. *Exp Eye Res* **2016,** *150*, 62-70.

20. Sakai, T.; Kondo, M.; Ueno, S.; Koyasu, T.; Komeima, K.; Terasaki, H., Supernormal ERG Oscillatory Potentials in Transgenic Rabbit with Rhodopsin P347L Mutation and Retinal Degeneration. *Invest Ophthalmol Vis Sci* **2009,** *50* (9), 4402-4409.

21. Jones, B. W.; Pfeiffer, R. L.; Ferrell, W. D.; Watt, C. B.; Marmor, M.; Marc, R. E., Retinal Remodeling in Human Retinitis Pigmentosa. *Exp Eye Res* **2016,** *150*, 149-165.

22. Marc, R. E.; Wei-Ley, S.; Kalloniatis, M.; Raiguel, S. F.; Van Haesendonck, E., Patterns of Glutamate Immunoreactivity in the Goldfish Retina. *J Neurosci* **1990,** *10* (12), 4006-4034.

23. Marc, R. E., Mapping Glutamatergic Drive in the Vertebrate Retina with a Channel-Permeant Organic Cation. *J Comp Neurol* **1999,** *407* (1), 47-64.

24. Anderson, J. R.; Jones, B. W.; Watt, C. B.; Shaw, M. V.; Yang, J. H.; Demill, D.; Lauritzen, J. S.; Lin, Y.; Rapp, K. D.; Mastronarde, D.; Koshevoy, P.; Grimm, B.; Tasdizen, T.; Whitaker, R.; Marc, R. E., Exploring the Retinal Connectome. *Mol Vis* **2011,** *17*, 355-379.

25. Marc, R. E.; Jones, B. W.; Watt, C. B.; Strettoi, E., Neural remodeling in retinal degeneration. *Prog Retin Eye Res* **2003,** *22* (5), 607-655.

26. Marc, R. E.; Cameron, D., A Molecular Phenotype Atlas of the Zebrafish Retina. *J Neurocytol* **2001,** *30* (7), 593-654.

27. Marc, R. E.; Jones, B. W., Molecular Phenotyping of Retinal Ganglion Cells. *J Neurosci* **2002,** *22* (2), 413-427.

28. Anderson, J. R.; Jones, B. W.; Yang, J. H.; Shaw, M. V.; Watt, C. B.; Koshevoy, P.; Spaltenstein, J.; Jurrus, E.; U, V. K.; Whitaker, R. T.; Mastronarde, D.; Tasdizen, T.;

Marc, R. E., A Computational Framework for Ultrastructural Mapping of Neural Circuitry. *PLoS Biol* **2009,** *7* (3), 493-512.

29. Pfeiffer, R. L.; Marc, R. E.; Kondo, M.; Terasaki, H.; Jones, B. W., Muller cell metabolic chaos during retinal degeneration. *Exp Eye Res* **2016**.

30. MacKenzie, D.; Arendt, A.; Hargrave, P.; McDowell, J. H.; Molday, R. S., Localization of Binding Sites for Carboxyl Terminal Specific Anti-Rhodopsin Monoclonal Antibodies Using Synthetic Peptides. *Biochemistry* **1984,** *23* (26), 6544-6549.

31. Chakraborty, D.; Ding, X. Q.; Fliesler, S. J.; Naash, M. I., Outer Segment Oligomerization of Rds: Evidence from Mouse Models and Subcellular Fractionation. *Biochemistry* **2008,** *47* (4), 1144-1156.

32. Zou, J.; Zheng, T.; Ren, C.; Askew, C.; Liu, X. P.; Pan, B.; Holt, J. R.; Wang, Y.; Yang, J., Deletion of PDZD7 Disrupts the Usher Syndrome Type 2 Protein Complex in Cochlear Hair Cells and Causes Hearing Loss in Mice. *Hum Mol Genet* **2014,** *23* (9), 2374-2390.

33. Cuenca, N.; Fernandez-Sanchez, L.; Campello, L.; Maneu, V.; De la Villa, P.; Lax, P.; Pinilla, I., Cellular Responses Following Retinal Injuries and Therapeutic Approaches for Neurodegenerative Diseases. *Prog Retin Eye Res* **2014,** *43*, 17-75.

34. Dettmer, U.; Newman, A. J.; Soldner, F.; Luth, E. S.; Kim, N. C.; von Saucken, V. E.; Sanderson, J. B.; Jaenisch, R.; Bartels, T.; Selkoe, D., Parkinson-Causing Alpha-Synuclein Missense Mutations Shift Native Tetramers to Monomers as a Mechanism for Disease Initiation. *Nat Commun* **2015,** *6*, 7314.

35. Brundin, P.; Kordower, J. H., Neuropathology in Transplants in Parkinson's Disease: Implications for Disease Pathogenesis and the Future of Cell Therapy. *Prog Brain Res* **2012,** *200*, 221-241.

36. Tran, H. T.; Chung, C. H.; Iba, M.; Zhang, B.; Trojanowski, J. Q.; Luk, K. C.; Lee, V. M., Alpha-Synuclein Immunotherapy Blocks Uptake and Templated Propagation of Misfolded Alpha-Synuclein and Neurodegeneration. *Cell Rep* **2014,** *7* (6), 2054-2065.

CHAPTER 6

DISCUSSION AND FUTURE DIRECTIONS

The purpose of this project was to understand the long-term effects of retinal remodeling on the neural retina and use this data to gauge likelihood of long-term success of different therapeutic interventions in late-stage degeneration. At the time of the project's inception, the belief in the field (including our laboratory) was that the degenerate neural retina would eventually hit a plateau phase of remodeling, where microneuromas would be prevalent with significant changes in retinal circuitry, some cell loss will have occurred, Müller glia will be altered, and RPE will have infiltrated, but that the neural retina will continue to survive in that remodeled state. The simple conclusion to be drawn from this project is that there is no such plateau in remodeling. Remodeling progresses long after photoreceptors have died but eventually gives way to a full neurodegeneration phenotype apparently similar to CNS neurodegenerations.

6.1 Müller Cell Metabolic Chaos

The first key finding of this project was significant alterations in Müller cell metabolism during late phase 3 remodeling. In aged human retinas, it is common to find variable levels of glutathione across Müller cells, which intuitively makes sense given its role in buffering against cellular damage caused by reactive oxygen species, with which

we come in regular contact, and given the varied experiences of normal humans (smoking, inflammation, obesity, alcoholism, stress, circadian variations, etc.,) However, in addition to glutathione, the increases in variability of glutamate, glutamine, taurine, and glutamine synthetase in Müller cells, as was found in degenerate retina, was unanticipated. If such changes were driven by the microenvironment, that is, if hypertrophic Müller cell columns changed their metabolic, gene, and protein expression in response to environmental cues generated by regional differences in photoreceptor degeneration, we would expect to find Müller cell metabolic variation along a gradient centered on regions of photoreceptor degeneration. This is not what we observe. Adjacent Müller cells appear to have individual metabolic profiles that vary irrespective of their surrounding environment in retinal degeneration. There are a number of avenues for investigation into the source of these changes.

First, we hypothesize a Müller cell synchrony signal that regulates metabolism and synchronizes cells across the normal retina. We expect that it will function based on a number of factors present within the intact retina, perhaps additional photoreceptor signals such as melatonin[1] or endothelin, as first described by Rattner and Nathans.[2] Many studies attempting to identify potential factors leading to Müller cell regulation use dissociated Müller cells.[3-8] If we are correct in our hypothesis that Müller cells are somehow synchronously regulated, dissociated cells are likely to express differing phenotypes than those found *in vivo*. In fact, gene expression studies have indicated heterogeneity in dissociated mouse Müller cells.[7] Even anatomical studies on dissociated cells[3] may result in misleading information. Though the level of diversity in Müller cells and the potential for multiple types is still in debate for adult Müller cells, it is likely that they do respond to

circadian rhythm. Müller cells have vasopressin receptors, which facilitate their response to the circadian variations in vasopressin secretion by some amacrine cells.[9] From this it is possible that there are circadian variations in Müller cell metabolism, but these potential variations would be expected to occur across the retina, not differentially in individual Müller cells. We have evaluated the small molecule signatures of many thousands of Müller cells from hundreds of samples, generated from dozens of species, and all normal retinas display a stereotyped $\tau^{+}Q^{+}E^{-}$ signature with exceedingly low variances between Müller cells. This indicates that despite possible genetic and anatomic variations between cells, regulating those metabolites within a narrow range is important to Müller cell function.

Second, in healthy retina we observe a clear formal tiling of the endfeet of Müller cells. In healthy retina, the processes originating from a Müller cell column do not intertwine with the processes from adjacent Müller cells, nor do Müller cell endfeet overlap. This motif is lost in degenerating retina (Chapter 5). Müller cell endfeet begin to invaginate to form finger-like projections that encroach upon neighboring Müller cells domains. It is unknown if this process is also occurring more apically as the Müller cells hypertrophy. This phenomenon of glial morphology variation coinciding with metabolic variability during neurodegeneration is not without parallel in the brain.[10] McKee et al. found that following repeated head injury astrocytic processes hypertrophied and became intertwined.[11] The impact of glial entanglement is currently unclear, however, its coincidence with high levels of metabolic variability raises a question of whether the tangles themselves may affect the metabolic interactions between neurons and glia and contribute to the variability.

These hypotheses are not exclusive. Both may play a role in the metabolic disruption seen throughout retinal degeneration, in addition to currently unidentified factors. Determining the functional impact of metabolic and anatomic disruption throughout retinal degeneration is still an ongoing question that will require further research in the future.

6.2 Excitotoxicity in the Retina

The concept of excitotoxicity in the brain is extensively cited in the field of neuroscience.[12-13] In the retina, it has been proposed that increased glutamate contributes to excitotoxicity in the retina during retinal degeneration.[14-15] For this to happen, glutamate near neurites expressing iGluRs must reach a concentration high enough to cause neuronal stress and death. Although glutamate was shown to be toxic and induce lesions in the retina of young mice in 1957[16] and was replicated through the 1960s,[17-18] it is important to consider what concentration of glutamate was used. Lucas and Newhouse report that to produce a lesion with a single subcutaneous injection they needed a near-lethal glutamate level, and to avoid this multiple smaller injections were given.[16] Still, these were increasing concentrations from 2mg to 30mg of L-glutamate per day, with a maximum concentration of 150M. For reference, the average retina has a total glutamate concentration of 1.5 mM;[19] with some ganglion cells containing the highest level of glutamate, ~10mM, bipolar cells ranging from 1-5 mM, and photoreceptors containing 1 mM or less depending on adaptation state. Glutamate is not transported across the blood retinal barrier or blood brain barrier at physiological levels,[20] it is possible the lesions seen in retina may have been caused by a separate mechanism, such as ischemia from particulate[21] or RBC[22] aggregates

following high glutamate exposure, rather than from the added glutamate directly. More recent studies have demonstrated that if the extracellular concentration is raised above 30-100μM and maintained there for a couple of hours it is sufficient to induce Müller cell swelling and some neuronal stress,[23] though these results are not consistent with previous literature[24] or any of our findings. In any case, a large number of glutamate-containing cells would have to die in a single region in an exceedingly short period of time (on the order of minutes), and extracellular glutamate would need to remain at that concentration for hours to induce an excitotoxic effect. To this end, the rate that Müller cells can transport glutamate away from neurons is of interest. Data from our lab have shown that the Müller cells continually buffer up to approximately 5mM extracellular glutamate,[25] more than 3 times the total glutamate of the retina.[26]

Therefore, for glutamate excitotoxicity to potentially contribute to the neurodegeneration seen in the retina, there would have to be significant disruption of glutamate transport by the Müller cells. It has been demonstrated conclusively in Chapter 4 of this dissertation that glutamate transport by the Müller cells is not significantly disrupted until very late stages of retinal degeneration, and most of that is in single Müller cells, not widespread populations. The timepoint at which the Müller cell transport begins to be widely compromised is in our 6-year-old rabbit, which has already undergone massive cell loss. Based on this, it is unlikely that glutamate excitotoxicity plays any significant role in retinal degeneration and future drugs or therapies based on this premise (e.g., neuroprotective glutamate receptor antagonists) are likely to have no effect on the progression of retinal degenerative diseases.

6.3 Retinal Neurodegeneration

During the course of retinal degeneration it is clear that both remodeling and neurodegeneration play important but differential roles in determining the final state of the neural retina. Previous studies evaluated the neural retina up to a year after the loss of photoreceptors.[27] Based on our analysis in Chapter 5, we conclude that retinal remodeling and neurodegeneration are separate overlapping processes occurring over the course of retinal degeneration (illustrated in Figure 6.1). Retinal remodeling begins in tandem with the loss of photoreceptors, and is characterized by progressive receptor alteration, neurite sprouting (followed by microneuroma formation), and early metabolic variation.[27-35] Retinal neurodegeneration on the other hand is what leads to the eventual decimation of the retina, and is characterized by metabolic chaos[36] and collapse within Müller cells, widespread cell death, debris accumulation, and likely has a proteinopathy component as evident by an increase in α-synuclein. Neurodegeneration begins after photoreceptors are lost and eventually supersedes remodeling years after the photoreceptors were lost, and continuing until the retina is entirely devoid of recognizable cells. Although this development is unfortunate for late-stage therapeutic interventions, this opens up a new potential for evaluating early disease progression in other synucleinopathies. Within the brain, neurodegenerative proteinopathies propagate slowly throughout affected regions following modifications of certain proteins making them prone to misfolding and aggregation.[37] One such protein is alpha-synuclein, which is associated with multiple neurodegenerative diseases.[38-40] Multiple mechanisms of alpha synuclein toxicity have been proposed, including proteasome impairment and stress, mitochondrial dysfunctions, ER stress, and membrane disruption and pore formation.[41] During the course of

degeneration, we see ultrastructural evidence for mitochondrial and ER stress. The increases seen in ubiquitin aggregation in the nuclei could also be attributed to the ubiquitin proteasome system being impaired.[42] All of these processes are slow progressing in the brain. We see similar signs of neurodegeneration occurring in the retina combined with focal increases in alpha synuclein. We posit that these processes are likely to occur at an accelerated rate in the retina in comparison to the brain in large part due to the close proximity of neurons to one another and relatively short axons, which can facilitate transneuronal propagation in a shorter time frame than that seen in the brain.

6.4 Implications for Therapeutic Interventions

Taken together, these findings show that the best time to intervene in retinal degenerative disease is as early as possible. When a specific genetic mutation is known, gene-replacement therapy shows the best promise for preventing widespread photoreceptor degeneration. Immediately following the onset of photoreceptor degeneration, optogenetics or photoswitches may be capable of restoring some, albeit coarse, vision to help provide independence; though complications due to rewiring will have to be addressed (see section 6.5, Future Directions). Later in disease, epi-retinal bionic implants may be a solution to bypass corrupted retinal circuits, though glial separation of ganglion cells from the vitreous and the progressive loss of ganglion cells will be an obstacle. However, Loizos et al. have shown by modeling that it is unlikely that epiretinal implants only stimulate ganglion cells.[43] It is unlikely that photoreceptor or whole retina replacement therapy will ever be the best choice. Photoreceptor replacement will always depend on our ability to prevent remodeling or even death of the transplanted cells,[44] and if we have that capability

the cellular replacements will likely be unnecessary. Whole retina replacement requires the ability to properly rewire the ganglion cell axons correctly to targets in the brain, which is an independently exceedingly difficult and probably insurmountable challenge. From the potential postphotoreceptor degeneration interventions, one fact is clear: preventing neurodegeneration progression will be crucial to long-term vision maintenance.

6.5 Future Directions

Based on our assessment of neurodegeneration being a large obstacle to late state retinal degeneration, we propose that the best timepoint for intervention will be as soon as possible after diagnosis. Because it is common for considerable photoreceptor loss to have occurred prior to a patient seeking treatment, remodeling will likely have already altered neural circuits in the inner retina. Prior studies have demonstrated neurite sprouting, with molecular markers indicative of active synapses,[33, 45] however, it remains to be seen whether the network topology of this system is correct. The synaptic and gap junction partners of neurons remaining in the retina during remodeling have not been addressed. To fully determine the extent of network alterations in the degenerating retina and their potential impacts on signaling capabilities of the remodeling retina, it will be necessary to construct connectomes for varying phases of remodeling and neurodegeneration. We have generated a preliminary pathoconnectome volume (RPC1) that combines the high resolution ultrastructure of automated TEM with the quantitative aspects of CMP, and is the first pathoconnectome ever generated. RPC1 consists of 948 serial sections spanning from the proximal ONL to the vitreous, with 1 of every 30 sections reserved for CMP data that are intercalated into the volume. In brief, sections were serially sectioned at 90nm and

prepared for TEM capture or CMP analysis. The resolution afforded by TEM is vastly superior to serial block face scanning electron microscopy (SBFSEM).[46] Our standard TEM acquisitions have a resolution of 2.18 nm/pixel, and because the grids are archival, we have the ability to reimage structures at a resolution of 0.27 nm/pixel. Alternatively, SBFSEM has a published resolution of 8-16 nm, which is too coarse to positively identify gap junctions or small synapses.[47] CMP lends itself to positive cell identification through classification enabled by the quantitation of small molecules,[19, 25, 48-50] which are stoichiometrically trapped during fixation,[19, 48, 51] in addition to glutaraldehyde/osmium-tolerant IgGs. For the identification of all cell structures and genetically labeled cells in the volumes we will use a combination of small molecule IgGs to GABA, glutamate, glutamine, glycine, and taurine, in addition to IgGs targeting GFAP, GFP/YFP, TH, Tomato lectin and GS. RPC1 was assembled using a modified version of the NCR toolkit[**]. Briefly, the toolkit combines individual images acquired from a JEOL electron microscope with a 16-Mpixel Gatan camera (EM sections) or a Leica light-microscope affixed with 8-bit CCD camera (CMP) and registers them into assembled mosaics before using automated registration to align adjacent sections throughout the volume (Figure 6.2).[46-47] Following the assembly of the connectome volume, navigation and annotation of the dataset will be done in the software Viking, which facilitates rapid navigation, visualization, and annotation of TEM and CMP data.[52] Viking annotations retain information about the size, structure, location, and may be queried for population statistics.[47, 53] From a Viking-annotated dataset, we can render 2D and 3D representations of cell including their

[**] http://www.sci.utah.edu/download/ncrtoolset

subcellular components (e.g., pre- and postsynaptic densities, organelles, gap junctions, etc.).[54]

Preliminary data reveal three distinct phenomena in early degeneration (10mo old P347L rabbit retina). First, dendritic structures of rod bipolar cells are significantly altered indicating the initiation of dendritic remodeling (Figure 6.3A) likely associated with reprogramming described by Marc et al.[35] Annotation of these dendrites will allow us to determine what combinations of photoreceptors contribute to the inputs of rod bipolar cells during the loss of rod photoreceptors. Second, by tracking neurite outgrowths from bipolar cells (that Marc et al., argued were supernumerary axons) it is clear that many of the ribbon synapses generated therein are morphologically altered (Figure 6.3B). The evaluation of these ribbons and their synaptic partners may yield insights regarding revised networks of the inner retina. Third, although it has been previously observed that high levels of electron density (presumed to be hyperosmication due to high levels of ribosomes, RNAs, aromatics, or unsaturated fatty acids) in Müller cells of degenerating retina, we had previously described it in the primary trunk. It is now clear that hyperosmication also appears in the finest processes of a Müller cell as it encroaches on a neighboring Müller cell's domain (Figure 6.3C). Continued evaluation of the ultrastructure of the Müller cells, combined with metabolic information afforded by CMP, will allow us to further evaluate the responses of Müller glia to retinal degeneration.

Figure 6.1 Retinal degeneration, a combination of remodeling and neurodegenerative processes. Retinal remodeling consists of the processes undergone by the retina in initial response to photoreceptor loss. In phase 1, rods begin to degenerate, and Rod bipolar cells retract their dendrites from rod spherules. Phase 2 continues the loss of photoreceptors with the loss of cone outer segments and complete loss of rods. Phase 2 is also characterized by initial metabolic variability seen in Müller cells. Phase 3 is initiated by the complete loss of photoreceptors. In the remodeling processes, neurite sprouting is abundant and leads to microneuroma formation. While remodeling continues to progress long after photoreceptors are absent, neurodegeneration processes eventually overwhelm the remnant neural retina. Retinal neurodegeneration is characterized by a complete lack of Müller cell coordination and increased α-syn in remaining neurons. As these initial processes persist, cell death occurs over large parts of the retina and coincides with debris accumulation. The timeline demonstrates the increasing impact of retinal neurodegeneration over the lifespan of rabbit and mouse. It is probable that mice do not live long enough for the end stages of retinal degeneration-induced neurodegeneration to be evident.

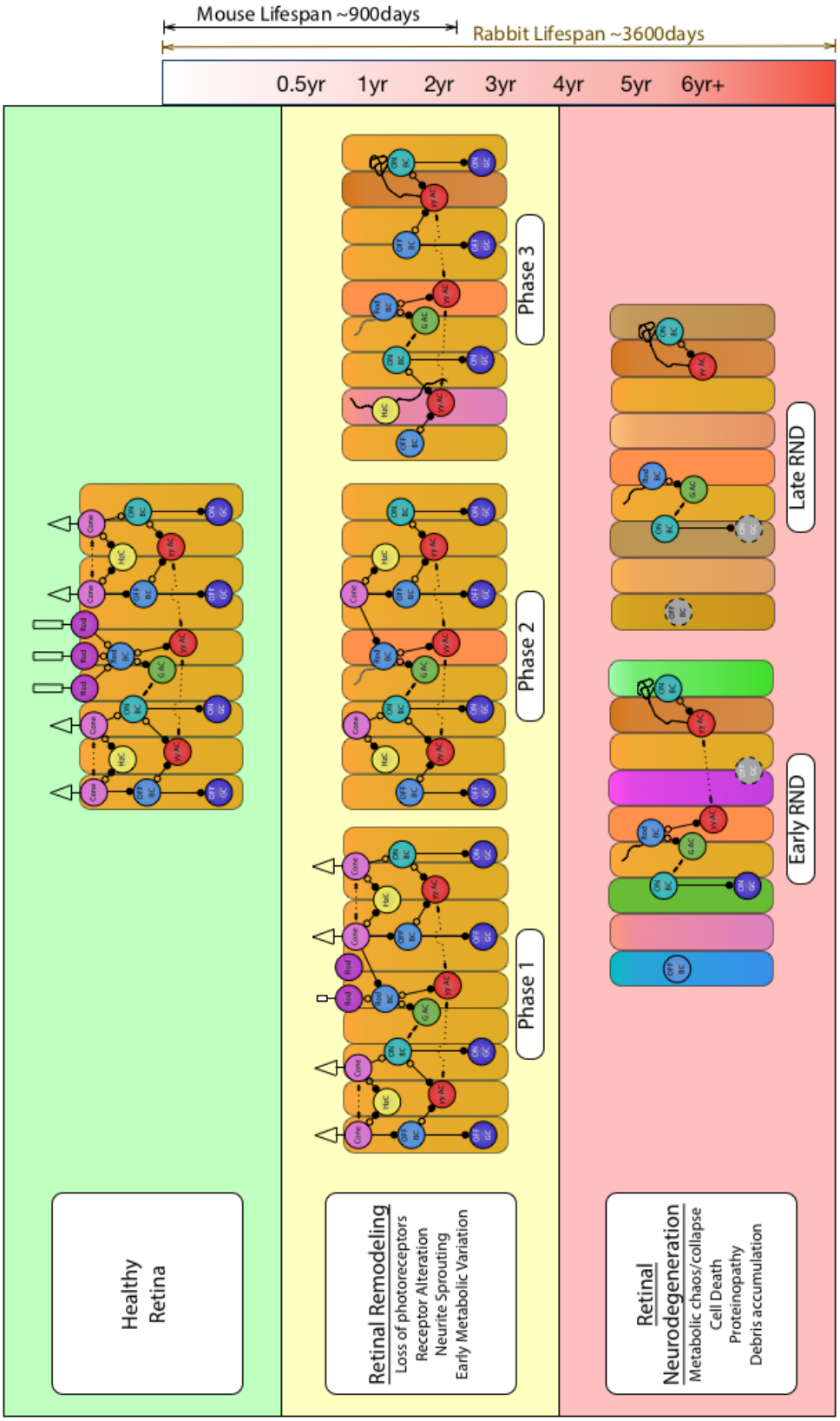
Mouse Lifespan ~900days
Rabbit Lifespan ~3600days
0.5yr
1yr
2yr
3yr
4yr
5yr
6yr+
Healthy Retina
Retinal Remodeling
Loss of photoreceptors
Receptor Alteration
Neurite Sprouting
Early Metabolic Variation
Retinal Neurodegeneration
Metabolic chaos/collapse
Cell Death
Proteinopathy
Debris accumulation
Phase 1
Phase 2
Phase 3
Early RND
Late RND

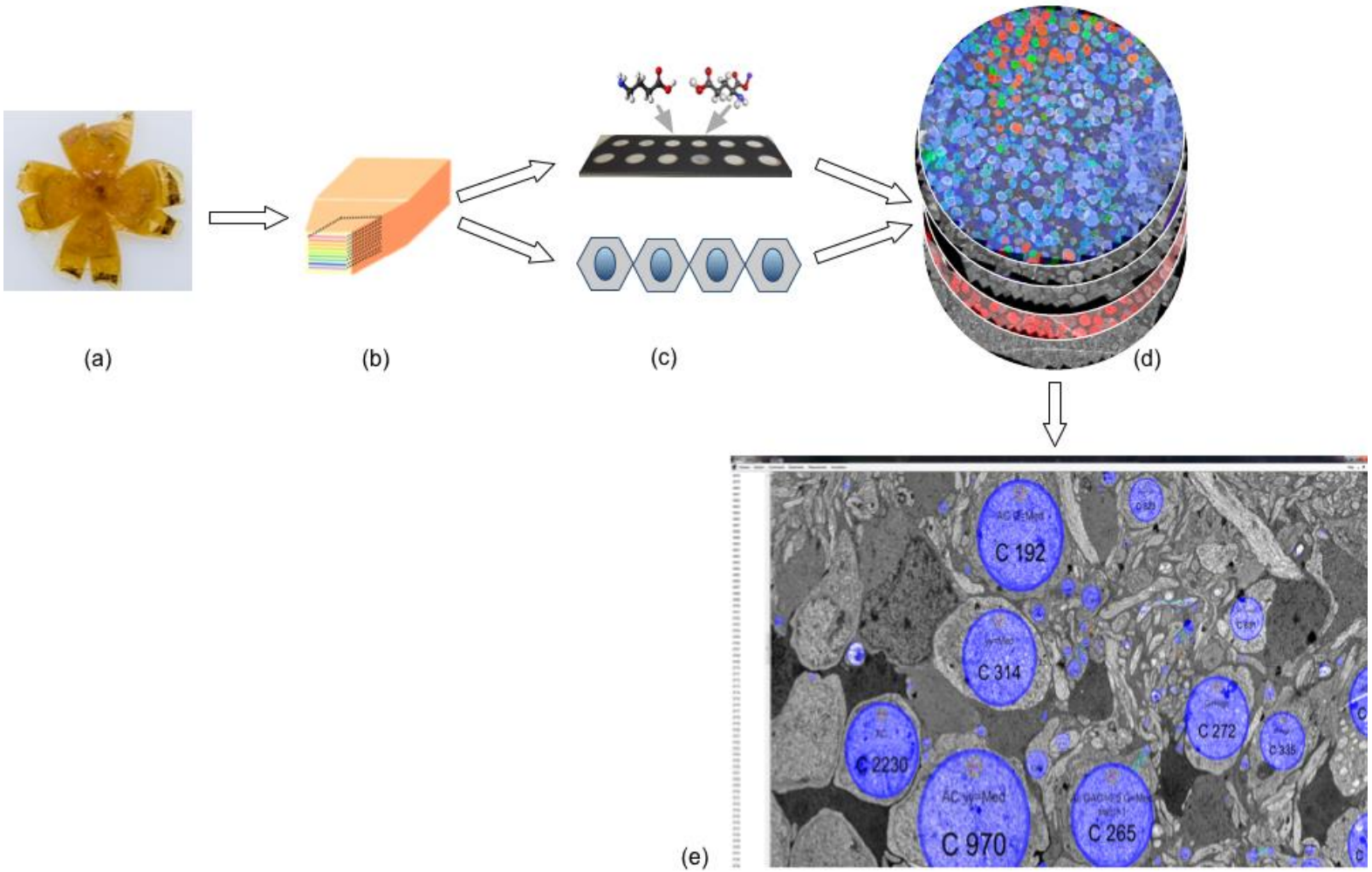

Figure 6.2 Workflow for generation of pathoconnectome. a) Tissue from a 10 month Tg P347L rabbit retina was prepared for TEM/CMP via osmication, b) embedded in epon blocs, and c) was serially sectioned at 90nm. Every 30 sections one was reserved for CMP analysis. D) TEM and CMP sections were imaged using a JEOL or Leica light microscope, respectively. Following image capture, sections were assembled, aligned, and imported into a Viking volume by custom software. E) Further annotation will continue in the Viking environment.

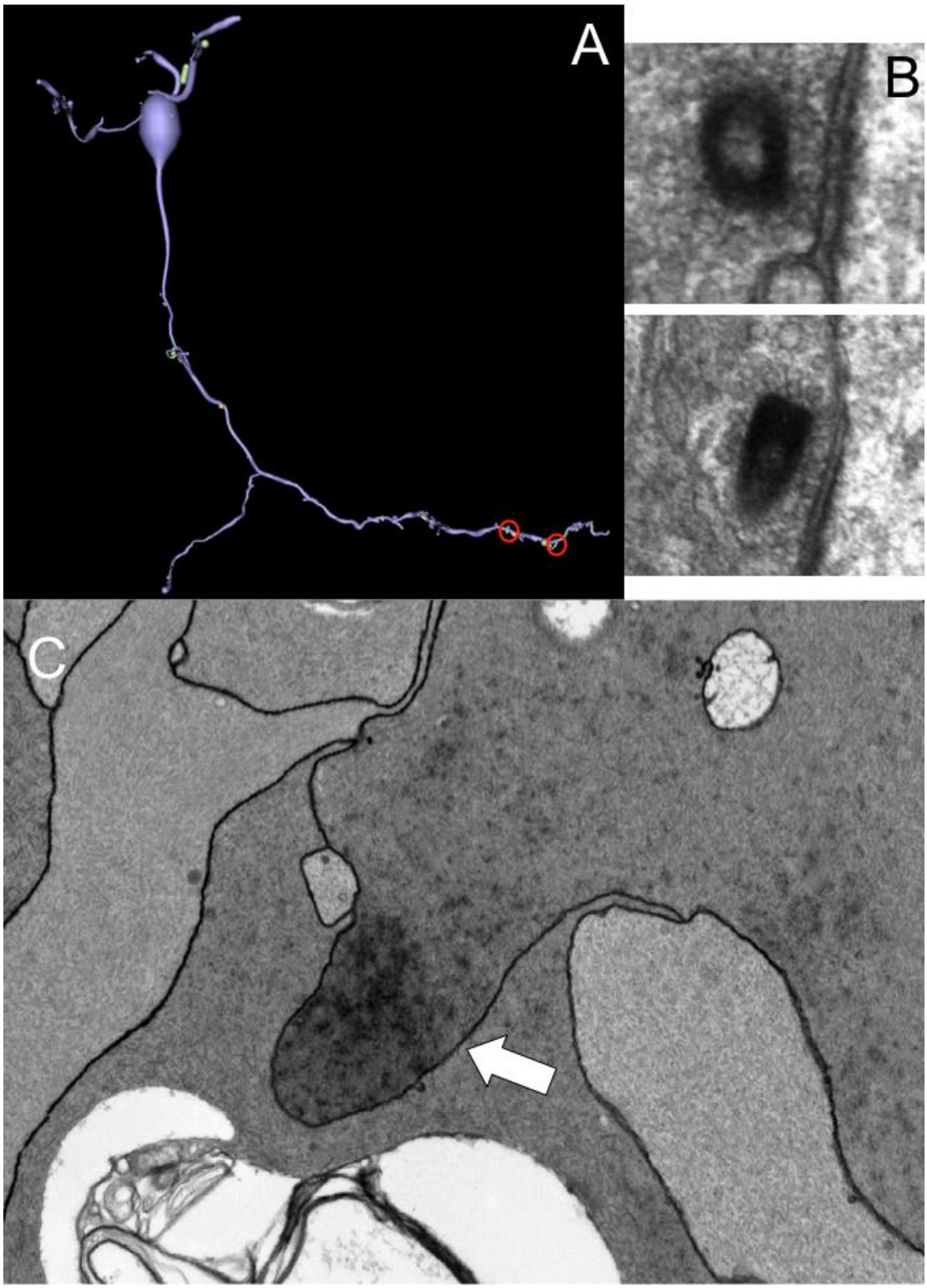

Figure 6.3 Preliminary RPC1 data. A) 3D reconstruction of rod bipolar cell annotated in Viking, rendered in VikingView. B) Abnormal morphology ribbon synapses from the regions indicated in A. C) Hyperosmication of the protruding tip of a Müller cell invading a neighbor's domain.

6.6 References

1. Hiragaki, S.; Baba, K.; Coulson, E.; Kunst, S.; Spessert, R.; Tosini, G., Melatonin Signaling Modulates Clock Genes Expression in the Mouse Retina. *PLoS One* **2014,** *9* (9), e106819.

2. Rattner, A.; Nathans, J., The Genomic Response to Retinal Disease and Injury: Evidence for Endothelin Signaling from Photoreceptors to Glia. *J Neurosci* **2005,** *25* (18), 4540-4549.

3. Anezary, L.; Medina, J. I.; Sanchez-Nogueiro, J.; Lopez-Gallardo, M.; Prada, C., Shape Diversity Among Chick Retina Muller Cells and their Postnatal Differentiation. *J Comp Neurol* **2001,** *438* (1), 32-49.

4. Dai, M.; Xia, X. B.; Xiong, S. Q., BDNF Regulates GLAST and Glutamine Synthetase in Mouse Retinal Muller Cells. *J Cell Physiol* **2012,** *227* (2), 596-603.

5. Poitry, S.; Poitry-Yamate, C.; Ueberfeld, J.; MacLeish, P. R.; Tsacopoulos, M., Mechanisms of Glutamate Metabolic Signaling in Retinal Glial (Muller) Cells. *J Neurosci* **2000,** *20* (5), 1809-1821.

6. Reichelt, W.; Pannicke, T.; Biedermann, B.; Francke, M.; Faude, F., Comparison Between Functional Characteristics of Healthy and Pathological Human Retinal Muller Glial Cells. *Surv Ophthalmol* **1997,** *42* S105-117.

7. Roesch, K.; Jadhav, A. P.; Trimarchi, J. M.; Stadler, M. B.; Roska, B.; Sun, B. B.; Cepko, C. L., The Transcriptome of Retinal Muller Glial Cells. *J Comp Neurol* **2008,** *509* (2), 225-238.

8. Roesch, K.; Stadler, M. B.; Cepko, C. L., Gene Expression Changes Within Müller Glial Cells in Retinitis Pigmentosa. *Mol Vis* **2012,** *18*, 1197-1214.

9. Koh, S. W.; Kyritsis, A.; Chader, G. J., Interaction of Neuropeptides and Cultured Glial (Muller) Cells of the Chick Retina: Elevation of Intracellular Cyclic AMP by Vasoactive Intestinal Peptide and Glucagon. *J Neurochem* **1984,** *43* (1), 199-203.

10. Acosta, C.; Anderson, H. D.; Anderson, C. M., Astrocyte Dysfunction in Alzheimer Disease. *J Neurosci Res* **2017,** *95* (12), 2430-2447.

11. McKee, A. C.; Cantu, R. C.; Nowinski, C. J.; Hedley-Whyte, E. T.; Gavett, B. E.; Budson, A. E.; Santini, V. E.; Lee, H. S.; Kubilus, C. A.; Stern, R. A., Chronic Traumatic Encephalopathy in Athletes: Progressive Tauopathy after Repetitive Head Injury. *J Neuropathol Exp Neurol* **2009,** *68* (7), 709-735.

12. Dong, X. X.; Wang, Y.; Qin, Z. H., Molecular Mechanisms of Excitotoxicity and Their Relevance to Pathogenesis of Neurodegenerative Diseases. *Acta Pharmacol Sin* **2009,** *30* (4), 379-387.

13. Lai, T. W.; Zhang, S.; Wang, Y. T., Excitotoxicity and Stroke: Identifying Novel Targets for Neuroprotection. *Prog Neurobiol* **2014,** *115*, 157-188.

14. Bringmann, A.; Grosche, A.; Pannicke, T.; Reichenbach, A., GABA and Glutamate Uptake and Metabolism in Retinal Glial (Muller) Cells. *Front Endocrinol* **2013,** *4*, 1-14.

15. Reichenbach, A.; Bringmann, A., New Functions of Muller Cells. *Glia* **2013,** *61* (5), 651-678.

16. Lucas, D. R.; Newhouse, J. P., The Toxic Effect of Sodium L-Glutamate on the Inner Layers of the Retina. *AMA Arch Ophthalmol* **1957,** *58* (2), 193-201.

17. Olney, J. W., Glutamate-Induced Retinal Degeneration in Neonatal Mice. Electron Microscopy of the Acutely Evolving Lesion. *J Neuropathol Exp Neurol* **1969,** *28* (3), 455-474.

18. Olney, J. W., The Toxic Effects of Glutamate and Related Compounds in the Retina and the Brain. *Retina* **1982,** *2* (4), 341-359.

19. Marc, R. E.; Murry, R. F.; Basinger, S. F., Pattern Recognition of Amino Acid Signatures in Retinal Neurons. *J Neurosci* **1995,** *15* (7 Pt 2), 5106-5129.

20. Yudkoff, M., Interactions in the Metabolism of Glutamate and the Branched-Chain Amino Acids and Ketoacids in the CNS. *Neurochem Res* **2017,** *42* (1), 10-18.

21. Tang, N.; Skibsted, L. H., Calcium Binding to Amino Acids and Small Glycine Peptides in Aqueous Solution: Toward Peptide Design for Better Calcium Bioavailability. *J Agric Food Chem* **2016,** *64* (21), 4376-4389.

22. Hossmann, K. A., Reperfusion of the Brain after Global Ischemia: Hemodynamic Disturbances. *Shock* **1997,** *8* (2), 95-101; discussion 102-103.

23. Izumi, Y.; Kirby, C. O.; Benz, A. M.; Olney, J. W.; Zorumski, C. F., Muller Cell Swelling, Glutamate Uptake, and Excitotoxic Neurodegeneration in the Isolated Rat Retina. *Glia* **1999,** *25* (4), 379-389.

24. Pow, D. V.; Robinson, S. R., Glutamate in Some Retinal Neurons is Derived Solely from Glia. *Neuroscience* **1994,** *60* (2), 355-366.

25. Marc, R. E., Mapping Glutamatergic Drive in the Vertebrate Retina with a Channel-Permeant Organic Cation. *J Comp Neurol* **1999,** *407* (1), 47-64.

26. Murry, R. F.; Marc, R. E., Muller's Cells are Not a Major Source of Excitotoxic Glutamate in Hypoxic/Hypoglycemic *in vitro* Retina. *Investigative Opthalmology & Visual Sciences* **1997,** *34* (4), 2836-B2526.

27. Jones, B. W.; Kondo, M.; Terasaki, H.; Watt, C. B.; Rapp, K.; Anderson, J.; Lin, Y.; Shaw, M. V.; Yang, J. H.; Marc, R. E., Retinal Remodeling in the Tg P347L Rabbit, a Large-Eye Model of Retinal Degeneration. *J Comp Neurol* **2011,** *519* (14), 2713-27133.

28. Jones, B. W.; Kondo, M.; Terasaki, H.; Lin, Y.; McCall, M.; Marc, R. E., Retinal remodeling. *Jpn J Ophthalmol* **2012,** *56* (4), 289-306.

29. Jones, B. W.; Marc, R. E., Retinal Remodeling During Retinal Degeneration. *Exp Eye Res* **2005,** *81* (2), 123-137.

30. Jones, B. W.; Marc, R. E.; Pfeiffer, R. L. Retinal Remodeling and Plasticity. http://webvision.med.utah.edu/.

31. Jones, B. W.; Pfeiffer, R. L.; Ferrell, W. D.; Watt, C. B.; Marmor, M.; Marc, R. E., Retinal Remodeling in Human Retinitis Pigmentosa. *Exp Eye Res* **2016,** *150*, 149-165.

32. Marc, R. E.; Jones, B. W.; Watt, C. B.; Strettoi, E., Neural remodeling in retinal degeneration. *Prog Retin Eye Res* **2003,** *22* (5), 607-655.

33. Jones, B. W.; Watt, C. B.; Marc, R. E., Retinal Remodeling *Clin Exp Optom* **2005,** *88* (5), 282-291.

34. Marc, R. E.; Jones, B. W., Retinal Remodeling in Inherited Photoreceptor Degenerations. *Mol Neurobiol* **2003,** *28* (2), 139-147.

35. Marc, R. E.; Jones, B. W.; Anderson, J. R.; Kinard, K.; Marshak, D. W.; Wilson, J. H.; Wensel, T.; Lucas, R. J., Neural Reprogramming in Retinal Degeneration. *Invest Ophthalmol Vis Sci* **2007,** *48* (7), 3364-3371.

36. Pfeiffer, R. L.; Marc, R. E.; Jones, B. W., Muller cell metabolic chaos during retinal degeneration. *Exp Eye Res* **2016**.

37. Sweeney, P.; Park, H.; Baumann, M.; Dunlop, J.; Frydman, J.; Kopito, R.; McCampbell, A.; Leblanc, G.; Venkateswaran, A.; Nurmi, A.; Hodgson, R., Protein Misfolding in Neurodegenerative Diseases: Implications and Strategies. *Transl Neurodegener* **2017,** *6* (6), 1-13.

38. Hu, R.; Luo, J.; Wang, W.; Wang, X. F.; Xi, Z. Q., Alpha-Synuclein is a Potential Biomarker in the Serum and CSF of Patients with Intractable Epilepsy. *Seizure-Eur J Epilepsy* **2015,** *27*, 6-9.

39. Polymeropoulos, M. H.; Lavedan, C.; Leroy, E.; Ide, S. E.; Dehejia, A.; Dutra, A.; Pike, B.; Root, H.; Rubenstein, J.; Boyer, R.; Stenroos, E. S.; Chandrasekharappa, S.; Athanassiadou, A.; Papapetropoulos, T.; Johnson, W. G.; Lazzarini, A. M.; Duvoisin, R. C.; DiIorio, G.; Golbe, L. I.; Nussbaum, R. L., Mutation in the Alpha-Synuclein Gene Identified in Families with Parkinson's Disease. *Science* **1997,** *276* (5321), 2045-2047.

40. Ganguly, G.; Chakrabarti, S.; Chatterjee, U.; Saso, L., Proteinopathy, Oxidative Stress and Mitochondrial Dysfunction: Cross Talk in Alzheimer's Disease and Parkinson's Disease. *Drug Des Dev Ther* **2017,** *11*, 797-810.

41. Gallegos, S.; Pacheco, C.; Peters, C.; Opazo, C. M.; Aguayo, L. G., Features of Alpha-Synuclein that Could Explain the Progression and Irreversibility of Parkinson's Disease. *Front Neurosci* **2015,** *9*, 59.

42. Zheng, Q.; Huang, T.; Zhang, L.; Zhou, Y.; Luo, H.; Xu, H.; Wang, X., Dysregulation of Ubiquitin-Proteasome System in Neurodegenerative Diseases. *Front Aging Neurosci* **2016,** *8*, 303.

43. Loizos, K.; Lazzi, G.; Lauritzen, J. S.; Anderson, J.; Jones, B. W.; Marc, R., A Multi-Scale Computational Model for the Study of Retinal Prosthetic Stimulation. *Conf Proc IEEE Eng Med Biol Soc* **2014,** *2014*, 6100-6103.

44. Seiler, M. J.; Aramant, R. B., Cell Replacement and Visual Restoration by Retinal Sheet Transplants. *Prog Retin Eye Res* **2012,** *31* (6), 661-687.

45. Marc, R. E.; Jones, B. W.; Watt, C. B.; Strettoi, E., Neural Remodeling in Retinal Degeneration. *Prog Retin Eye Res* **2003,** *22* (5), 607-655.

46. Anderson, J. R.; Jones, B. W.; Yang, J. H.; Shaw, M. V.; Watt, C. B.; Koshevoy, P.; Spaltenstein, J.; Jurrus, E.; U, V. K.; Whitaker, R. T.; Mastronarde, D.; Tasdizen, T.; Marc, R. E., A Computational Framework for Ultrastructural Mapping of Neural Circuitry. *PLoS Biol* **2009,** *7* (3), 493-512.

47. Marc, R. E.; Jones, B. W.; Lauritzen, J. S.; Watt, C. B.; Anderson, J. R., Building Retinal Connectomes. *Curr Opin Neurobiol* **2012,** *22* (4), 568-574.

48. Marc, R. E.; Cameron, D., A Molecular Phenotype Atlas of the Zebrafish Retina. *J Neurocytol* **2001,** *30* (7), 593-654.

49. Marc, R. E.; Jones, B. W., Molecular Phenotyping of Retinal Ganglion Cells. *J Neurosci* **2002,** *22* (2), 413-427.

50. Marc, R. E.; Murry, R. F.; Fisher, S. K.; Linberg, K. A.; Lewis, G. P.; Kalloniatis, M., Amino Acid Signatures in the Normal Cat Retina. *Invest Ophthalmol Vis Sci* **1998,** *39* (9), 1685-1693.

51. Ottersen, O. P., Postembedding Immunogold Labelling of Fixed Glutamate: An Electron Microscopic Analysis of the Relationship Between Gold Particle Density and Antigen Concentration. *J Chem Neuroanat* **1989,** *2* (1), 57-66.

52. Anderson, J. R.; Jones, B. W.; Watt, C. B.; Shaw, M. V.; Yang, J. H.; Demill, D.; Lauritzen, J. S.; Lin, Y.; Rapp, K. D.; Mastronarde, D.; Koshevoy, P.; Grimm, B.; Tasdizen, T.; Whitaker, R.; Marc, R. E., Exploring the Retinal Connectome. *Mol Vis* **2011,** *17*, 355-379.

53. Lauritzen, J. S.; Anderson, J. R.; Jones, B. W.; Watt, C. B.; Mohammed, S.; Hoang, J. V.; Marc, R. E., ON Cone Bipolar Cell Axonal Synapses in the OFF Inner Plexiform Layer of the Rabbit Retina. *J Comp Neurol* **2013,** *521* (5), 977-1000.

54. Lauritzen, J. S.; Sigulinsky, C. L.; Anderson, J. R.; Kalloniatis, M.; Nelson, N. T.; Emrich, D. P.; Rapp, C.; McCarthy, N.; Kerzner, E.; Meyer, M.; Jones, B. W.; Marc, R. E., Rod-Cone Crossover Connectome of Mammalian Bipolar Cells. *J Comp Neurol* **2016**.